CDF/ANAL/EXOTIC/GROUP/9101
April 5, 2008

A Limit on the Branching Ratio of the Flavor-Changing Top Quark Decay $t \to Z^0 c$

Alexander Paramonov[1] and Henry Frisch[2]

Enrico Fermi Institute, University of Chicago

Abstract

We measure an upper limit of 8.3% (95% C.L.) on the branching ratio of the flavor-changing top quark decay $t \to Z^0 c$ for 100% longitudinally polarized Z-bosons using 1.52 fb^{-1} of data. We parametrize the upper limit as a function of Z-boson's helicity to cover the full range of possible decay structures. The analysis is based on the comparison of two processes: $p\bar{p} \to t\bar{t} \to WbWb \to l\nu bjjb$ and $p\bar{p} \to t\bar{t} \to Z^0 cWb \to l^+l^- cjjb$. The use of these two decay modes together allows cancellation of major systematic uncertainties of acceptance, efficiency, and luminosity. We validate the MC modeling of acceptance and efficiency for lepton identification over the multi-year dataset by a precision measurement of the ratio of the inclusive production of W- and Z-bosons. To improve the discrimination, we calculate the top mass for each event with two leptons and four jets assuming it is a $t\bar{t}$ event with one of the top quarks decaying to $Z^0 c$. The calculation of the top mass is performed with a fitter on an event-by-event basis. The upper limit on the Br($t \to Z^0 c$) is estimated from a 2-dimensional likelihood of the $l^+l^- cjjb$ top mass distribution and the number of "$l + \not\!\!E_{\rm T} + 4jets$" events. The results are limited by statistics at present.

[1] paramon@hep.uchicago.edu
[2] frisch@hep.uchicago.edu

Contents

1 Introduction

The Standard Model (SM) Lagrangian does not contain any flavor changing neutral terms such as $d \to s$ as an algebraic consequence of its SU(2) structure [1]. The Tevatron affords us the unique opportunity to search for a flavor changing neutral current (FCNC) $t \to c$ in top quark decays. In the Standard Model the FCNC decay $t \to Z^0 c$ is highly suppressed, proceeding only through radiative corrections, with a predicted branching ratio $\mathrm{Br}(t \to Z^0 c)$ of about 10^{-14} [2]. However, some extensions of the SM predict measurable rates [1, 3, 4]. Any observation of an excess over SM background in this decay channel must therefore be a sign of new physics.

We assume that the $\mathrm{Br}(t \to Z^0 c)$ is small and the top quark decays mostly to Wb. Specifically, the assumption is $\mathrm{Br}(t \to Z^0 c) + \mathrm{Br}(t \to Wb) = 100\%$

The production of top quark pairs, $t\bar{t}$, is the best channel to observe FCNC, as single top production would have too small a cross section and has enormous QCD backgrounds in the $Z^0 c$ final state. We search for the case in which one of the top quarks decays to $Z^0 c$ and the other one decays to Wb. We ask for the leptonic decays of the Z^0-boson, $Z^0 \to ee$ and $Z^0 \to \mu\mu$, in order to get a sample of better purity. In this scenario, the FCNC signature is a pair of oppositely-charged leptons forming a Z^0 and four jets (the Z^0-boson decays leptonically and W-boson decays hadronically), with the event being kinematically consistent with the FCNC $t\bar{t}$ decay hypothesis. In addition, we require at least one displaced vertex (B-tag) as a sign of heavy-flavor quark (b or c-quark) to further suppress hadronic backgrounds.

To measure a branching fraction we face the problem of correctly estimating the systematic uncertainties on the efficiencies, acceptances, and luminosity. We have developed a technique which allows us to cancel out many of these uncertainties. The idea is based on the comparison of two processes:

1. $p\bar{p} \to t\bar{t} \to WbWb \to l\nu bjjb$,
2. $p\bar{p} \to t\bar{t} \to Z^0 cWb \to l^+l^- cjjb$,

In addition we study inclusive production of W- and Z- bosons as a sanity check of lepton identification. Specifically we consider these two decay modes:

- $p\bar{p} \to Z^0 + jets \to l^+l^- + jets$,
- $p\bar{p} \to W + jets \to l\nu + jets$.

Comparison of inclusive W and Z production allows us to validate the lepton identification (ID) efficiencies in the Monte Carlo (MC) samples. We measure the value of the ratio R as a cross-check, where R is defined as [5]:

$$R = \frac{\sigma(W^{\pm}) \cdot BR(W \to e\nu)}{\sigma(Z^0) \cdot BR(Z^0 \to e^+e^-)} \tag{1}$$

We also compare the observed top cross-section $\sigma(p\bar{p} \to t\bar{t})$ with the Standard Model prediction as an additional cross-check.

Another difficulty we face is Monte Carlo modeling of "Z + 4 jets" production. This is especially difficult in the presence of Heavy Flavor (HF) quarks. As we have mentioned above, the "Z+c-jet +b-jet + 2 jets" category is crucial for this analysis and the result heavily depends on the MC predictions. We exploit the MC generator Alpgen [6] with MLM matching [7] to get a better estimate of the SM contributions. Most other SM processes are described using Pythia [8] and Alpgen. Contributions from 'fake' electrons, fake muons, and fake B-tags ('mistags') are estimated with data.

The present study employs leptonic decays of W's and Z's using data collected at CDF Run II at the Tevatron up to 31st of January of 2007. The data correspond to an integrated luminosity of 1.52 fb^{-1} . All events are triggered with high-P_T electrons and muons.

The direct observation on the branching ratio for $t \to Z^0 c$ cited by the PDG [9] is from CDF using data from Run I of the Tevatron; the limit is 33% at 95% C.L. [10]. The limit from indirect precision measurements at LEP is lower, 13.7% at 95% C.L. [11]. The latest CDF limit on the branching ratio is 10.4% at 95% C.L. [12].

The structure of this note is as follows. Section 2 gives an overview of the analysis strategy and procedures. Section 3 describes the details of the lepton identification cuts and corrected efficiencies. Jet identification is described in Section 4, and the selection criteria for W- and Z- bosons are given in Section 6. Section 7 gives the details of b-tagging and the mistag matrix. The datasets used, both in data and Monte Carlo, are presented in section 8. We use the comparison of the measurement and the precise prediction for R, the ratio of W and Z cross-sections, as a check of the lepton identification efficiencies and geometric acceptances and the faithfulness of the MC simulation over this run range; this is presented in Section 9.

Moving on to the limit on FCNC, Section 10 describes Standard Model top pair production, and Section 11 describes MC generation of the FCNC decay $t\bar{t} \to Z^0 cWb$, the top mass fitter program used to identify the signature, and the extraction of the limit. Systematic uncertainties are described in Section 12. The calculation of the limit including uncertainties is given in Section 13, followed by the conclusions in Section 14.

2 Analysis Procedure Overview

We consider only two decay chains of the $t\bar{t}$ pairs: $p\bar{p} \to t\bar{t} \to Z^0 cWb \to l^+l^- bcjj$ and $p\bar{p} \to t\bar{t} \to WbWb \to l\nu bbjj$, where the final state notation is:

- l is a lepton (e or μ),
- j is a jet,
- ν is a neutrino which is observed via missing transverse energy ($\not\!\!E_{\rm T}$),
- the missing transverse energy ($\not\!\!E_{\rm T}$) can be produced by missing a real lepton due to inefficiency in the identification procedure for leptons or to limited detector coverage,

- b is a bottom-quark, and c is a charm-quark.

Note that both decay channels have at least one charged lepton in the final state, allowing a single dataset to be formed from an inclusive high-Pt lepton trigger.

In the beginning let us consider the case when we observe events in two final states: $N(l\nu + 4jets)$ and $N(l^+l^- + 4jets)$ by applying some set of selection requirements. We will generalize this approach to any fixed number of final states later and now we will discuss only two for simplicity. Also, we assume that the top quark has only two decay channels:

$$Br(t \to Wb) + Br(t \to Z^0 c) = 1, \tag{2}$$

where below we will be using the following notation:

$$B_Z = Br(t \to Z^0 c). \tag{3}$$

The number of expected $t\bar{t}$ pairs is

$$N_{t\bar{t}} = \sigma(p\bar{p} \to t\bar{t}) \cdot \int Ldt, \tag{4}$$

where $\sigma(p\bar{p} \to t\bar{t})$ can be taken a priori since it does not depend on the FCNC physics at all.

The expected numbers of events in each of the decay modes are estimated in the following way:

$$\begin{aligned} E(l\nu + 4jets) = \quad & Bgr(l\nu + 4jets) + N_{t\bar{t}} \cdot \{ \\ & 2B_Z(1 - B_Z) \cdot (Br(Z^0 \to jj) \cdot Br(W \to l\nu) \cdot (A * \epsilon)_{Z^0 cWb \to l+\nu+4jets} + \\ & Br(Z^0 \to l^+l^-) \cdot Br(W \to jj) \cdot (A * \epsilon)_{Z^0 cWb \to l+\not{E}_T+4jets}) + \\ & 2(1 - B_Z)^2 Br(W \to l\nu) \cdot Br(W \to jj) \cdot (A * \epsilon)_{WbWb \to l+\nu+4jets} + \\ & 2B_Z^2 \cdot Br(Z^0 \to l^+l^-) \cdot Br(Z^0 \to jj) \cdot (A * \epsilon)_{Z^0 cZ^0 c \to l+\not{E}_T+4jets}\} \end{aligned} \tag{5}$$

and

$$\begin{aligned} E(l^+l^- + 4jets) = \quad & Bgr(l^+l^- + 4jets) + N_{t\bar{t}} \cdot \{ \\ & 2B_Z(1 - B_Z) \cdot Br(Z^0 \to l^+l^-) \cdot Br(W \to jj) \cdot (A * \epsilon)_{Z^0 cWb \to l^+l^- + 4jets} + \\ & 2B_Z^2 \cdot Br(Z^0 \to l^+l^-) \cdot Br(Z^0 \to jj) \cdot (A * \epsilon)_{Z^0 cZ^0 c \to l^+l^- + 4jets}\}, \end{aligned} \tag{6}$$

where Bgr(X) are non-top contributions (backgrounds) to a given channel 'X', $(A * \epsilon)_Y$ is acceptance multiplied by efficiency[3] for a decay mode 'Y', and $Br(A \to B)$ is a branching fraction of 'A' decaying to 'B'.

To simplify the formulae we introduce the following notations for constant terms:

$$A_1 = 2Br(Z^0 \to l^+l^-) \cdot Br(Z^0 \to jj) \cdot (A * \epsilon)_{Z^0 cZ^0 c \to l^+l^- + 4jets}, \tag{7}$$

[3] The efficiency includes so called pre-tag and tagging efficiencies.

$$A_2 = 2Br(Z^0 \to l^+l^-) \cdot Br(W \to jj) \cdot (A * \epsilon)_{Z^0cWb \to l^+l^- + 4jets}, \quad (8)$$

$$\begin{aligned} A_3 = \quad & 2Br(Z^0 \to jj) \cdot Br(W \to l\nu) \cdot (A * \epsilon)_{Z^0cWb \to l\nu + 4jets} + \\ & 2Br(Z^0 \to l^+l^-) \cdot Br(W \to jj) \cdot (A * \epsilon)_{Z^0cWb \to l + \not{E}_T + 4jets}, \end{aligned} \quad (9)$$

$$A_4 = 2Br(W \to l\nu) \cdot Br(W \to jj) \cdot (A * \epsilon)_{WbWb \to l\nu + 4jets}, \quad (10)$$

and

$$A_5 = 2Br(Z^0 \to l^+l^-) \cdot Br(Z^0 \to jj) \cdot (A * \epsilon)_{Z^0cZ^0c \to l + \not{E}_T + 4jets}. \quad (11)$$

Then the expected numbers of events can be rewritten in the following way:

$$E(l\nu + 4jets) = Bgr(l\nu + 4jets) + N_{t\bar{t}} \cdot \{A_4 + B_Z \cdot (A_3 - 2A_4) + B_Z^2(A_4 - A_3 + A_5)\} \quad (12)$$

and

$$E(l^+l^- + 4jets) = Bgr(l^+l^- + 4jets) + N_{t\bar{t}} \cdot \{(A_1 - A_2) \cdot B_Z^2 + A_2 \cdot B_Z\}. \quad (13)$$

As you can see, these two are functions of $N_{t\bar{t}}$ and B_Z only.

The probability density (i.e. likelihood) function is

$$\begin{aligned} & P(N(l\nu + 4jets), N(l^+l^- + 4jets)|B_Z, N_{t\bar{t}}) = P(N(l\nu + 4jets)|E(l\nu + 4jets)) \cdot \\ & P(N(l^+l^- + 4jets)|E(l^+l^- + 4jets)), \end{aligned} \quad (14)$$

where

$$P(N|E) = \frac{E^N e^{-E}}{N!} \quad (15)$$

is a regular Poisson distribution. Here we will be using the following notation:

$$L(B_Z, N_{t\bar{t}}) = P(N(l\nu + 4jets), N(l^+l^- + 4jets)|B_Z, N_{t\bar{t}}). \quad (16)$$

We should mention that the likelihood $L(B_Z, N_{t\bar{t}})$ is defined in the physical region of parameters $N_{t\bar{t}} \geq 0$ and $0 \leq B_Z \leq 1$.

We use a standard numerical integration technique to calculate the likelihood function (See [13]). This technique allows us to incorporate systematic uncertainties properly. More details on the calculation procedure can be found in the Section 13.

In this analysis we utilize the discriminating power of the top-mass distribution (M_{top}) for "Z+4jets" events to get a better separation between the SM backgrounds and the FCNC signal. The signal has a distinguishable peak at about 170-175 GeV. Therefore, instead of using a probability function for a single observable $P(N(l^+l^- + 4jets)|E(l^+l^- + 4jets))$ we combine probabilities for each bin of the M_{top} distribution

$$\prod_i P(N_i(l^+l^- + 4jets)|E_i(l^+l^- + 4jets)), \quad (17)$$

where the index i stands for bins of the top-mass distribution. This requires calculating acceptances $A_1 = A_{1,i}$ and $A_2 = A_{2,i}$ for each bin of the M_{top} histogram. We note that

the electron and muon decay modes of the top quarks are treated separately up to this point of the analysis in order to better understand the systematics of both. The two channels are then included together in the final likelihood function $L(B_Z, N_{t\bar{t}})$.

The likelihood function can be used to construct a one-dimensional posterior probability density $P(B_Z|observables)$ or a two-dimensional posterior distribution $P(B_Z, N_{t\bar{t}}|observables)$, where *observables* are $(\mathbf{N}(l\nu + 4jets), \mathbf{N}(l^+l^- + 4jets))$. We use the one-dimensional function to set a limit on the $Br(t \to Z^0c)$, and we use the two-dimensional probability density function to draw "1σ"- and "2σ"- contours in $(B_Z, N_{t\bar{t}})$-space.

The one-dimensional posterior probability $P(B_Z|observables)$ is obtained using a Bayesian approach in the following way:

$$P(observables|B_Z) = \int L(B_Z, N_{t\bar{t}}) \cdot \pi_0(N_{t\bar{t}}) dN_{t\bar{t}} \tag{18}$$

$$P(B_Z|observables) = \frac{P(observables|B_Z) \cdot \pi_1(B_Z)}{\int P(observables|B_Z) \cdot \pi_1(B_Z) dB_Z}, \tag{19}$$

where $\pi_0(N_{t\bar{t}})$ is the a priori probability density function of $N_{t\bar{t}}$ (here we assume that $N_{t\bar{t}}$ and B_Z are physically independent parameters) and $\pi_1(B_Z)$ is the a priori distribution of B_Z which is flat in the physical region (it is 1.0 for $0 \leq B_Z \leq 1$ and zero everywhere else). The distribution of $\pi_0(N_{t\bar{t}})$ represents the knowledge about top pair production cross-section $\sigma(p\bar{p} \to t\bar{t})$, which ideally should be just a δ-function since you there is a fixed number of top pairs produces. In this analysis we consider two choices of $\pi_0(N_{t\bar{t}})$ distribution:

- a flat distribution (which is not very appropriate from a mathematical point of view) that does not contains any information regarding the theoretical predictions of $\sigma(p\bar{p} \to t\bar{t})$ and
- a "Gaussian" distribution derived using the theoretical estimates of top pair production cross-section $\sigma(p\bar{p} \to t\bar{t})$ [14] as a function of top quark mass M_{top}, the measured M_{top} (with its uncertainties) and the uncertainty on the integrated luminosity.

The two-dimensional posterior probability is defined as follows with a Bayesian approach as well:

$$P(B_Z, N_{t\bar{t}}|observables) = \frac{L(B_Z, N_{t\bar{t}}) \cdot \pi_1(B_Z) \cdot \pi_0(N_{t\bar{t}})}{\int dB_Z \int dN_{t\bar{t}} \{L(B_Z, N_{t\bar{t}}) \cdot \pi_1(B_Z) \cdot \pi_0(N_{t\bar{t}})\}}. \tag{20}$$

Drawing the "2σ"-contour (corresponding to 95% C.L.) for $P(B_Z, N_{t\bar{t}}|observables)$ (in the two-dimensional space of $(N_{t\bar{t}}, B_Z)$) requires a closed set of points which has an integral of 0.95 and the boundary points have equal values of probability density. The "1σ"-contour is obtained the same way by taking the integral to be approximately 0.68.

2.1 Tagging Efficiency

The tagging efficiency per event is the probability of identifying at least one Heavy Flavor jet in the event. The existing Monte Carlo simulations require additional corrections to be applied. The corrections scale the MC efficiency to be the same as for the data, *i.e.*, we re-weight every MC event depending on the number of B-tags observed. The scaled MC efficiencies are in good agreement with data in the $P_T(jet)$-range from 20 to 200 GeV. More information on the B-tagging can be found in Section 7.

2.2 Pretag Efficiency

The quantity 'pretag $A \cdot \epsilon$' includes geometrical acceptance, and trigger and identification efficiencies. The acceptance is defined as the fraction of events that satisfy geometrical and kinematic requirements. The identification of leptons and jets are limited by coverage of the calorimeters, muon systems, and tracking systems. The reconstructed leptons and jets are required to pass a minimum E_T requirement, which contributes to the acceptance. In addition we require $\not\!\!E_{\rm T} > 25$ GeV for events with $W \to l\nu$, and the dilepton invariant mass of $Z^0 \to l^+l^-$ is restricted (See 6). We use Monte Carlo samples to estimate the acceptance for each of the processes.

The identification efficiencies are different for events in data and Monte Carlo though they demonstrate a very similar energy dependence. To eliminate this inconsistency we use correction factors (scale factors) to re-weight the MC events. The largest discrepancy is for central muons, being 8%. The scale factors are described in more detail in Section 3.

2.3 Using R as a Precise check of the Pretag Acceptance $A \cdot \epsilon$

To validate the modeling of the lepton ID and acceptances, we use inclusive W and Z events, and calculate the ratio R, where R is defined as:

$$R = \frac{\sigma(W) * Br(W \to l\nu)}{\sigma(Z^0) * Br(Z^0 \to l^+l^-)} \tag{21}$$

$$\sigma(p\bar{p} \to Z + jets) * Br(Z^0 \to l^+l^-) = \frac{N_{obs}(Z^0 \to l^+l^-) - N_{bck}(Z^0 \to l^+l^-)}{(A * \epsilon)_{MC}(Z^0 \to l^+l^-) * \int Ldt} \tag{22}$$

$$\sigma(p\bar{p} \to W + jets) * Br(W \to l\nu) = \frac{N_{obs}(W \to l\nu) - N_{bkg}(W \to l\nu)}{(A * \epsilon)_{MC}(W \to l\nu) * \int Ldt} \tag{23}$$

Therefore,

$$R = \frac{N_{obs}(W \to l\nu) - N_{bkg}(W \to l\nu)}{N_{obs}(Z^0 \to l^+l^-) - N_{bck}(Z^0 \to l^+l^-)} * \frac{(A * \epsilon)_{MC}(Z^0 \to l^+l^-)}{(A * \epsilon)_{MC}(W \to l\nu)} \tag{24}$$

Note that the luminosity does not contribute directly to these equations. The ratio R has been calculated at NNLO by Stirling et al., and is predicted to be 10.67 ± 0.15 [15], providing a precise check of lepton acceptances, efficiencies, and the W- and Z- boson selection criteria both in data and the MC. A check at this level of precision is especially important to validate the reproduction by the Monte Carlo of the many changes in the muon systems, the tracking systems, and other systems over the multiple years of data taking, including the dramatic growth in luminosity in that time.

3 Lepton Identification

We use standard CDF definitions for identification (ID) of electrons and muons. The same lepton ID requirements are applied to data and Monte Carlo events. "Larry's corrections" [16] are applied to the COT tracks. Details of the reconstruction of W- and Z- bosons are listed in Tables 1, 2, and 3.

Variable	Tight	Loose
P_T, GeV	> 20	> 12
E_{EM}, GeV	< 2+max(0,p-100)$*$0.0115	< 2+max(0,p-100)$*$0.0115
E_{HAD}, GeV	< 6+max(0,p-100)$*$0.028	< 6+max(0,p-100)$*$0.028
$isolation/P_T$	< 0.1	< 0.1
#SL with ≥ 5 hits	≥ 3 stereo and axial	≥ 3 axial and ≥ 2 stereo
χ^2_{COT}/DOF	< 3	< 4
$\|Z0\|$, cm	< 60	< 60
ΔX_{CMU}, cm	< 7	
ΔX_{CMP}, cm	< 7[a]	
ΔX_{CMX}, cm	< 6 for run > 150144	
COT exit radius	> 140 cm	
Muon Detector	CMUP or CMX	
Cosmic Filter	On	On
Fiducial Requirements	Yes	

[a] We use a wider cut than the default of 5.0 cm since the MC does not reproduce the distribution of ΔX_{CMP} well enough.

Table 1: Summary of the muon identification cuts (see Ref. [17]).

3.1 Corrections to the Lepton ID Efficiency

We re-weight Monte Carlo events to take into account the difference between the identification efficiencies used for data and simulations. The list of scale factors for each lepton type is presented in Table 4. The correction coefficients have been taken from the CDF Joint Physics web page. In addition to correcting for lepton ID we take into

Variable	Tight	Loose
E_T, GeV	> 20	> 12
Track P_T, GeV	> 10	> 10
Track $Z0$, cm	< 60	< 60
E/P	< 2 or $P_T > 50$ GeV	
charge signed ΔX, cm	< 1.5 and > -3.0	
# of Sl with ≥ 5 hits	≥ 3 axial and ≥ 2 stereo	≥ 3 axial and ≥ 2 stereo
Conversion Filter	On	On
Had/EM	$< 0.055 + 0.00045*E$	$< 0.055 + 0.00045*E$
Lshr	$< .2$	
χ^2_{strip}	< 10	
Calorimeter Iso./E_T	$< .1$	$< .1$
Fiducial Requirements	$X_{CES} < 21.5$ cm and $9 < Z_{CES} < 230$ cm	$X_{CES} < 21.5$ cm and $9 < Z_{CES} < 230$ cm

Table 2: Summary of the central (CEM) electron identification cuts (see Refs. [18] and [19]).

Variable	Cut
Type	Phoenix
E_T, GeV	> 12
$\lvert\eta_{det}\rvert$	$1.2 < \lvert\eta_{det}\rvert < 2.5$
Track type	phoenix
Track $Z0$, cm	< 60
SVX Hits	> 2
Had/EM	< 0.05
χ^2_{tree}	< 10
Frac. Cal. Iso.	$< .1$
PES 5X9 U	> 0.65
PES 5X9 V	> 0.65
PEM fit towers	$\neq 0$

Table 3: Summary of the plug (PEM) electron identification cuts (see Ref. [20]).

account the corresponding trigger inefficiencies. The events are triggered with high-P_T leptons (electrons and muons) so we re-weight every Monte Carlo event which contains less than two leptons satisfying trigger requirements. The trigger efficiency estimates are given in Table 5;

Type	Scale Factor
CEM Tight	$0.983 \pm 0.002(stat.) \pm 0.003(syst.)$
CEM Loose	$1.000 \pm 0.001(stat.) \pm 0.003(syst.)$
PEM	$0.937 \pm 0.003(stat.) \pm 0.003(syst.)$
Tight CMUP Muon	0.9257 ± 0.005
Tight CMX Muon (Arches)	0.9927 ± 0.006
Tight CMX Muon (MS + KS)	0.9159 ± 0.092
Loose (Stubbles) Muon	1.036 ± 0.01

Table 4: A summary of the lepton scale factors. The Monte Carlo efficiencies are *multiplied* by these to match those in the data. See [17, 21].

Trigger	Efficiency
ELECTRON_CENTRAL18	$0.9585(7) * (1 - 89593 * exp(-0.7127 * E_T))$, where E_T is of the trigger electron
MUON_CMUP18	0.917 ± 0.003
MUON_CMX18 (Arches)	0.953 ± 0.003
MUON_CMX18 (MS+KS)	0.759 ± 0.010

Table 5: A summary of the lepton trigger efficiencies. The Monte Carlo events are re-weighted to correct for the trigger inefficiencies. The electron triggering is described in [22]. In case of MUON_CMX18 we actually consider all triggers that start with the syntax "MUON_CMX18".

4 Jet Identification

Jets are reconstructed using the standard CDF cone clustering algorithm with a cone radius of $R = 0.4$ and within $|\eta| < 2.4$. The raw energy of the jets must be greater then 8 GeV and the corrected energy is required to be greater than 15 GeV. Jet energy scale corrections (JES) at Level 5 are applied to every jet [23] by using the JetCorr08 package. Also jets can not coincide with identified electrons or photons (i.e. each calorimeter cluster can be associated with either a jet, an electron, or a photon which have mutually exclusive definitions to avoid any ambiguities).

5 Photon Identification

High-Pt photons are not rare in busy events, and are precisely measured in the electromagnetic calorimeters, without the necessity of large jet corrections. While in principle photons in the Monte Carlo samples are mis-reconstructed on average in the same way as those in the data, individual events with photons can be mis-reconstructed, possibly important in analysis leading to small signal samples, as in this analysis. The identification criteria for photons are given in Table 6. The identified photons are used for

jet identification and calculation of missing transverse energy.

Variable	Cut
Corrected Et, GeV	> 25
CES X and Z Fiducial	Ces $\|X\| < 21$ cm, $9 <$ Ces $\|Z\| < 230$ cm
Had/Em	$< 0.125 \,\|\|\, < 0.055 + 0.00045$ * ECorr
Cone 0.4 IsoEtCorr (new correction- see notes)	EtCorr<20: < 0.1*EtCorr EtCorr>20: $< 2.0+0.02$*(EtCorr-20.0)
Chi2 (Strips+Wires)/2.0	< 20
N track (N3D)	≥ 1
Track Pt	$< 1+0.005$*EtCorr GeV
Cone 0.4 Track Iso	$< 2.0+0.005$*EtCorr
2nd CES cluster E*sin(theta) (both strip and wire E individually)	EtCorr<18: < 0.14*EtCorr EtCorr>18: $< 2.4+0.01$*EtCorr

Table 6: Summary of cuts for Central Photons. See [24].

6 Definitions of W- and Z-bosons

Events with inclusive W- and Z-bosons (W/Z + anything) decaying via the leptonic decay channels are selected using high-P_T electrons and muons: $Z^0 \to ee$, $Z^0 \to \mu\mu$, $W \to e\nu$, and $W \to \mu\nu$.

6.1 Z Boson Selection

To be identified as a Z-boson a pair of opposite-sign electrons or muons must have a reconstructed invariant mass in the mass window from 66 GeV to 116 GeV. The selection of $Z^0 \to ee$ events requires a tight CEM electron (see Table 2) and a "loose CEM" or a PEM electron (see Tables 2 and 3). A tight CEM electron passes all the loose cuts. The $Z^0 \to \mu\mu$ event selection requires a tight and a loose muon (see Table 1). The muons are required to be coming the same vertex ($|Z(\mu_1) - Z(\mu_2)| < 4$ cm).

6.2 Missing E_T Reconstruction

Missing transverse energy ($\not\!\!E_{\rm T}$) is the negative two-dimensional vector sum of $\vec{E}_T$ of all identified objects in the event: electrons (See Section 3), muons (See Section 3), photons (See Section 5), jets (See Section 4), and unclustered energy. The unclustered energy is calculated as raw calorimeter energy (it is a two-dimensional vector) without energies deposited by identified jets, electrons, muons, and photons. Appropriate JES corrections (See [23]) are used for the identified jets when we calculate $\not\!\!E_{\rm T}$.

6.3 W Boson Selection

For W-bosons, the transverse mass ($M_T(W)$) reconstructed from the lepton and the missing transverse energy is required to be greater than 20 GeV. The selection of $W \to e\nu$ events requires a tight central electron and $\not\!\!E_{\rm T}$ greater than 25 GeV. The selection of $W \to \mu\nu$ events requires a tight muon and $\not\!\!E_{\rm T}$ greater than 25 GeV. Also we require each W-event to have only one tight lepton and no loose leptons.

6.4 Kinematic Variables Used in a Comparison between Data and MC

The kinematic structure of the events is studied from the distributions in the following variables:

- H_T (Scalar sum of E_T of all reconstructed objects (electrons, muons, photons, jets, missing transverse energy, and unclustered energy)),
- Missing transverse energy ($\not\!\!E_{\rm T}$) (Negative vector sum of $\vec{E}_T$ of all reconstructed objects (electrons, muons, photons, jets, and unclustered energy)),
- Number of jets,
- Pt(W) or Pt(Z),
- Rapidity (y) of the Z-boson,
- E_T of the leptons,
- Pseudo-rapidity (η) of the leptons (+ and - separately for W's)

7 B-tagging and the Mistag Matrix

We use the loose SecVtx (Secondary Vertex, so called B-tag) tagger to identify decays of bottom and charm quarks (Heavy Flavor). To model the tagged events in data we use data to estimate the mistag rate (number of tags coming from the falsely tagged jets) and MC to get the contribution from heavy flavor jets.

The mistag rate is estimated by applying the mistag matrix parametrization to each event in data (See [25, 26]). The parametrization gives each jet a probability to be falsely tagged. The calculation of the rate is performed in the following steps:

1. We cache all jets with $E_T > 10$ GeV and $|\eta| < 2.4$ that are not identified as electrons or photons (this is important since we have at least one lepton in each event).
2. We apply the mistag matrix to all cached jets.

3. We loop through jets satisfying the selection requirements and find the probability for each jet to be tagged. These probabilities are combined into a probability of the whole event to have at least one B-tag. The probability of a jet to be tagged is obtained using the *my_mistag->mistagRate(i)* method where 'i' is the index of the corresponding jet.

The contribution from real HF jets is estimated by applying the loose SecVtx tagger to Z+HF and W+HF MC samples (see Table 7). Events with at least one B-tag are selected. Each selected event is weighted by $(1-(1-0.95)^{N_{tags}})$, where N_{tags} is the number of B-tagged jets in the event, to take into account the difference in the tagging efficiencies between data and simulation.

Specifically, we exploit the CDF packages BTagObjects (btag_1500invpb_v1) and BTagMods using cdfsoft 6.1.4 (See [25, 26]).

8 Datasets

The data and trigger paths used in this analysis are described in Section 8.1 below. Calculating the SM expectations required extensive Monte Carlo work, described in Section 8.2.

8.1 Data

The observed events are triggered on high-P_T electrons and muons selected by the ELECTRON_CENTRAL_18, MUON_CMUP_18, and MUON_CMX_18 triggers, respectively. We require the SVX detector to be functional by taking events from the silicon Good Run list, V16, defined by the DQM group (the bits are (1,1,1,1)). The electron datasets (bhel0d, bhel0h, and bhel0i) contain 75466634 events and correspond to an integrated luminosity of 1.52 fb^{-1} . The muon datasets (bhmu0d, bhmu0h, and bhmu0i) have 21251395 events and correspond to a luminosity of 1.52 fb^{-1} . We use the partial runs included in the good run list. The luminosity comes from LUMI_INTEGRAL_OFFLINE entry in the database, multiplied by the correction factor of 1.019.

8.2 Standard Model Monte Carlo

The Standard Model expectations are calculated from Monte Carlo. The processes and datasets are shown in Table 7.

The Z + light jets datasets are produced using Pythia v6.216 with a $M(\gamma^*/Z) >$ 30 GeV cut, Tune A, and the 'Willis Sakumoto' corrections applied. The Z + HF samples are produced with ALPGEN v2.10-prime (which has built-in MLM matching) and showered with PYTHIA v 6.325.

The MC contributions from the various SM processes are combined into inclusive samples (i.e. describing any number of partons/hadrons) using weights proportional to

the cross-sections of each contribution. These summed MC-samples are then compared to the observed events in the electron and muon decay modes of W- and Z-bosons separately.

The MC samples were processed with the CDF "realistic" simulation (i.e. events were assigned real run numbers proportionally to the luminosities of the runs. This is intended to help model the operation of the SVX detector more precisely.).

The MC samples are studied with the same analysis code and selection criteria as the data but there is a difference. The Monte Carlo events are weighted to take into account differences in lepton ID efficiencies, triggering, and B-tagging. The appropriate scale factors are listed in Section 3.

Table 7: The Monte Carlo samples used for the SM backgrounds in this search. "K" stands for a scale factor which is used to reflect the difference between LO and NLO calculations.

Process	Dataset	Generator	σ (pb) / Comment
$W \to e\nu$ + jets	wtop1i	Pythia	2687
$W \to \mu\nu$ + jets	wewk8m	Pythia	2687
$W \to \tau\nu$ + jets	wewkat	Pythia	2687
WW	wtop1w	Pythia	13.25
WZ	wtop1z	Pythia	3.96
ZZ	ztopcz	Pythia	1.39
$Z^0 \to ee$ + jets	ztop7i	Pythia	251.3
$Z^0 \to ee$ + jets	ztopbi	Pythia	251.3
$Z^0 \to \mu\mu$ + jets	zewk9m	Pythia	251.3
$Z \to \tau\tau$ + jets	ztop4i	Pythia	251.3
$t\bar{t} \to WbWb$	ttop75	Pythia	7.6
$W^+ + b\bar{b}$ + 0p, $W \to e\nu$	btop0w	Alpgen + Pythia	2.98
$W^+ + b\bar{b}$ + 1p, $W \to e\nu$	btop1w	Alpgen + Pythia	0.888
$W^+ + b\bar{b}$ + 2p, $W \to e\nu$	btop2w	Alpgen + Pythia	0.287
$W^+ + b\bar{b}$ + 0p, $W \to \mu\nu$	btop5w	Alpgen + Pythia	2.98
$W^+ + b\bar{b}$ + 1p, $W \to \mu\nu$	btop6w	Alpgen + Pythia	0.889
$W^+ + b\bar{b}$ + 2p, $W \to \mu\nu$	btop7w	Alpgen + Pythia	0.286
$W^+ + c\bar{c}$ + 0p, $W \to e\nu$	ctop0w	Alpgen + Pythia	5.00
$W^+ + c\bar{c}$ + 1p, $W \to e\nu$	ctop1w	Alpgen + Pythia	1.79
$W^+ + c\bar{c}$ + 2p, $W \to e\nu$	ctop2w	Alpgen + Pythia	0.628
$W^+ + c\bar{c}$ + 0p, $W \to \mu\nu$	ctop5w	Alpgen + Pythia	5.00
$W^+ + c\bar{c}$ + 1p, $W \to \mu\nu$	ctop6w	Alpgen + Pythia	1.79
$W^+ + c\bar{c}$ + 2p, $W \to \mu\nu$	ctop7w	Alpgen + Pythia	0.628
W^+ + c + 0p, $W \to e\nu$	stopw0	Alpgen + Pythia	17.1
W^+ + c + 1p, $W \to e\nu$	stopw1	Alpgen + Pythia	3.39

Continued on the next page

Process	Dataset	Generator	σ (pb) / Comment
W^+ + c + 2p, $W \to e\nu$	stopw2	Alpgen + Pythia	0.507
W^+ + c + 3p, $W \to e\nu$	stopw3	Alpgen + Pythia	0.083
W^+ + c + 0p, $W \to \mu\nu$	stopw5	Alpgen + Pythia	17.1
W^+ + c + 1p, $W \to \mu\nu$	stopw6	Alpgen + Pythia	3.39
W^+ + c + 2p, $W \to \mu\nu$	stopw7	Alpgen + Pythia	0.507
W^+ + c + 3p, $W \to \mu\nu$	stopw8	Alpgen + Pythia	0.083
Z + $b\bar{b}$ + 0p, $Z^0 \to ee$	ztopb0	Alpgen + Pythia	0.511
Z + $b\bar{b}$ + 1p, $Z^0 \to ee$	ztopb1	Alpgen + Pythia	0.134
Z + $b\bar{b}$ + 2p, $Z^0 \to ee$	ztopb2	Alpgen + Pythia	0.0385
Z + $b\bar{b}$ + 0p, $Z^0 \to \mu\mu$	ztopb5	Alpgen + Pythia	0.511
Z + $b\bar{b}$ + 1p, $Z^0 \to \mu\mu$	ztopb6	Alpgen + Pythia	0.134
Z + $b\bar{b}$ + 2p, $Z^0 \to \mu\mu$	ztopb7	Alpgen + Pythia	0.0385
Z + $c\bar{c}$ + 0p, $Z^0 \to ee$	ztopc0	Alpgen + Pythia	1.08
Z + $c\bar{c}$ + 1p, $Z^0 \to ee$	ztopc1	Alpgen + Pythia	0.331
Z + $c\bar{c}$ + 2p, $Z^0 \to ee$	ztopc2	Alpgen + Pythia	0.107
Z + $c\bar{c}$ + 0p, $Z^0 \to \mu\mu$	ztopc5	Alpgen + Pythia	1.08
Z + $c\bar{c}$ + 1p, $Z^0 \to \mu\mu$	ztopc6	Alpgen + Pythia	0.332
Z + $c\bar{c}$ + 2p, $Z^0 \to \mu\mu$	ztopc7	Alpgen + Pythia	0.107
$Z^0 \to \mu\mu$+ 0p	ztopp5	Alpgen + Pythia	K*158
$Z^0 \to \mu\mu$+ 1p	ztopp6	Alpgen + Pythia	K*21.6
$Z^0 \to \mu\mu$+ 2p	ztopzt	Alpgen + Pythia	K*3.46
$Z^0 \to \mu\mu$+ 3p	ztop8p	Alpgen + Pythia	K*0.548
$Z^0 \to \mu\mu$+ 4p	ztop9p	Alpgen + Pythia	K*0.0992
$t\bar{t} \to ZcWb$	texo0w	Madgraph + Pythia	2.5M events
$t\bar{t} \to ZcZc$	texo0z	Madgraph + Pythia	2.5M events

8.3 FCNC Modeling

We use a modified version of the MadGraph Monte Carlo event generator[4] (See [27]) to produce tree-level diagrams for the $t\bar{t} \to ZcWb$ and $t\bar{t} \to ZcZc$ processes, which are then hadronized using Pythia. The generated datasets are listed in Table 7.

We note that the helicity structure of a possible $t \to Z^0c$ vertex is not known, although there are strong limits on left-handed couplings from precision tests of the SM assuming unitarity of the CKM matrix, and the right-handed couplings have only weak limits [28]. We cover the full range of possible helicities so as to be assumption-independent.

All kinematic properties of $t \to Z^0c \to l^+l^-c$ and $t \to Wb \to l\nu b$ decays are encoded in the angular distributions of the decay products. All the distributions can be described by introducing an angle θ^* which is taken in the rest frame of the Z-boson

[4]We are grateful to Michel Herquet for explaining to us how to make these changes and then installing the model in MadGraph.

between the direction of the top-quark and a fermion of the same charge as the top-quark. For example, the angular distribution of θ^* has the following form for the decay of $t \to Wb \to l\nu b$:

$$f(\theta^*) = a_0 \cdot f_0(\theta^*) + a_1 \cdot f_1(\theta^*) + a_2 \cdot f_2(\theta^*), \tag{25}$$

where a_0, a_1, and a_2 are constants whose sum is one ($a_0+a_1+a_2 = 1$), and the functions $f_i(\theta^*)$ are given by:

$$f_0(\theta^*) = \frac{3}{4}(1 - \cos^2(\theta^*)), \tag{26}$$

$$f_1(\theta^*) = \frac{3}{8}(1 + \cos(\theta^*))^2, \tag{27}$$

and

$$f_2(\theta^*) = \frac{3}{8}(1 - \cos(\theta^*))^2. \tag{28}$$

The angular distribution of the decay products of $t \to Wb \to l\nu c$ are parametrized taking appropriate values of the a_i. The coefficients a_0, a_1, and a_2 are the fractions of longitudinal, left-handed, and right-handed helicities of the W-boson, respectively.

The FCNC decay of the top are different from thoses in the SM since the W is coupled only to left-handed fermions but Z is coupled to both right-handed and left-handed. Decays of longitudinally polarized Z's are described with the same function $f_0(\theta^*)$ as that for W's, but decays of the left-handed and right-handed Z's have different angular distributions:

$$f_1(\theta^*) \simeq 0.21 \cdot (1 + \cos\theta^*)^2 + 0.16 \cdot (1 - \cos\theta^*)^2 \tag{29}$$

and

$$f_2(\theta^*) \simeq 0.21 \cdot (1 - \cos\theta^*)^2 + 0.16 \cdot (1 + \cos\theta^*)^2, \tag{30}$$

where $0.21 + 0.16 \simeq 3/8$ and

$$0.21 \simeq \frac{3}{8}\frac{\Gamma(Z^0 \to f_L\bar{f}_R)}{\Gamma(Z^0 \to f_L\bar{f}_R) + \Gamma(Z^0 \to f_R\bar{f}_L)}. \tag{31}$$

As an example we draw a distribution of $\cos(\theta^*)$ for $t \to Zc$ where 65% (this is the fraction of longitudinally polarized W's in $t \to Wb$ decay) of the Z-bosons are longitudinally polarized. The distribution is shown in Figure 1.

We have mentioned that Z's couple to left-handed and right-handed fermions when W's couple only to left-handed fermions. This alters the functional form of $f_1(\theta^*)$ and $f_2(\theta^*)$ in the following way:

$$f_1(\theta^*) = \frac{3}{8}\left(\frac{\Gamma(Z^0 \to f_L\bar{f}_R) \cdot (1 + \cos\theta^*)^2}{\Gamma(Z^0 \to f_L\bar{f}_R) + \Gamma(Z^0 \to f_R\bar{f}_L)} + \frac{\Gamma(Z^0 \to f_L\bar{f}_R) \cdot (1 - \cos\theta^*)^2}{\Gamma(Z^0 \to f_L\bar{f}_R) + \Gamma(Z^0 \to f_R\bar{f}_L)}\right) \tag{32}$$

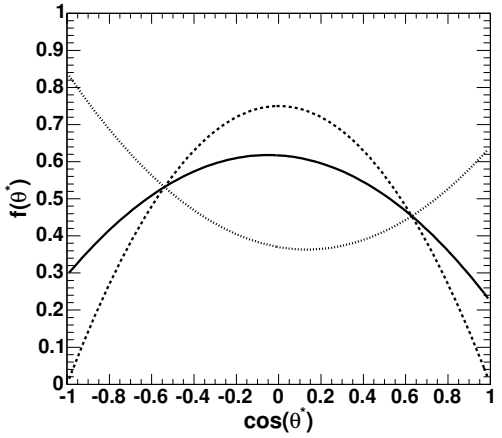

Figure 1: The distributions of $\cos(\theta^*)$ for three fractions of longitudinally polarized Z-bosons: 65% (solid line), 100% (dashed line), and 0% (dotted line). The left-right asymmetry is much smaller than that of $t \to Wb$ decay.

and

$$f_2(\theta^*) = \frac{3}{8}\left(\frac{\Gamma(Z^0 \to f_L\bar{f}_R)\cdot(1-\cos\theta^*)^2}{\Gamma(Z^0 \to f_L\bar{f}_R)+\Gamma(Z^0 \to f_R\bar{f}_L)} + \frac{\Gamma(Z^0 \to f_L\bar{f}_R)\cdot(1+\cos\theta^*)^2}{\Gamma(Z^0 \to f_L\bar{f}_R)+\Gamma(Z^0 \to f_R\bar{f}_L)}\right), \tag{33}$$

where f_L stands for left-handed fermions and f_R - right handed ones. The ratio of the decay widths can be obtain at tree level from the SM Lagrangian of the Z-currents:

$$\frac{\Gamma(Z^0 \to f_L\bar{f}_R)}{\Gamma(Z^0 \to f_R\bar{f}_L)} = \frac{(0.5-|Q_f|\sin^2\theta_W)^2}{(|Q_f|\sin^2\theta_W)^2}. \tag{34}$$

A distribution of $\cos(\theta^*)$ resulting from any possible FCNC coupling can always be described by choosing appropriate values for the constants a_i. Also we note that the acceptances of the FCNC top quark decays A_i depend solely on the angular distributions of its decay products. This lead us to a conclusion that the acceptances are functions of a_0 and a_1 (i.e. $A_i = A_i(a_0, a_1)$). The other important fact is that Z-bosons decay to $l\bar{l}$ or $q\bar{q}$ so that the top quark decay is symmetric with respect to the charge of the fermion and therefore acceptances of fully right-handed and fully left-handed decays are identical. This means that the acceptances A_i depend only on the fraction of longitudinally polarized Z's (i.e. $A_i = A_i(a_0, 1-a_0) = A_i(a_0)$).

Unfortunately the FCNC Monte-Carlo samples (texo0z and texo0w) have a problem. The problem is that helicities of the W- and Z-bosons were not used by Pythia properly. However, the distributions of $\cos(\theta^*)$ can be and have been corrected manually by re-weighting events.

We compute each acceptance A_i for a few helicity structures in order to estimate the dependence of the acceptances $A_i = A_i(a_0)$. The acceptance A_4 is a constant term since it does not have any FCNC vertexes. The other acceptances A_1, A_2, and A_3

have linear or quadratic dependence on the fraction of the longitudinal helicity of the Z-bosons:

$$A_1(a_0) = a_0^2 \cdot A_1^{longitudinal} + 2 \cdot a_0 \cdot (1 - a_0) \cdot A_1^{corr} + (1 - a_0)^2 \cdot A_1^{left}, \quad (35)$$

$$A_2(a_0) = a_0 \cdot A_2^{longitudinal} + (1 - a_0) \cdot A_2^{left}, \quad (36)$$

$$A_3(a_0) = a_0 \cdot A_3^{longitudinal} + (1 - a_0) \cdot A_3^{left}, \quad (37)$$

and

$$A_5(a_0) = a_0^2 \cdot A_5^{longitudinal} + 2 \cdot a_0 \cdot (1 - a_0) \cdot A_5^{corr} + (1 - a_0)^2 \cdot A_5^{left}, \quad (38)$$

where $A_i^{longitudinal}$ is the acceptance of the longitudinally-polarized component of the Z-decays and A_i^{left} is the acceptance of the left-handed component. The acceptance A_1 depends quadratically on a_0 since it accounts for two FCNC decays of the top and anti-top quarks. The exact values of the acceptances are listed later in the paper (See 10 and 11).

The coefficients $A_i^{longitudinal}$, A_i^{left}, and A_i^{corr} are calculated using measured acceptances $A_i(a_0)$ in the following way:

$$A_i^{longitudinal} = A_i(1.0), \quad (39)$$

$$A_i^{left} = A_i(0.0), \quad (40)$$

and

$$A_i^{corr} = \frac{4A_i(0.5) - A_i(1.0) - A_i(0.0)}{2}. \quad (41)$$

The acceptances $A_i(a_0)$ are obtained for a sef of values of a_0 by reweighting events in the corresponding Monte Carlo sammples. The MC samples are reweighted in order to correct the angular distributions of θ^* of the FCNC decays.

9 Production of W's and Z's as a Control Region

9.1 Inclusive W Production

Production of W and Z gauge bosons is a very sensitive tool to check the cross-sections, lepton ID efficiencies, and trigger efficiencies. Also it provides a valuable validation of energy scales and detector coverage of the MC samples.

Production of W-bosons observed via their leptonic decays is sensitive to the corresponding high-Pt leptonic triggers since each reconstructed event usually contains only one tight lepton. Z-bosons, however, have two leptons, and thus are much less sensitive to trigger inefficiencies.

The contributions from the Standard Model processes in the histograms below are absolutely normalized. We have taken into account every significant irreducible SM process which contains an isolated lepton and large missing energy.

The non-W contribution is estimated with data by using events with low $\not\!\!E_T$ and fitting the $\not\!\!E_T$-distribution with an anti-selected-electron (or just anti-electron) component and the MC components mentioned earlier. The exact procedure is discussed later in Section 9.3.3.

Later on we are going to use the measured acceptance and numbers of observed $W \to l\nu$ events to calculate the R-ratio (See Equation 24).

Figure 2 shows the measured and expected distributions in transverse mass for the $W \to e\nu$ and $W \to \mu\nu$ selection criteria of Section 6. All the other histograms include only events where $M_T > 20$ GeV. The distributions in transverse momentum of the W boson are shown in Figure 3. The discrepancy at large p_T in the electron sample seems to be a feature of the wtopli sample, but has negligible effect on this analysis.

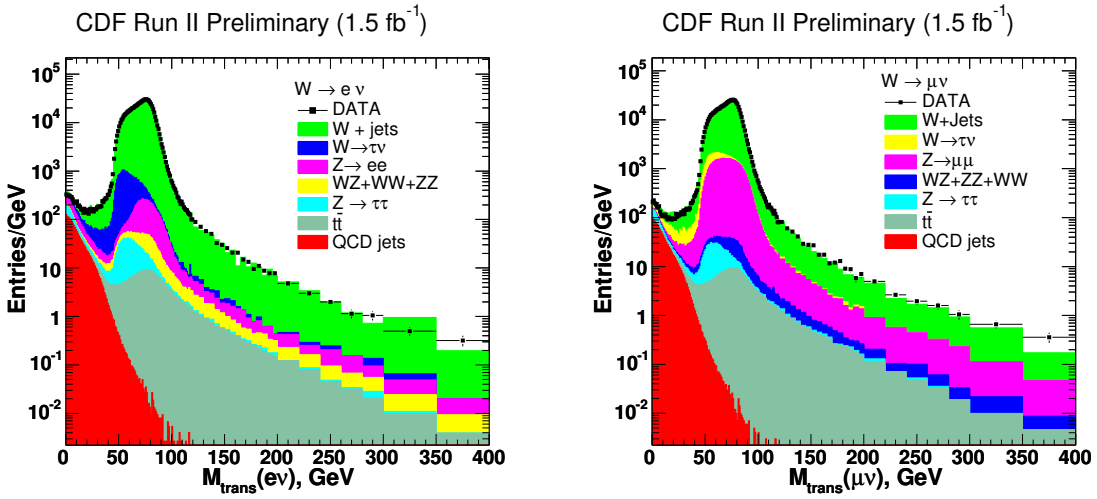

Figure 2: The observed (points) and expected ("stacked" histogram) distributions in transverse mass for $W \to e\nu$ (left) and $W \to \mu\nu$ (right).

Process	Generated	Reconstructed	$A * \epsilon$
$W \to e\nu$	1304237	250722	0.1922
$W \to \mu\nu$	5571556	833985	0.1497

Table 8: A summary of the acceptance times efficiency for inclusive W production measured from the Monte Carlo samples.

The agreement in all the distributions for the W-bosons is quite good.

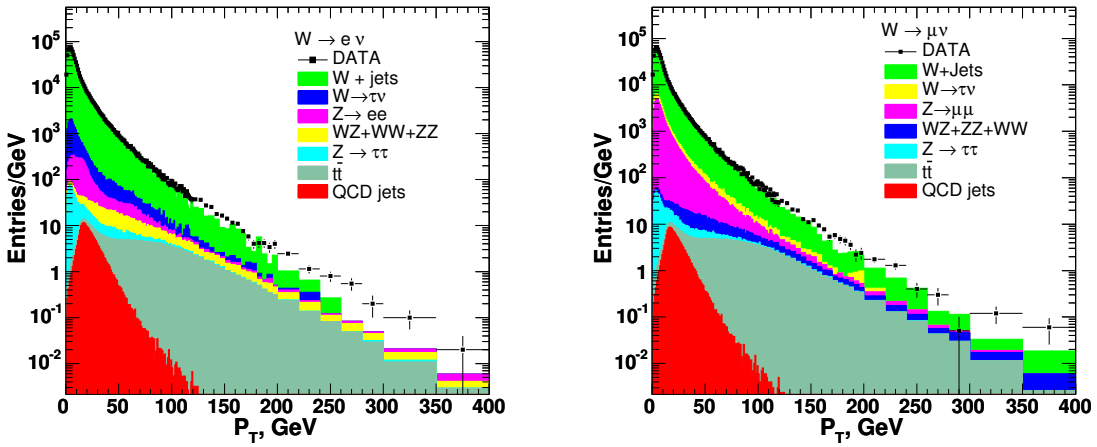

Figure 3: The observed (points) and expected (stacked histogram) distributions in the transverse momentum of the W boson for $W \to e\nu$ (left) and $W \to \mu\nu$ (right) with $M_T > 20$ GeV. (The discrepancy at large p_T in the electron sample seems to be a feature of the wtopli sample, but has negligible effect on this analysis.)

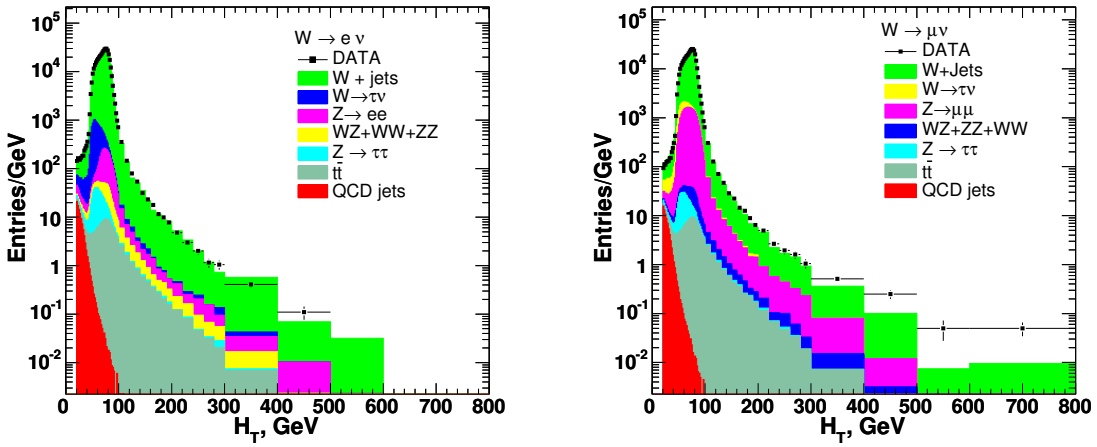

Figure 4: The observed (points) and expected (stacked histogram) distributions in H_T for $W \to e\nu$ (left) and $W \to \mu\nu$ (right) with $M_T > 20$ GeV. The discrepancy at large H_T in the wewk8m muon sample does not appear in the analogous plot for $Z^0 \to \mu\mu$, and so has no effect on this analysis (we show it for others to beware of).

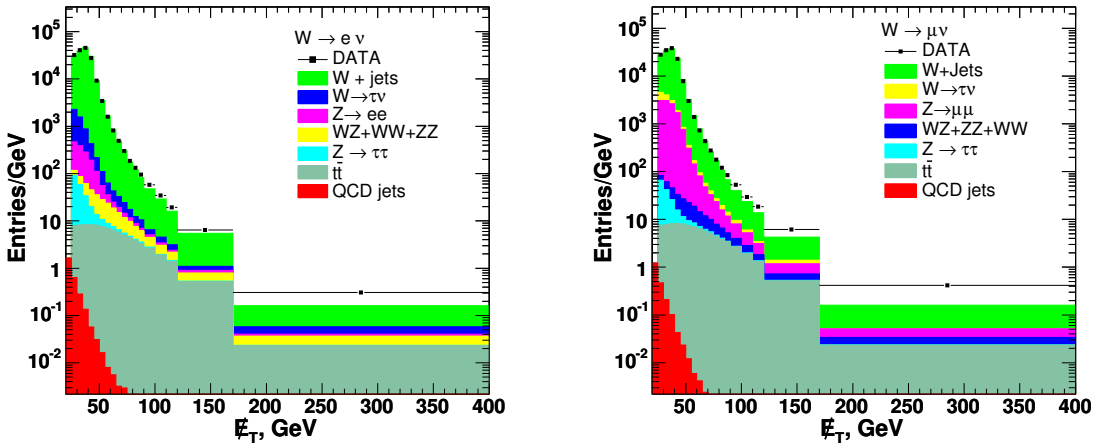

Figure 5: The observed (points) and expected (stacked histogram) distributions in $\not\!\!E_T$ for $W \to e\nu$ (left) and $W \to \mu\nu$ (right). We select only events with $M_T > 20$ GeV to make the distribution.

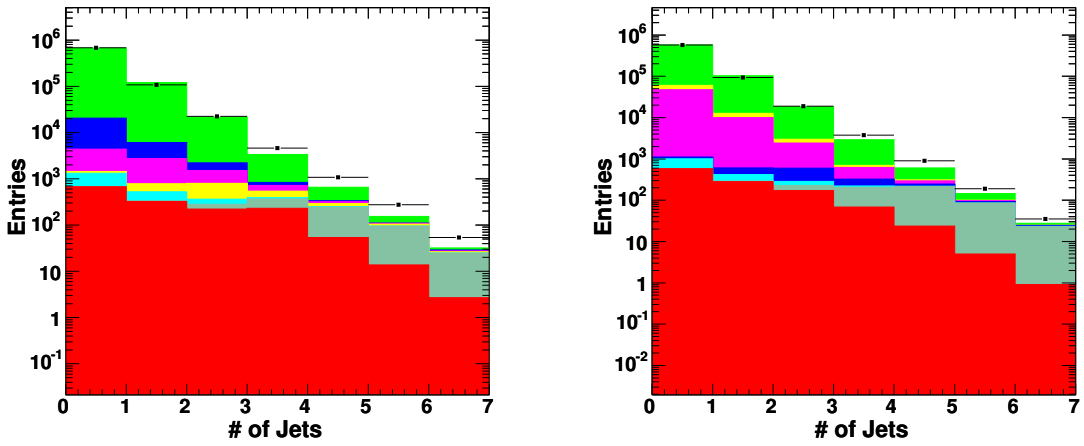

Figure 6: The observed (points) and expected (stacked histogram) distributions in the number of jets, N_{jets}, for $W \to e\nu$ (left) and $W \to \mu\nu$ (right) with $M_T > 20$ GeV.

Process	Observed	Expected "W+jets"	Background Fraction
$W \to e\nu$	814746	786005	3.5%
$W \to \mu\nu$	694651	618226	11%

Table 9: A summary of the numbers of "W+jets" events observed in the data compared to the Monte Carlo expectations. The Background Fraction corresponds to events which are not "W+jets" events where the W-boson is decaying to a lepton of a proper flavor.

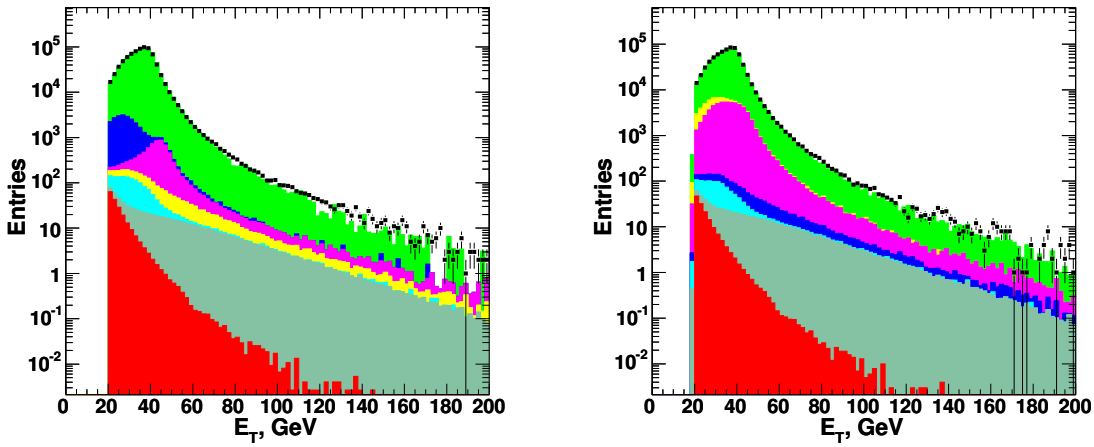

Figure 7: The observed (points) and expected (stacked histogram) distributions in the P_T of the lepton for $W \to e\nu$ (left) and $W \to \mu\nu$ (right) with $M_T > 20$ GeV.

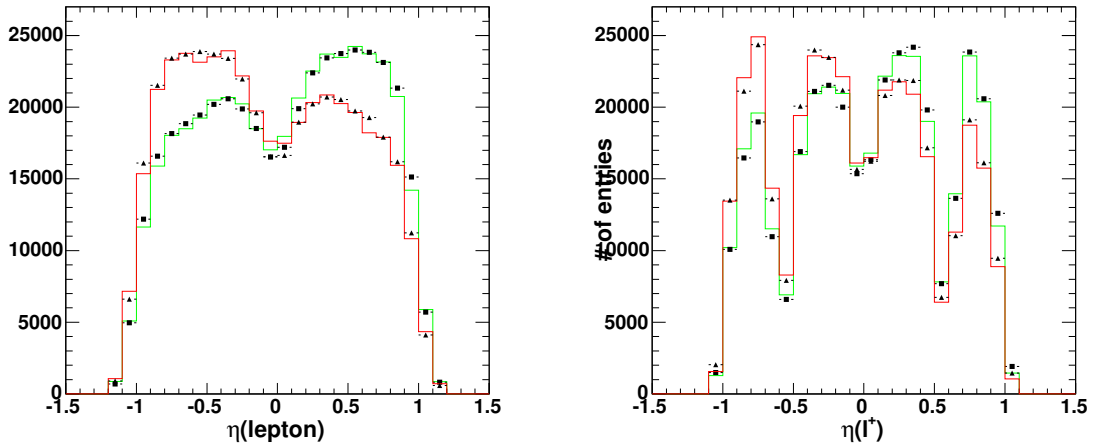

Figure 8: A further check of the lepton and $\not\!\!E_{\rm T}$ modeling of the MC: The observed (points) and expected distributions in the η of the lepton for $W \to e\nu$ (left) and $W \to \mu\nu$ (right). Positive-charge leptons are shown by squares (data) and the green histogram (MC); negative-charge by triangles (data) and the red histogram (MC).

9.2 Inclusive Z Production

The detection of Z-bosons is not very sensitive to the lepton trigger efficiencies since there are at least two leptons in each event. However, Z-bosons are a good way to check lepton ID efficiencies and energy scales of the leptons and jets. To make a detailed study of the physical quantities we perform the following comparisons of the observed and expected distributions (See Figures 9, 10, 11, 12, 13, 14, 15, and 16) and we see excellent agreement everywhere.

Each of the contributions from Standard Model processes is normalized absolutely. We take into account all significant irreducible processes which contain two isolated leptons of the same flavor and opposite charge. The number of events with fake (misidentified) Z-bosons is negligibly small and considered only for the $Z^0 \rightarrow ee$ events (See Section 9.3.1).

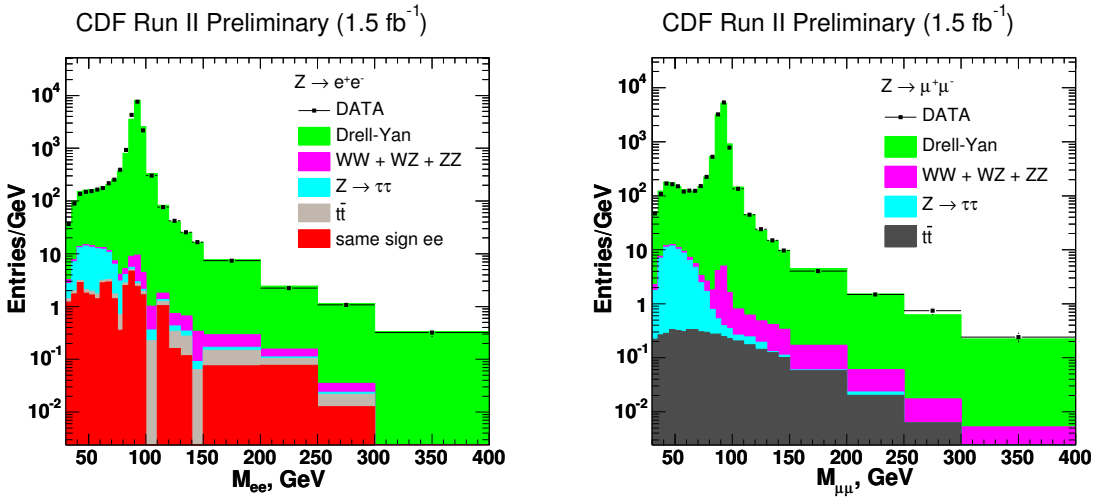

Figure 9: The observed (points) and expected (stacked histogram) distributions in the invariant mass for $Z^0 \rightarrow ee$ (left) and $Z^0 \rightarrow \mu\mu$ (right).

Process	Generated	Reconstructed	$A * \epsilon$
$Z^0 \rightarrow ee$	4043452	859332	0.2125
$Z^0 \rightarrow \mu\mu$	3465140	467415	0.1349

Table 10: A summary of the acceptance times efficiency for inclusive Z production measured from the Monte Carlo samples.

9.3 Backgrounds from Fake W- and Z-bosons

The background compositions of the jet multiplicity distributions in Figures 6 and 13 are presented in Tables 24, 26, 28, and 30. The relative fractions of the backgrounds are also calculated (see Tables 25, 27, 29, and 31).

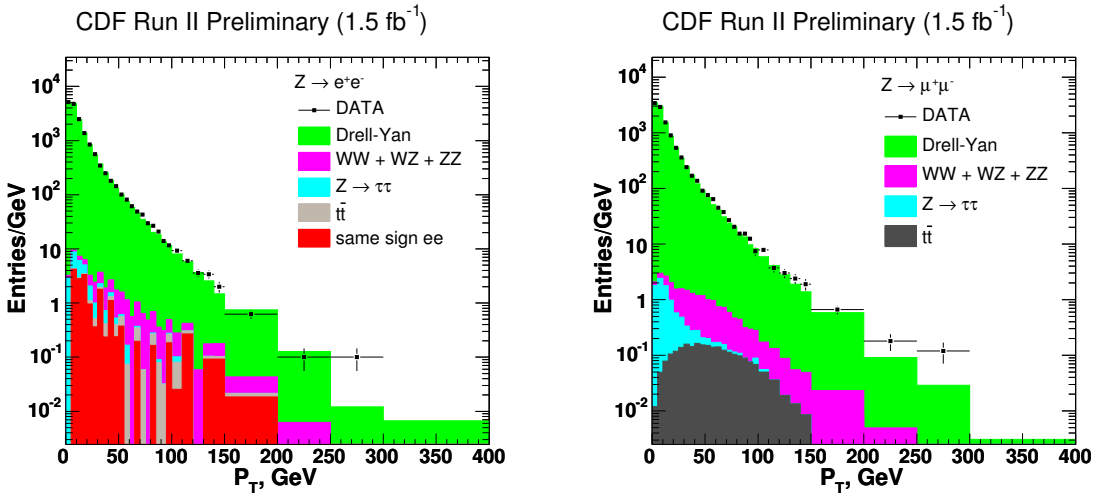

Figure 10: The observed (points) and expected (stacked histogram) distributions in transverse mass for $Z^0 \to ee$ (left) and $Z^0 \to \mu\mu$ (right). We select events with $66 < M(l^+l^-) < 116$ GeV for the histograms.

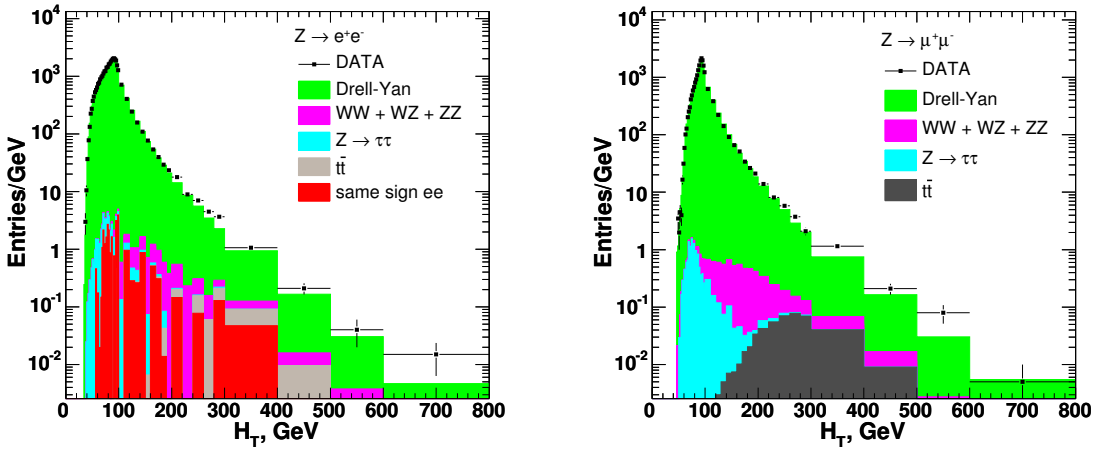

Figure 11: The observed (points) and expected (stacked histogram) distributions in H_T for $Z^0 \to ee$ (left) and $Z^0 \to \mu\mu$ (right). We select events with $66 < M(l^+l^-) < 116$ GeV for the histograms.

Process	Observed	Expected "Z+jets"	Background Fraction
$Z^0 \to ee$	82901	82641	0.4%
$Z^0 \to \mu\mu$	53368	53237	0.25%

Table 11: A comparison of the numbers of observed "Z+jets" events versus expectations.

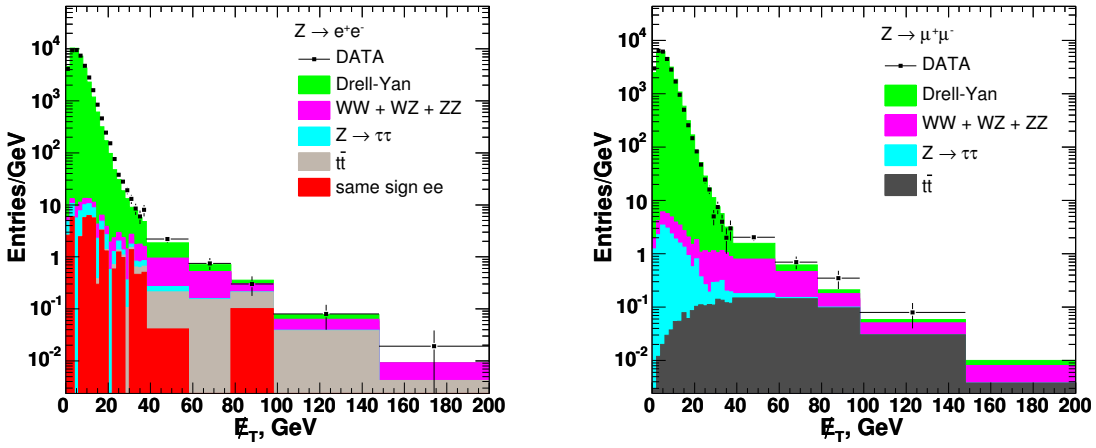

Figure 12: The observed (points) and expected (stacked histogram) distributions in $\not\!\!E_{\rm T}$ for $Z^0 \to ee$ (left) and $Z^0 \to \mu\mu$ (right). We select events with $66 < M(l^+l^-) < 116$ GeV for the histograms.

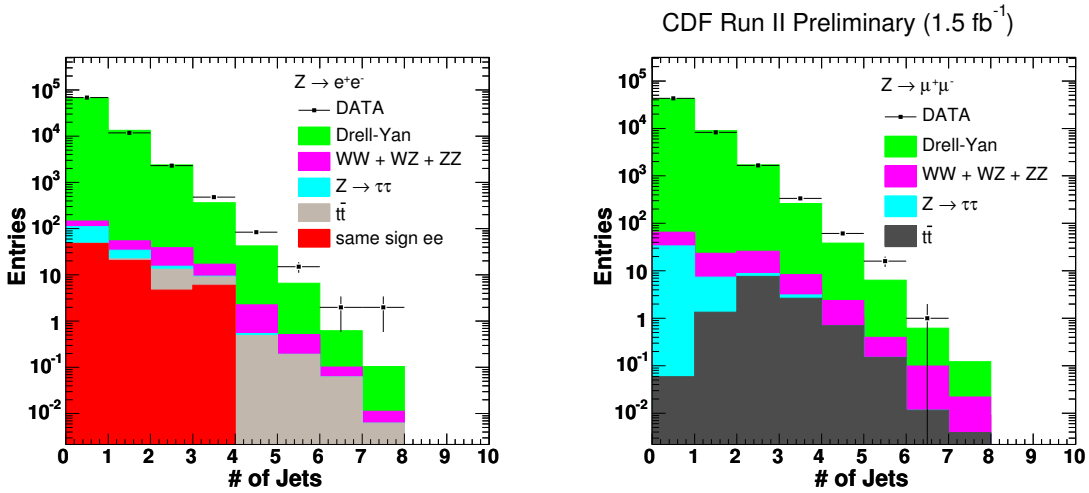

Figure 13: The observed (points) and expected (stacked histogram) distributions in the number of jets, N_{jets}, for $Z^0 \to ee$ (left) and $Z^0 \to \mu\mu$ (right). We select events with $66 < M(l^+l^-) < 116$ GeV for the histograms.

9.3.1 Fake Z Background from Hadron Jets

This background consists of events in which one or more leptons are "fake", i.e. jets misidentified as leptons. We expect that in our samples the two fake leptons, or, more often, one real lepton and one fake lepton, making up the Z in the background events

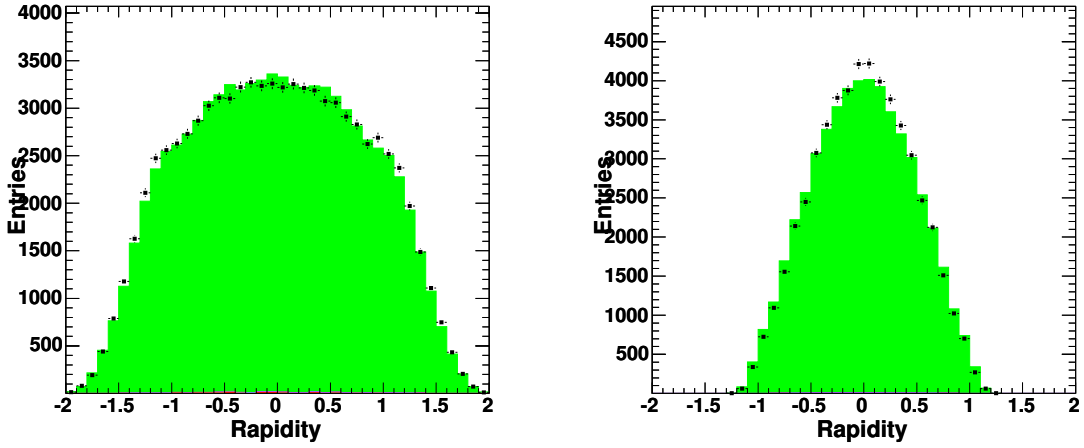

Figure 14: The observed (points) and expected (stacked histogram) distributions in the rapidity of the Z-bosons for $Z^0 \to ee$ (left) and $Z^0 \to \mu\mu$ (right). We select events with $66 < M(l^+l^-) < 116$ GeV for the histograms.

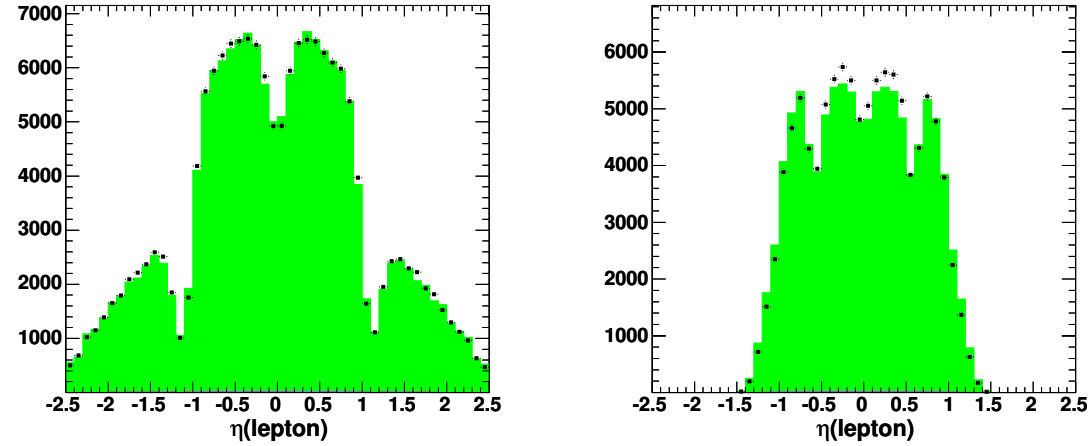

Figure 15: The observed (points) and expected distributions in the η of the lepton for $Z^0 \to ee$ (left) and $Z^0 \to \mu\mu$ (right).

have no charge correlation [5]. This assumption means that the number of same-sign and opposite-sign pairs in Z+multi-jet events are about equal. As the number of fake Z's is small, we use the number of same sign lepton pairs to estimate the hadron jet background in the $\gamma^*/Z^0 \to l^+l^-$ sample.

The $Z^0 \to \mu\mu$ sample (66 GeV $< M_{inv}(ll) <$ 116 GeV) contains only 8 events with muons of the same sign. We consider the background to be negligibly small in

[5]There is a small ($\sim$ 10%) charge correlation in W+1jet with the jet faking a lepton- this background is small here.

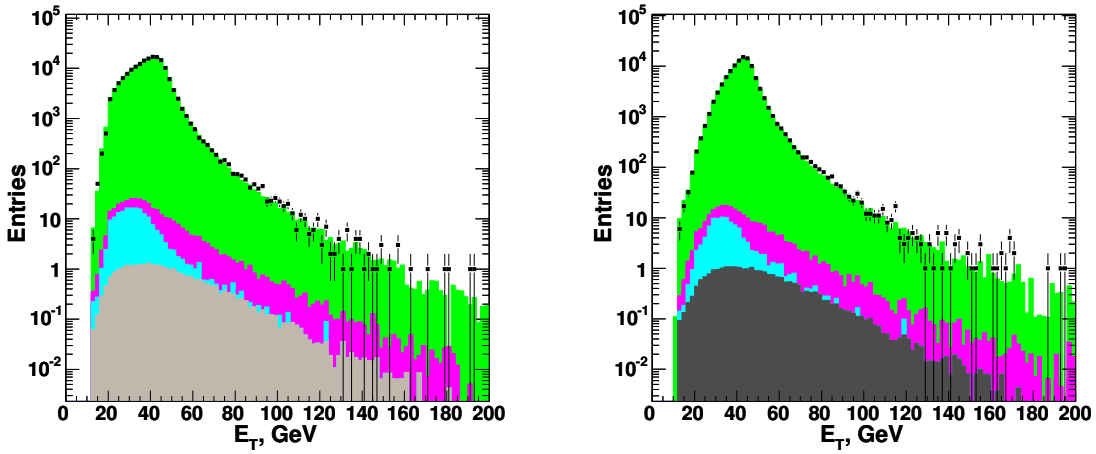

Figure 16: The observed (points) and expected (stacked histogram) distributions in the P_T of the lepton for $Z^0 \to ee$ (left) and $Z^0 \to \mu\mu$ (right).

the muon channel.

The number of same-sign electron pairs in the $Z^0 \to ee$ sample is corrected for the number of real e^+e^- pairs mis-reconstructed as e^+e^+ or e^-e^- using the MC predictions for $Z^0 \to ee$ production.

We observe 398 same-sign electron pairs and 82901 e^+e^- pairs. We remove the contribution of real $\gamma^*/Z^0 \to e^+e^-$ events from the number of observed events by subtracting the number of observed e^+e^- events scaled by the fraction of same-sign to opposite-sign events in the Monte-Carlo samples for $Z^0 \to ee$. The remaining number of same-sign electron pairs is used to estimate the hadron jet background in the $Z^0 \to ee$ sample (see Fig. 9).

9.3.2 Electroweak Backgrounds

Several electroweak processes mimic $\gamma^*/Z^0 \to l^+l^-$ and $W \to l\nu$ production. The processes are $Z^0 \to \tau^+\tau^-$, W^+W^-, WZ, ZZ, $W \to \tau\nu$, and $t\bar{t}$ production. Their contributions to W- and Z-boson production are estimated from the corresponding MC-simulated samples.

9.3.3 Fake W backgrounds from Hadron jets

The ubiquitous QCD processes produce events which mimic leptonic decays of the W-boson's by faking a tight isolated lepton and large missing energy ($\not\!\!E_{\rm T}$). To make a precise estimate of the non-W background coming from hadron jets we follow the procedure described in [29]. This approach provides a better kinematic modeling of the background sample in many variables (observables) than the traditional "$\not\!\!E_{\rm T}$ vs. Iso" technique.

The number of fake W bosons is estimated by fitting the $\not\!\!E_T$-distributions for electron and muon modes separately. The fits are performed for the $\not\!\!E_T$-distributions from 0 to 60 GeV of events that contain only one tight lepton with the transverse mass of the lepton and $\not\!\!E_T$ above 20 GeV. The fits are also performed separately for events with 0, 1, 2, 3, and $\geq$4 jets. The fraction of the non-W events in each bin of the jet multiplicity is estimated by propagating the "anti-selected-electron" events mimicking the background into the region with $\not\!\!E_T > 25$ GeV.

The estimated fractions of the non-W events coming from jets are summarized in Table 12. The fractions are given for each category of the jet multiplicity for events with $\not\!\!E_T > 25$ GeV and $M_T(l + \not\!\!E_T) > 20$ GeV. The fitted distributions are shown in Figures 17 and 18.

Jet Multiplicity	0 jets	1 jet	2 jets	3 jets	$\geq$4 jets
$W \rightarrow e\nu$ + jets	0.6%	1.9%	7%	14%	20%
$W \rightarrow \mu\nu$ + jets	0.1%	0.3%	0.9%	1.8%	2.6%

Table 12: Fractions of the non-W QCD events in events with $\not\!\!E_T$ >25 GeV and $M_{TRANS}(l + \not\!\!E_T) > 20$ GeV.

We put a systematic uncertainty of 26% on the fractions of events with the fake W-bosons (see Table 12) as suggested in [29]. The systematic uncertainty comes from how well the anti-electron sample models the $\not\!\!E_T$ distribution of the fake electrons in data and the Monte Carlo modeling of the electroweak processes (mostly W+jets).

The contributions of fake W-bosons to inclusive production of $W \rightarrow e\nu$ and $W \rightarrow \mu\nu$ are on the order of 1% and 0.2%, respectively, and we neglect them in the inclusive part of the analysis (which is only a sanity check of lepton ID).

9.3.4 Cosmic Ray Backgrounds

High-energy cosmic muons traverse the CDF detector at a significant rate and are reconstructed as $\mu^+\mu^-$ pairs. We remove the cosmic muons with the cosmic ray tagging algorithm (See [30]) which basically fits the two tracks of the $\mu^+\mu^-$ pair with a single arc. If the fit is successful, the muon pair is tagged as cosmic muons and removed from the $Z^0 \rightarrow \mu\mu$ and $W \rightarrow \mu\nu$ sample [30]. The algorithm is 99.75 ± 0.05% efficient and the mistag rate is 0.03 ± 0.02%.

An independent estimate of the number of cosmic muons surviving the cosmic-ray filter can be made from the distribution $|\vec{P}(Z)|$ of the muon pair. This is an elegant way of combining the usual 'back-to-back' and momentum balance criteria into a single distribution, as cosmic $\mu^+\mu^-$ pairs have a very narrow peak at 0 GeV, while real $Z^0 \rightarrow \mu\mu$ decays have negligibly small phase space at low $|\vec{P}(Z)|$). Using the $|\vec{P}(Z)|$ distribution, the most probable number of cosmic ray events in the sample surviving the cosmic filter is zero.

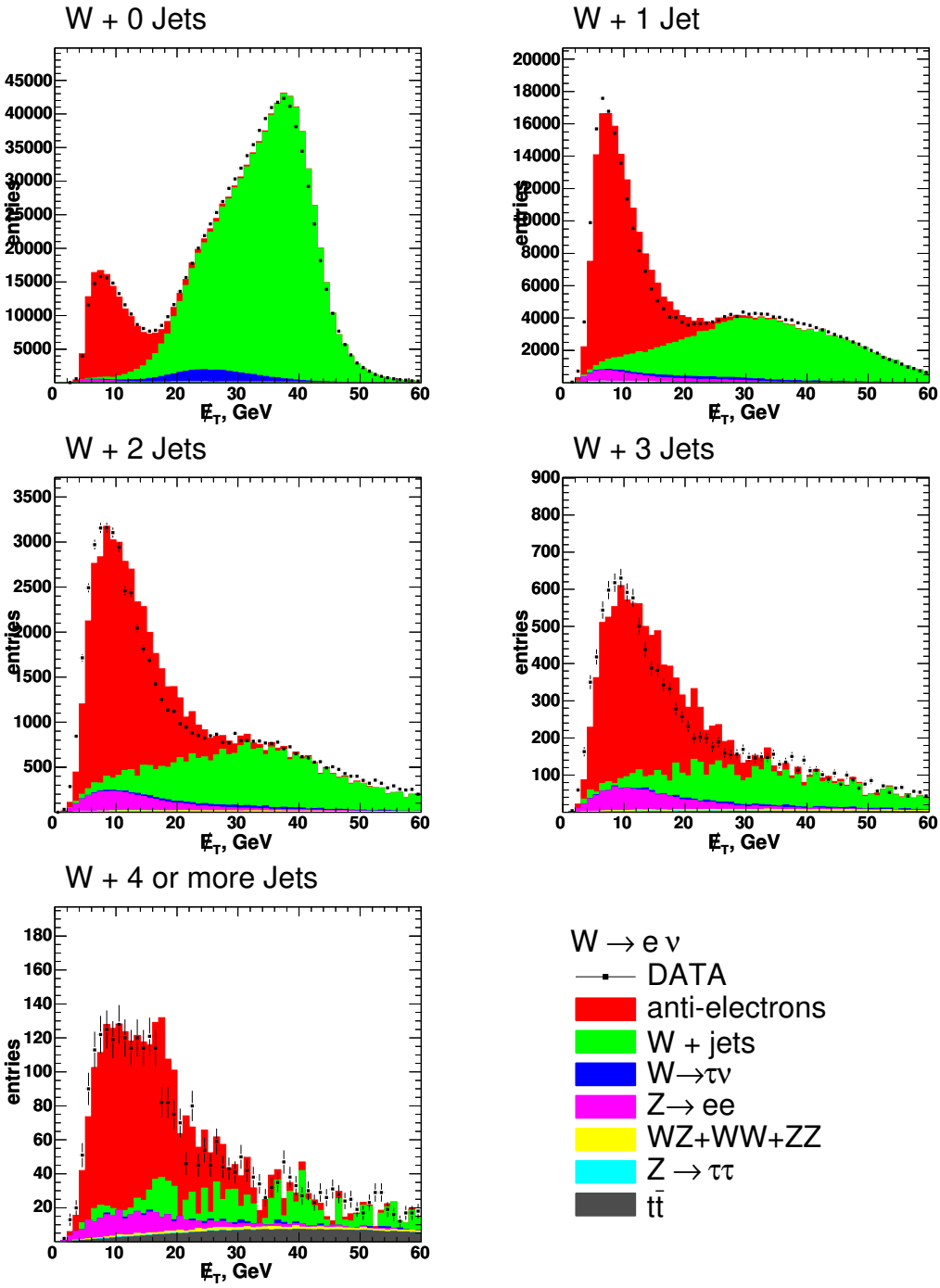

Figure 17: The measured distribution in $\not\!\!E_{\rm T}$ for events with 1,2,3, and 4 or more jets in events with a single tight electron and missing energy forming a transverse mass more than 20 GeV. The distributions are compared to SM expectations and anti-selected-electron samples. We let the normalization of the non-QCD processes float.

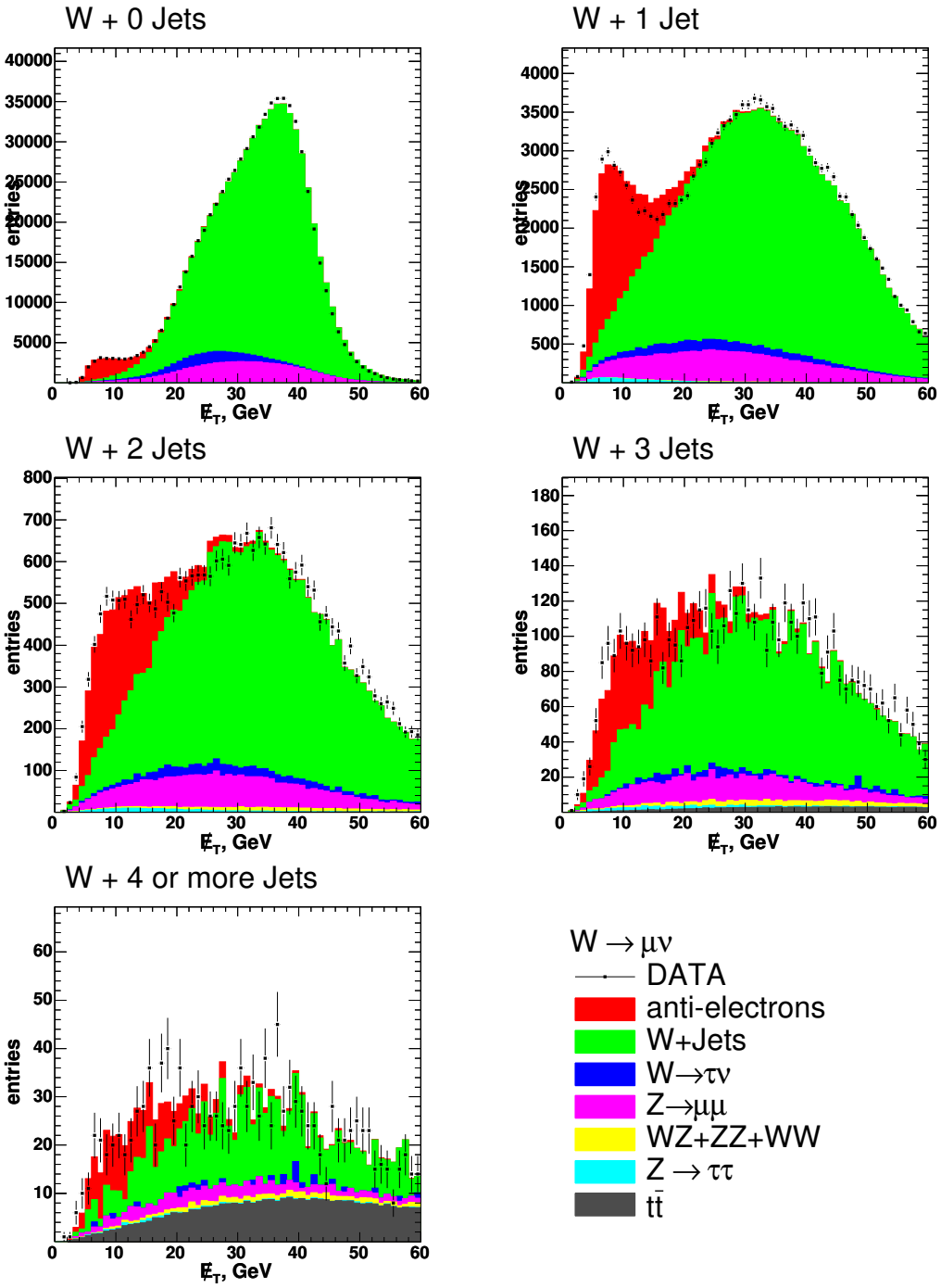

Figure 18: The measured distribution in $\not\!\!E_T$-distributions for events with 1,2,3, and 4 or more jets in events with a single tight muon and missing energy which make transverse mass more than 20 GeV. The distributions are compared to SM expectations and anti-selected-electron samples. We let the normalization of the non-QCD processes float.

9.4 The R-ratio as a Precision Check of Lepton Identification

We calculate the R-ratio for electron and muon channels separately as their individual cross-checks.

$$R = \frac{\sigma(W) * Br(W \to l\nu)}{\sigma(Z^0) * Br(Z^0 \to l^+l^-)} \tag{42}$$

We measure the following numbers for electrons and muons:

$$R(electrons) = 10.52 \tag{43}$$

$$R(muons) = 10.46 \tag{44}$$

The expectation for the ratio is 10.67 ± 0.15. The observed values are within a 2σ agreement with the expectation considering only the theoretical uncertainty. The systematic and statistical uncertainties on the measured ratios are not estimated at this point but we expect them to be comparable to the uncertainty on the theory prediction. The mean values of the ratios agree within 2%. We use this difference between the observed and the predicted numbers to estimate the contribution from the lepton identification to the systematic uncertainty on the ratio

$$\frac{(A \cdot \epsilon)_{pretag}(t\bar{t} \to l^+l^-bcjj)}{(A \cdot \epsilon)_{pretag}(t\bar{t} \to l\not{E}_{\mathrm{T}}bbjj)} \tag{45}$$

which contributes almost directly to the FCNC limit value.

10 Standard Model Production of $t\bar{t}$ Pairs

We define the 'W+HF' sample to be events with an identified W-boson (a lepton and $\not{E}_{\mathrm{T}}$ - see Section 6) and at least one B-tagged jet. Estimation of the SM production for 'W+HF' events requires normalization of three key components: $t\bar{t}$, $W + b\bar{b}$, $W + c\bar{c}$, $W + c$,and non-W events. This is done in four steps:

1. We assume that fractions of non-W events are negligible and $\sigma(t\bar{t})$ is equal to 7.6 pb. The theoretical estimate of the top pair production cross-section is based on [14] using the measured top-quark mass of 170.9 ± 1.8 GeV [31]. We determine the normalization of the Standard Model's contribution to the "W+HF" (i.e. "W+$b\bar{b}$", "W+c" and "W+$c\bar{c}$") processes by rescaling their cross-sections to match the total number events observed the "W + 2 jets" bin. We assume that the overall normalization of "$W + b\bar{b}$ + jets", "$W + c\bar{c}$ + jets", and "$W + c$ + jets" can be corrected by a single scale factor (which is the same for the electron and muon channels).

2. We take the normalization of "W+HF" samples from step "1" to estimate the contribution from fake W's. The procedure is described later in this section.

3. By repeating "1" again we recalculate the fraction of real "W+HF" events using the non-zero estimates of fake W's obtained in step "2".

4. We rescale $\sigma(t\bar{t})$ (it is 7.6 pb a priori) to match the "W + 4 jets" bin for illustrative purposes (see Fig 22). We do not vary any other scale factors when we normalize the $t\bar{t}$ component. The scale factor for W+HF processes ($W + b\bar{b}$, $W + c\bar{c}$, and $W + c$) does not depend strongly on the number of $t\bar{t}$ events since the $t\bar{t} \to WbZc$ and $t\bar{t} \to WbWb$ modes contribute mostly to a final state with a W and four jets in the final state.

The obtained jet multiplicity distributions for 'W + B-tag' are shown in Figure 21.

The motivation for normalizing to the two-jet multiplicity bin is based on the matrix-element structure of associated heavy flavor production in W and Z events. The real problem is that different diagrams contribute differently to the N=1 and the N=2 jet multiplicity bins; taking into account the (large, particularly for charm) NLO corrections is tricky since the corrections differ significantly for the different processes. In contrast, the radiation of additional jets and jet matching procedures are fairly well understood and have been studied elsewhere quite carefully. As we do not use the 1-jet bin we avoid all these issues by normalizing to the 2nd jet bin.

A preliminary estimate of the top-pair production rate (assuming that there is no FCNC) can be done by computing the difference between the observed and the expected non-$t\bar{t}$ events in the W+4jets bin. To illustrate this we scale $\sigma(t\bar{t} \to WbWb)$ to match the calculated difference in the "W+4jets" bin. The H_T- distributions with the rescaled $\sigma(t\bar{t} \to WbWb)$ agree well with those of top-pair decays (See Fig 22).

The number of fake W bosons is estimated by fitting the $\not\!\!E_{\rm T}$-distribution for each jet multiplicity bin in events with one a tight lepton and M_T higher than 20 GeV where the transverse mass M_T is calculated for the lepton and $\not\!\!E_{\rm T}$ (this is done to match kinematic properties of the events). Basically, we repeat the same thing we have done earlier for the inclusive W-bosons (See 9.3.3). The fitted distributions are presented in Figures 19 and 20. The obtained fractions of the fake W-events after applying the $\not\!\!E_{\rm T}$-cut ($\not\!\!E_{\rm T}$>25 GeV) are presented in Table 13.

Jet Multiplicity	1 jet	2 jets	3 jets	≥4 jets
$W \to e\nu$ + jets	2.0%	4.9%	7.6%	4.7%
$W \to \mu\nu$ + jets	0.3%	0.9%	1.3%	–%

Table 13: Fractions of the non-W QCD events in events with a tight lepton (e or μ), $\not\!\!E_{\rm T}$ >25 GeV, $M_{TRANS}(l + \not\!\!E_{\rm T}) > 20$ GeV, and at least one B-tagged jet. (Fit for $W \to \mu\nu$+4 jets returned 0 events due to low statistics of the sample. In any case this number should be comparable with the one for inclusive W's so we take the inclusive number as that for the tagged sample.)

The observed efficiencies and event counts for the "W + 4 jets" bin are presented in Tables 14 and 15.

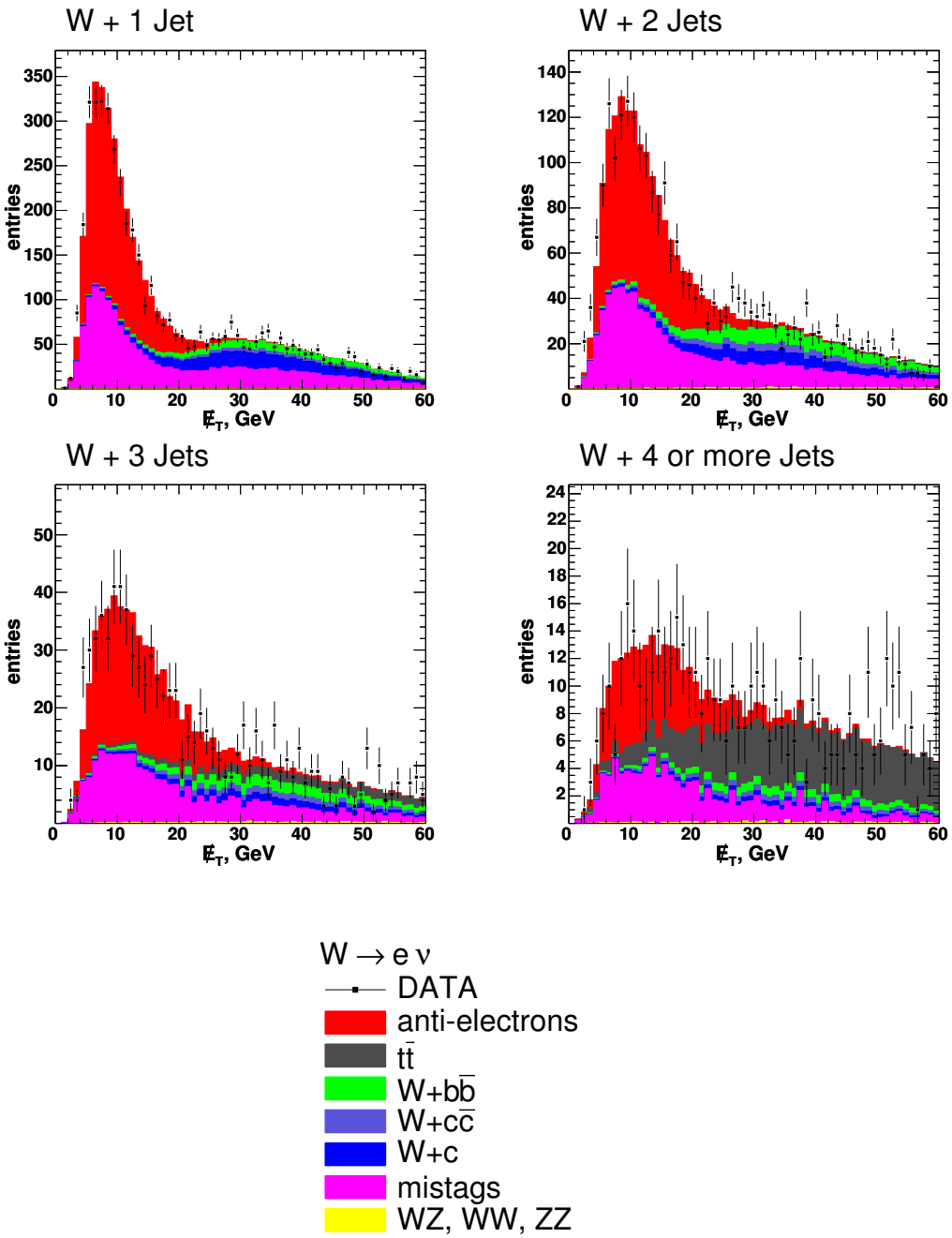

Figure 19: The measured distribution (points) in $\not\!\!E_{\rm T}$-distributions for events with 1,2,3, and 4 or more jets (at least one jet is B-tagged) in events with a single tight electron and missing energy which make transverse mass more than 20 GeV. The distributions are compared to SM expectations (stacked histograms) and anti-selected-electron samples. We let the normalization float.

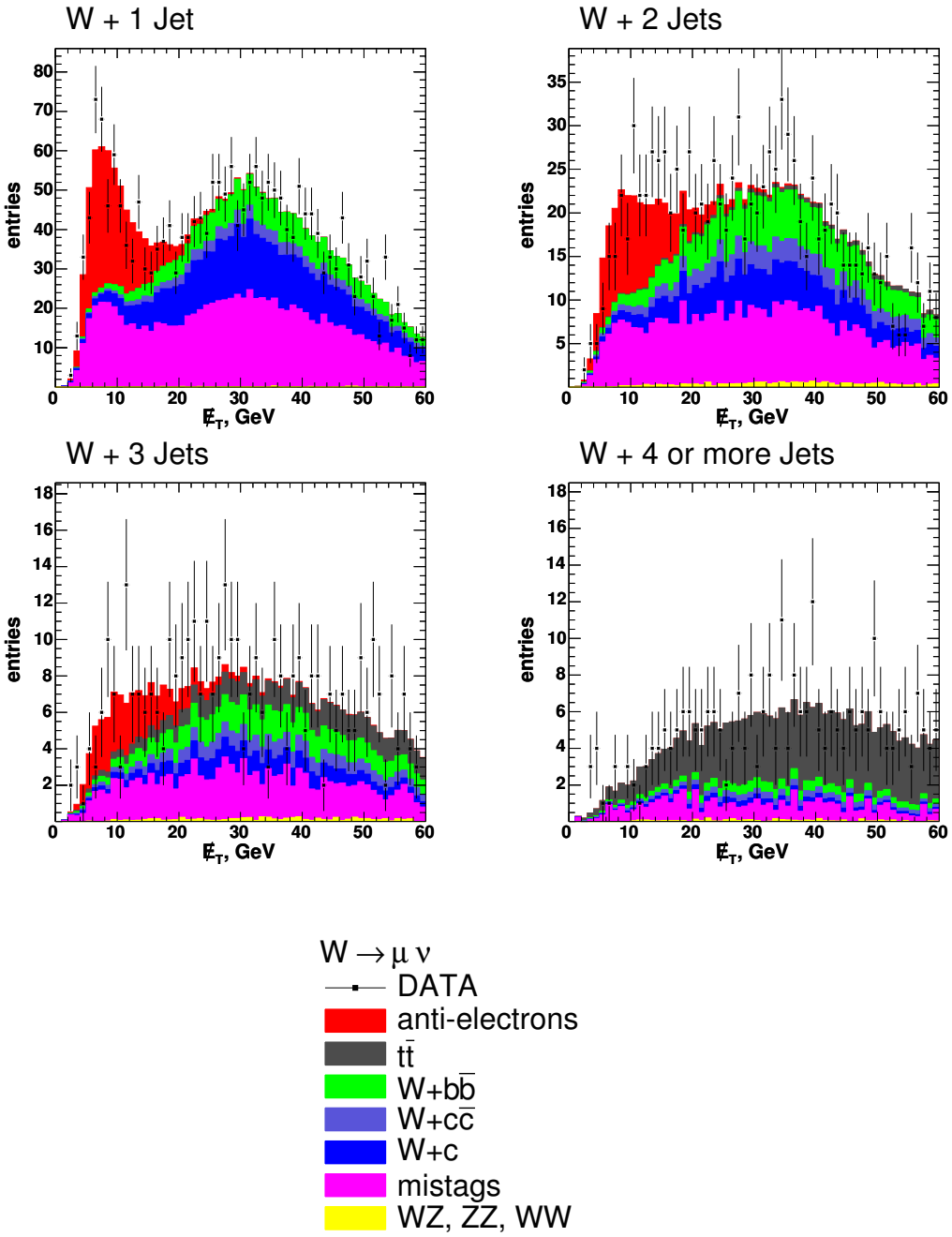

Figure 20: The measured distribution (points) in $\not\!\!E_{\mathrm{T}}$-distributions for events with 1,2,3, and 4 or more jets (at least one jet is B-tagged) in events with a single tight muon and missing energy which make transverse mass more than 20 GeV. The distributions are compared to SM expectations (stacked histograms) and anti-selected-electron samples. We let the normalization float.

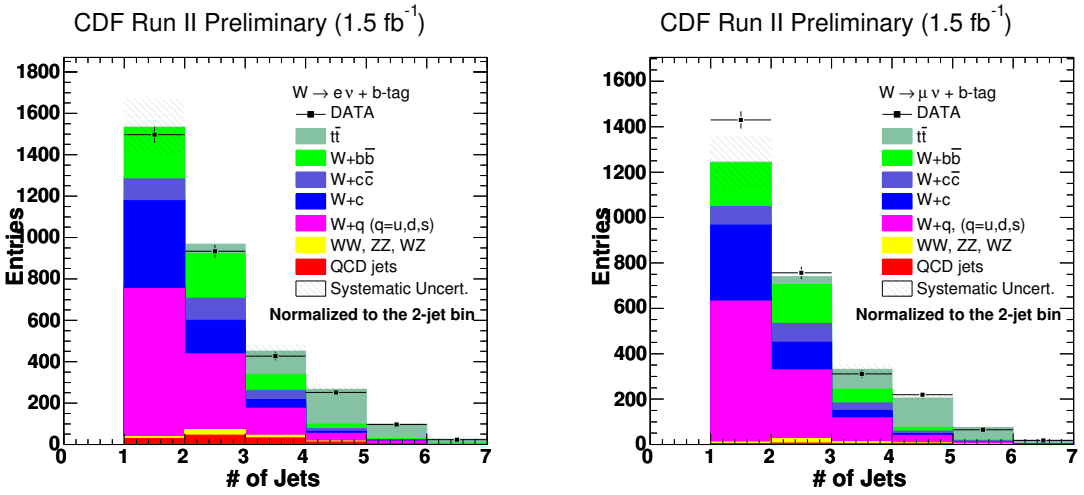

Figure 21: The measured distributions (points) in the number of jets in $Z^0 \to ee$ and $Z^0 \to \mu\mu$ events, respectively, with a W and a b-tag, compared to SM expectations (stacked histogram.) The content of the distributions is summarized in Tables 32, 33, 34, and 35.

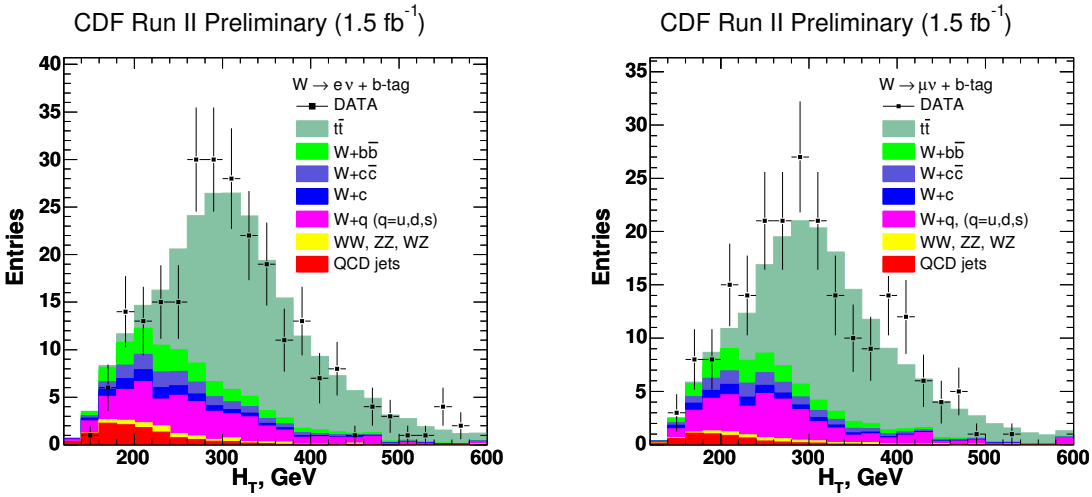

Figure 22: The measured distribution (points) in H_T in events with a W and a b-tag, compared to SM expectations (stacked histogram), for the electron channel (left) and muon channel (right).

Process	Generated	Pre- tag	Tagged	A_4	$\epsilon_{tagging}$
$t\bar{t} \to WbWb \to e\not{E}_T + bcjj$	4710280	88808.9	60258	0.01279	0.6785
$t\bar{t} \to WbWb \to \mu\not{E}_T + bcjj$	4710280	68496.2	46819	0.00994	0.6835

Table 14: A summary of the acceptance times efficiency (A_4) for inclusive $t\bar{t} \to$ WbWb production measured from the Monte Carlo samples.

Final state	Observed	Background (non-$t\bar{t}$)
$e + \not\!\!E_{\mathrm{T}} + 4jets$	252	98.7
$\mu + \not\!\!E_{\mathrm{T}} + 4jets$	219	75.2

Table 15: A summary of the numbers of "W + 4 jets" events. At least one jet in each event is required to be B-tagged.

11 FCNC $t\bar{t} \to ZcWb$ and $t\bar{t} \to ZcZc$ production

At this stage we consider only events which have two leptons consistent with a Z-boson and at least one B-tagged jet. We use the jet multiplicity distribution (See Fig. 23) to constrain the number of not-top Z+4jet events. We do this by scaling the whole "Z+HF" component to the number of (observed - mis-tagged) Z+2 jets events in the electron and muon modes simultaneously. The number of events with a fake Z-boson is less than 0.5% and we neglect it.

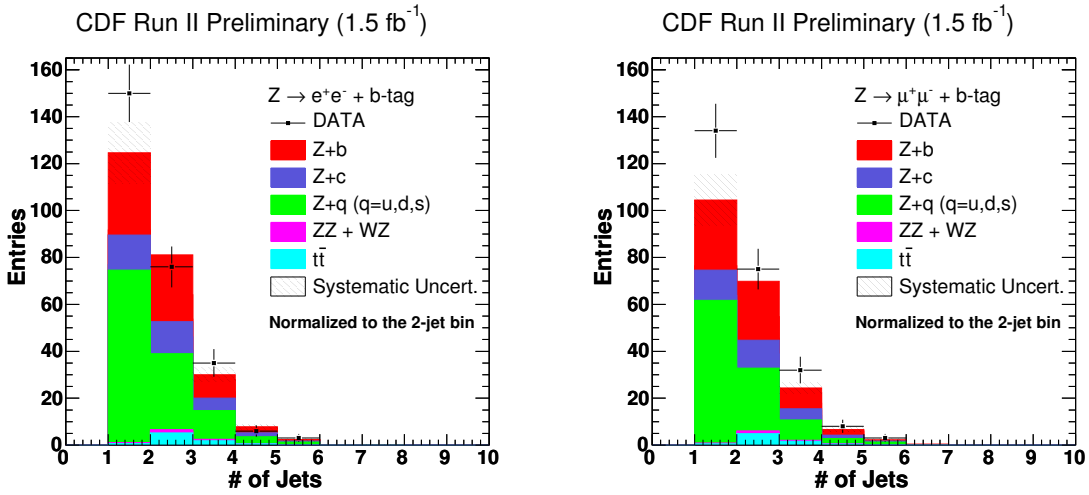

Figure 23: The measured distribution (points) in the number of jets in events with a Z and a b-tag, compared to SM expectations (stacked histogram), for the electron channel (left) and muon channel (right). The content of the distributions is summarized in Tables 36, 37, 38, and 39. We normalize to the average of the $Z^0 \to ee$ and $Z^0 \to \mu\mu$ 2 jet bins. We normalize to the 2-jet bin in order to avoid the difficult relative normalization problem for the 1-jet bin, which is unique in being especially sensitive to the Q^2 scale used in 2-2 diagrams involving an incoming b-quark; the 1-jet bin is not used at all in this analysis.

We have made an estimate of the uncertainty on the limit due to the discrepancy in the 1-jet bin as suggested by Beate. We note that a fundamental strategy of this analysis is that we do *not* use the 1-jet bin. We have avoided for a physics reason - it's dependent on a different Q-squared scale, as there is a diagram that depends on bottom-quark and charm-quark fusion, and these have strong Q-squared dependences (see F. Maltoni, Z. Sullivan and S. Willenbrock, Phys. Rev. D **67**, 093005 (2003)- we had Zack Sullivan working on this with us for several months here at UC.).

Assuming we go to a lower-Q^2 scale for the fusion diagrams (Compton diagram), we assume that the Compton diagram doubles. The Compton diagram is $\sim 40\%$ of the total cross-section; let us double it. The Behrends-Kleiss scaling gives about a factor of 5 per extra jet, so that we have thus added 8% to the 2-jet bin. This adds 1.6% to the 3-jet bin, and 0.3% to the 4-jet bin. The partial derivative of the limit with respect

to the Z+4jets background is about 0.1; i.e., a 10% change in the Z+4jets background gives a 1% (absolute- i.e. a 10% limit would go to 11%)) change in the limit. So the total change in the limit is $\sim 3 \times 10^{-4}$, i.e. it's negligible.

The FCNC signal contribution is divided into two parts: ZcWb mode and ZcZc mode since the B-tagging rates are different. We summarize the acceptance and the efficiency measurements for the "Z + 4 jets" channel in Tables 17, 16, 18, and 19. The case when a leptonic decay of a Z-bosons fakes a leptonic decay of a W-boson is taken into account in tables 18 and 19.

The M_{top}-dependent acceptances $A_{1,i}$ and $A_{2,i}$ are obtained by multiplying the cumulative acceptance A_j by a fraction of events contribution to the i'th bin of the top mass distribution:

$$A_{j,i} = A_j \cdot \frac{N_i}{\sum_k N_k}. \tag{46}$$

Process	Generated	Pre- tag	Tagged	A_1	$\epsilon_{tagging}$
Longitudinal fraction is a_0=0.00					
$t\bar{t} \to ZcZc \to e^+e^- + 4jets$	383748	32401.8	10537.5	0.001848	0.325
$t\bar{t} \to ZcZc \to \mu^+\mu^- + 4jets$	383748	28914.6	10141.7	0.001779	0.351
Longitudinal fraction is a_0=0.50					
$t\bar{t} \to ZcZc \to e^+e^- + 4jets$	380939	35238	11508.2	0.002034	0.327
$t\bar{t} \to ZcZc \to \mu^+\mu^- + 4jets$	380939	30782.5	10847.7	0.001917	0.352
Longitudinal fraction is a_0=1.00					
$t\bar{t} \to ZcZc \to e^+e^- + 4jets$	377971	37978.2	12486.8	0.002224	0.329
$t\bar{t} \to ZcZc \to \mu^+\mu^- + 4jets$	377971	32556.4	11504.4	0.002049	0.353

Table 16: A summary of the acceptance times efficiency for the inclusive FCNC decay of $t\bar{t} \to ZcZc \to l^+l^- + ccjj$ measured from the Monte Carlo samples.

Process	Generated	Pre- tag	Tagged	A_2	$\epsilon_{tagging}$
Longitudinal fraction is a_0=0.00					
$t\bar{t} \to ZcWb \to e^+e^- + 4jets$	375526.7	31278.2	15337.4	0.002749	0.490
$t\bar{t} \to ZcWb \to \mu^+\mu^- + 4jets$	375526.7	27611	14880.9	0.002667	0.539
Longitudinal fraction is a_0=1.00					
$t\bar{t} \to ZcWb \to e^+e^- + 4jets$	375753	35499.4	17443.7	0.003125	0.491
$t\bar{t} \to ZcWb \to \mu^+\mu^- + 4jets$	375753	30393.4	16361.6	0.00293	0.538

Table 17: A summary of the acceptance times efficiency for the inclusive FCNC decays of $t\bar{t} \to ZcWb \to l^+l^- + bcjj$ measured from the Monte Carlo samples.

Process	Generated	Pre- tag	Tagged	A_3	$\epsilon_{tagging}$
Longitudinal fraction is a_0=0.00					
$t\bar{t}\rightarrow WbZc \rightarrow e\nu + bcjj$	4710280	89118	43668	0.009271+	0.490
$t\bar{t}\rightarrow WbZc \rightarrow e\not{E}_{\rm T} + bcjj$	375526.7	19928.1	10010.3	+0.001794	0.502
$t\bar{t}\rightarrow WbZc \rightarrow \mu\nu + bcjj$	4710280	69242.2	37280	0.007915+	0.538
$t\bar{t}\rightarrow WbZc \rightarrow \mu\not{E}_{\rm T} + bcjj$	375526.7	22882.9	12161.8	+0.002180	0.531
Longitudinal fraction is a_0=1.00					
$t\bar{t}\rightarrow WbZc \rightarrow e\nu + bcjj$	4710280	92967	45554	0.009671+	0.490
$t\bar{t}\rightarrow WbZc \rightarrow e\not{E}_{\rm T} + bcjj$	375753	20387.5	10326.1	+0.001850	0.507
$t\bar{t}\rightarrow WbZc \rightarrow \mu\nu + bcjj$	4710280	71473.9	38481	0.008169+	0.538
$t\bar{t}\rightarrow WbZc \rightarrow \mu\not{E}_{\rm T} + bcjj$	375753	23743.2	12662.1	+0.002268	0.533

Table 18: A summary of the acceptance times efficiency for the inclusive FCNC decays of $t\bar{t}\rightarrow WbZc \rightarrow l\not{E}_{\rm T}+bcjj$ (decay of a Z fakes decay of a W) and $t\bar{t}\rightarrow WbZc \rightarrow l\nu+bcjj$ measured from the Monte Carlo samples. The acceptance A_3 is the sum of acceptances for the both decay modes which contribute to the signature of $l + \not{E}_{\rm T} + 4jets$.

Process	Generated	Pre- tag	Tagged	A_5	$\epsilon_{tagging}$
Longitudinal fraction is a_0=0.00					
$t\bar{t}\rightarrow ZcZc \rightarrow e + \not{E}_{\rm T} + 4jets$	383748	16068.3	4976.49	0.000873	0.310
$t\bar{t}\rightarrow ZcZc \rightarrow \mu + \not{E}_{\rm T} + 4jets$	383748	20621.9	7248.1	0.001271	0.351
Longitudinal fraction is a_0=0.50					
$t\bar{t}\rightarrow ZcZc \rightarrow e + \not{E}_{\rm T} + 4jets$	380939	15708.6	4855.15	0.000858	0.309
$t\bar{t}\rightarrow ZcZc \rightarrow \mu + \not{E}_{\rm T} + 4jets$	380939	21095.9	7448.1	0.001316	0.353
Longitudinal fraction is a_0=1.00					
$t\bar{t}\rightarrow ZcZc \rightarrow e + \not{E}_{\rm T} + 4jets$	377971	15349.3	4707.03	0.000838	0.307
$t\bar{t}\rightarrow ZcZc \rightarrow \mu + \not{E}_{\rm T} - +4jets$	377971	21655.5	7681.28	0.001368	0.355

Table 19: A summary of the acceptance times efficiency for the inclusive FCNC decay of $t\bar{t}\rightarrow ZcZc \rightarrow l+\not{E}_{\rm T}+ccjj$ (here $Z \rightarrow l^+l^-$ fakes $W \rightarrow l\nu$) measured from the Monte Carlo samples.

11.1 Top Mass Fitter

We reconstruct the value of M_{top} for each candidate event that contains at least two leptons consistent with a Z-boson and at least four jets. The procedure is very similar to that of the regular top mass measurement (See [32]). The value of M_{top} is determined by a kinematic fit of χ^2.

The χ^2 includes all the top-specific corrections and energy resolutions used in the single lepton top mass measurement. The reconstructed top mass agrees well with the generated one. The difference between the reconstructed and the generated masses does not contribute to the final result and we neglect it.

The value of M_{top} is calculated by minimizing the χ^2 distribution, which is based on the assumption that the event is $p\bar{p} \to t\bar{t} \to Z^0 + 4jets \to l^+l^- + 4jets$. The minimization takes into account every combination of the jets in the event since we do not know the true jet-parton assignments. The top mass distribution obtained for $t\bar{t} \to ZcZc \to l^+l^- + 4jets$ decays does not differ significantly from that of $WbZc$ decay. The exact formula for the χ^2 has the following structure:

$$\chi^2(M_{top}) = \sum_{l_1,l_2,jets} \frac{(\hat{Et}_i - Et_i)^2}{\sigma_i^2} + \sum_{x,y} \frac{(\hat{Et}_i^{uncl} - Et_i^{uncl})^2}{\sigma_i^2} + \frac{(M(j_1j_2) - M_W)^2}{\Gamma_W^2} + \frac{(M(l^+l^-) - M_Z)^2}{\Gamma_Z^2} + \frac{(M(W+j) - M_{top})^2}{\Gamma_{top}^2} + \frac{(M(Z+j) - M_{top})^2}{\Gamma_{top}^2}. \quad (47)$$

The first term contains the fitted transverse energies of the leptons and four jets within the corresponding experimental resolutions. The second term includes the x- and y- components of the unclustered energy. The formula also contains terms for the reconstructed masses of the W, Z, and the two top-quarks.

We process all the "Z+4jets" events in data and simulations with the same top mass fitter so that we can compare the M_{top} distributions to set the limit (See fig. 24).

The χ^2 function we use does not have the proper shape since each term in the sum should be distributed as a squared Gaussian with the mean of 1. The observed distributions are shown in Figure 25.

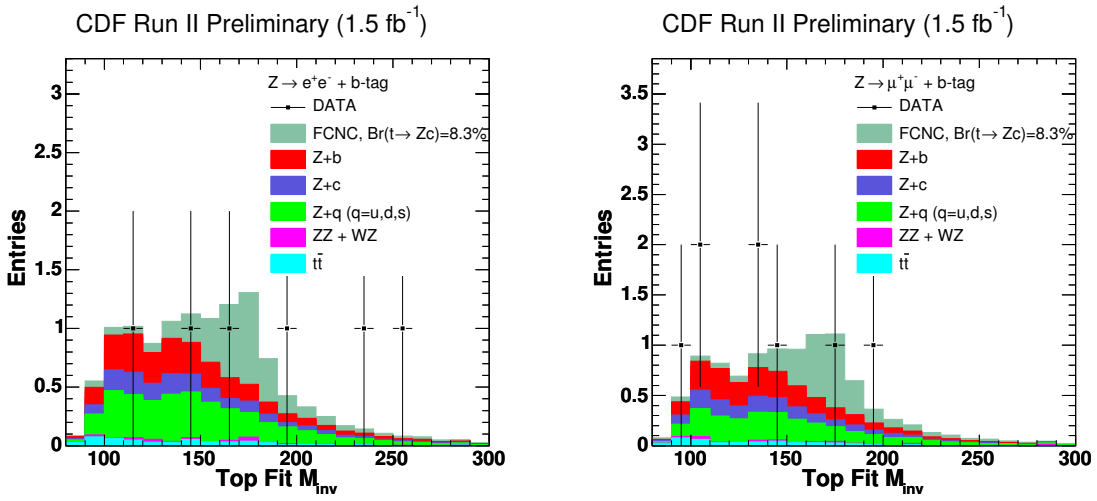

Figure 24: The measured distribution (points) in the fitted top mass in events with a Z and four jets with at least one B-tagged jet, compared to the SM expectations (stacked histogram), for the electron channel (left) and muon channel (right). The magnitude of the FCNC contribution represents the observed limit of 8.3% on the branching fraction assuming that the Z's are 100% longitudinally polarized. We use high-statistics Monte Carlo simulations to build the tempaltes for mistagged events.

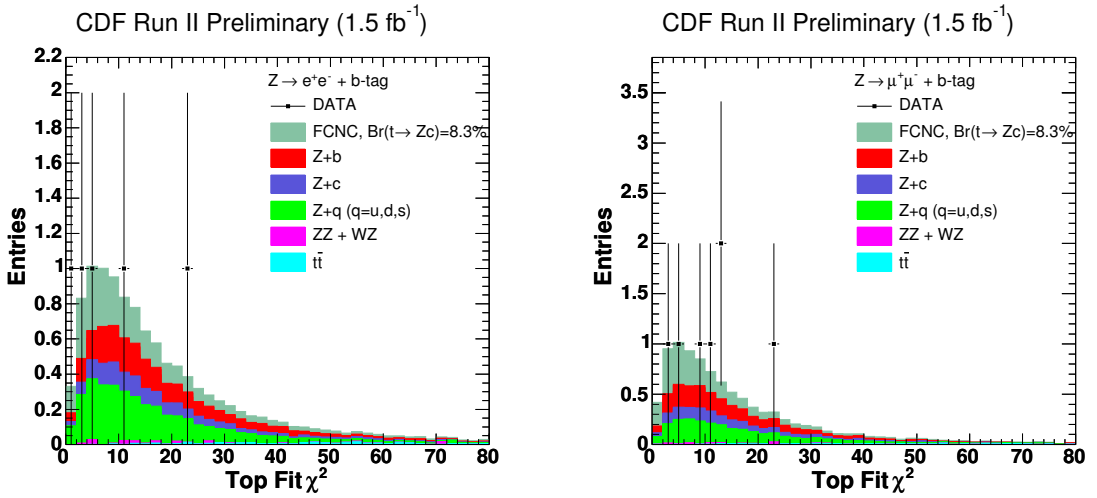

Figure 25: The measured distribution (points) in the fitted top χ^2 in events with a Z and four jets with at least one B-tagged jet, compared to the SM expectations (stacked histogram), for the electron channel (left) and muon channel (right). The magnitude of the FCNC contribution represents the observed limit of 8.3% on the branching fraction assuming that the Z's are 100% longitudinally polarized. We use high-statistics Monte Carlo simulations to build the tempaltes for mistagged events.

12 Systematic uncertainties

We have shown earlier (See 2) that the expected numbers of observed events depend on acceptances and backgrounds. We discuss systematic uncertainties involving the acceptances and the background in the following two subsections.

12.1 Systematic Uncertainties on the Acceptances

To estimate the systematic uncertainty on the acceptances (A_1, A_2, A_3, A_4, and A_5) we vary each of the parameters listed below by one standard deviation ($\pm\sigma$) and then we recalculate the acceptances A_i (i=1,..,5). We take into account correlations between the individual uncertainties. The sources of uncertainty are as follows:

- *Jet Energy Scale.* We estimate the effect of uncertainties in the calibration of jet energies by varying the Jet Energy Correction by $\pm 1\sigma$ (one standard deviation). The systematic uncertainties are positively correlated for all the A_i. The individual uncertainties due to the JES systematics are presented in Table 21.

- *Lepton ID + Lepton trigger.* The acceptances A_i are influenced by uncertainties in the identification of W- and Z-bosons, and have been studied earlier in the paper (Section 9). We assume that the reconstruction and the triggering efficiencies of electrons and muons are not correlated, but acceptances of W's and Z's decaying to leptons of the same flavor are correlated. This means that A_1 would be 'off' by the same percentage as A_2 for leptons of the same flavor. The same principle is true for A_3, A_4, and A_5. (The uncertainty on the luminosity does not matter because it factors out in $N_{t\bar{t}}$).

  The observed R-ratios (See 9.4) agree with the NNLO predictions to within 2%. However the crossection $\sigma(Z \to \mu^+\mu^-)$ differs from the NNLO prediction by 2.7% (this is the largest discrepancy). A simple explanation of why the uncertainty in the R-ratio is smaller than that on an individual cross-section is that the $\sigma(W \to l\nu)$ is proportional to the product of efficiencies of the high-P_T lepton trigger and lepton reconstruction, but $\sigma(Z \to l^+l^-)$ is proportional only to the square of the efficiency of the lepton reconstruction. The uncertainty for the W then is linear in the uncertainties on both the reconstruction and the trigger, while the uncertainty for the Z is dominated by twice the uncertainty on the acceptance. The uncertainty on R, the ratio of W to Z, thus depends on both the uncertainty on the reconstruction and the uncertainty on the trigger. If the reconstruction uncertainty is the larger, then R will be better measured than the individual cross-sections. This is the case in the muon channel.

  The systematic uncertainties in the A_i for electrons and muons depend on the reconstruction and trigger efficiencies in the following way:

$$\sigma(A_1) = \sigma(A_2) = 2\sigma_{Rec} \tag{48}$$

and

$$\sigma(A_3) = \sigma(A_4) = \sigma(A_5) = \sigma_{Rec} + \sigma_{Trig}, \quad (49)$$

where σ_{Rec} is the (relative) standard deviation of the reconstruction efficiency (which includes acceptance), and σ_{Trig} is the relative standard deviation of the trigger efficiency. The deviations σ_{Rec} and σ_{Trig} are treated independently for electrons and muons. The obtained values for the relative deviations are listed in Table 20.

Lepton Flavor	σ_{Rec}	σ_{Trig}
electrons	0.8%	-0.9%
muons	1.4%	-0.5%

Table 20: A summary of the systematic uncertainties in the reconstruction and trigger efficiencies for electrons and muons. The negative signs of σ_{Trig} represent a negative correlation between σ_{Rec} and σ_{Trig}.

We assume that σ_{Rec} and σ_{Trig} are both affected by modeling of leptons in the same manner so we take them as negatively correlated. This procedure allows us to constrain the uncertainty on the R-ratio (it can not be bigger than 2%).

- *ISR and FSR.* The effect of initial and final radiation (ISR and FSR) on A_4 was studied in [33]. We expect that FSR will contribute to the uncertainties in the other three A_i in the same way since we require four jets in the final state for all four channels and the samples are triggered on leptons. The ISR error should also contribute identically to the uncertainties of the four acceptances A_i. The uncertainties are 0.5% for the ISR and 0.6% for the FSR, and they are 100% correlated across all A_i.

- *Parton Distribution Functions (PDF).* The PDF uncertainties can also propagate into the acceptance. However, these affect only production of the $t\bar{t}$ pairs and not their decays. The effect of the uncertainties is studied carefully in Ref [33]. The total uncertainty is 0.9% and is 100% correlated for the four A_i.

- *Heavy quark Tagging.* The b-tagging scale factor (which is used to take into account an over-efficiency of B-tagging in MC events) comes with a systematic uncertainty. The scale factor is 0.95 ± 0.05 [34]. We vary the scale factor within its uncertainty and recalculate the tagging efficiency for ± 1 σ.

- *Charm quark Tagging.* We assume that the b-tagging scale factor for a jet with a charm-quark decay is the same as that for a jet with a bottom-quark decay. However, there are no direct measurements of this hypothesis in Run 2. We follow the prescription used in the top cross-section measurement [33]. To estimate the systematics we set the b-tagging scale factor to 0.95 and we use 0.8 for b-taggs caused by decays of charm-quarks.

- *Top Quark Mass.* The uncertainty on the top quark mass is now close to 1% [31]. This will introduce an uncertainty similar to, but much smaller than and correlated with, that from the jet energy scale.

- *Monte Carlo Statistics.* The statistics of the signal samples is large enough so it does not contribute as a major uncertainty. However, the uncertainty is taken into account for each individual channel (histogram bin).

We summarize the systematic uncertainties of the acceptances in Table 21.

Systematics	$\frac{\sigma(A_1)}{A_1}$, %	$\frac{\sigma(A_2)}{A_2}$, %	$\frac{\sigma(A_3)}{A_3}$, %	$\frac{\sigma(A_4)}{A_4}$, %	$\frac{\sigma(A_5)}{A_5}$, %
JES	2.5	2.6	2.7	2.4	6.4
ISR	0.5	0.5	0.5	0.5	0.5
FSR	0.6	0.6	0.6	0.6	0.6
Lepton ID	$2\sigma_{Rec}$	$2\sigma_{Rec}$	$\sigma_{Rec} + \sigma_{Trig}$	$\sigma_{Rec} + \sigma_{Trig}$	$\sigma_{Rec} + \sigma_{Trig}$
PDFs	0.9	0.9	0.9	0.9	0.9
HF Tagging	3.4	3.6	3.6	3.9	3.4
Charm Tagging	9.7	3.5	3.5	1.4	10.0
Total	10.6 $\oplus$ lept.	5.8 $\oplus$ lept.	5.8 $\oplus$ lept.	4.9 $\oplus$ lept.	12.4 $\oplus$ lept

Table 21: A summary table of the systematic uncertainties on the acceptances. Correlations are taken into account in the calculation of the limit. The abbreviation "lept." stands for the systematic uncertainty due to lepton ID.

12.2 Systematic Uncertainties of the Backgrounds

We consider the following sources of the major systematic uncertainties in $Bgr(l\nu + 4jets)$ and $Bgr(l^+l^- + 4jets)$:

- *The expected number of W/Z+HF events: Alpgen's parametrization.* The Z+HF and W+HF backgrounds are modeled by Alpgen, and hadronized with Pythia. The predictions suffer from uncertainties in the modeling procedure. In particular, the expected number of events in the "W/Z + 4 jets" category enters directly into the calculation for the final result. Here we make an estimate of the uncertainty on the expected number of W/Z+HF events.

  We assume that there is a set or parameters which allows Alpgen to model data perfectly. A deviation from the "ideal set" can be estimated using inclusive Z + jets events with jet multiplicity below three. A comparison between data and Alpgen simulations is shown in Figure 26. The observed deviation on radiation of one extra jet in the inclusive sample is less than 5%. We thus take 10% as the estimate of the uncertainty on this Alpgen prediction for the radiation of 2 extra jets in the inclusive sample. However, the slopes of the N-jet distribution are predicted to be different in the inclusive and HF samples, with the factors

for each additional jet being 5.0 and 2.7 in the inclusive and b-tagged samples, respectively.The ratio of 5.0 to 2.7 makes a relative difference of 1.85 between radiating an extra jet in inclusive and tagged samples. We consequently increase the 10% deviation by a factor of 2 (rounding 1.85 up), to 20%.

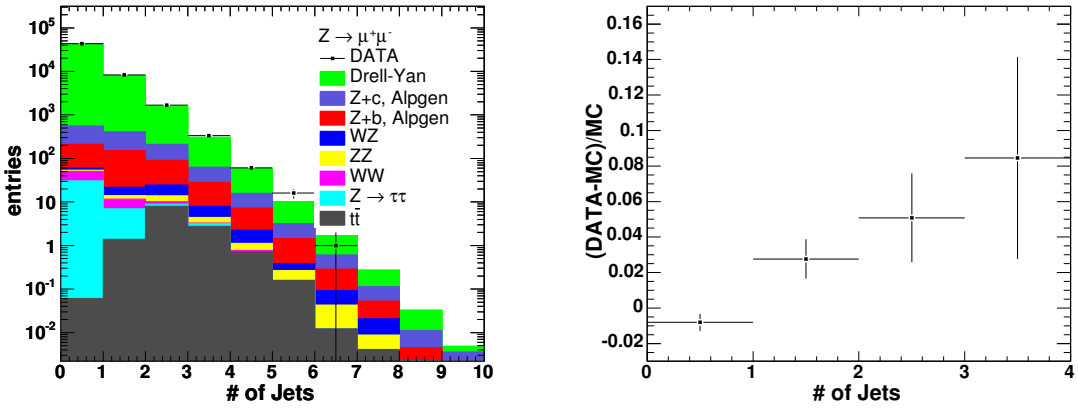

Figure 26: The measured distribution (points) in the number of jets in events with an inclusive decay of $Z^0 \rightarrow \mu\mu$, compared to SM expectations (stacked histogram.) The content of the distributions is summarized in Tables 40 and 41. The "Z+Jets" processes (Drell-Yan, Z+b, and Z+c) are modeled with Alpgen. In this analysis we consequently normalize the Alpgen predictions with events in the 2-jet bin to study events with four jets in the final state. The uncertainty we estimate for the number of expected Alpgen events in the 4-jet bin of the tagged sample is 20%.

- *Sensitivity of the Limit to the number of 4-jet Z+HF events.* We have used pseudo-experiments to calculate the sensitivity of the final limit to the number of SM Z+4-jet tagged events. The limit was calculated with this systematic uncertainty set to zero, set to 20% (nominal), and set to 40%. The respective shifts in the limit are -0.1%, zero (by construction), and +0.1%, respectively.

  The reason for the relatively weak dependence of the limit on the Z+4-jet background is subtle [6]. The measured number of events in the bin is fixed, of course. An increase in the estimated number of SM background events decreases the average of $N_{t\bar{t}}$ of the likelihood $L(B_Z, N_{t\bar{t}})$ distribution and it makes it more consistent with the SM prior $\pi_0(N_{t\bar{t}})$. These leads to an increase of the expected limit.

- *Normalization procedure.* The background contributions from W+HF and Z+HF events are not absolute; they are normalized to match the number of observed events with 2 jets (we discuss it in more detail in Sections 10 and 11). This leads to

[6] Sasha says it's clear. HJF

an uncertainty which is caused by the finite statistics of the data. The estimated uncertainties of the normalization procedure are 2.5% for $Bgr(l\nu + 4jets)$ and 8% for $Bgr(l^+l^- + 4jets)$.

- *Mistag modeling.* The method of predicting mistag rates by applying the mistag matrix to data introduces significant systematic uncertainty. We vary the mistag probability by 15% (See [35] and [36]) to estimate the systematics.

- *Jet Energy Scale.* Changing the jet energy scale changes the Behrends scaling factor in the Njet distribution for Z+Njets; i.e. the slope of the Njet distribution in the N+2jet and higher bins depends on the JES scale. The systematic uncertainty due to any uncertainty on the JES scale is thus already estimated in the uncertainties in the Alpgen modeling and it should not be double-counted.

- *Luminosity.* The 6% uncertainty of the measured luminosity affects only processes that are normalized absolutely. These processes are WW, WZ, and ZZ production. The contribution from this events to the final result is negligible ($< 0.1\%$).

We summarize the systematic uncertainties of backgrounds in Table 22.

Systematics	"$l + \not\!\!E_T + 4jets$", %	"$l^+l^- + 4jets$", %	Correlation
Alpgen	20	20	1
Mistags	15	15	1
Normalization	2.5	8	0

Table 22: A summary table of the relative systematic uncertainties on the backgrounds for each final state. The given correlations are taken into account in the computation of the limit.

13 Data Analysis and Measurement of the Limit on Br($t \to Z^0c$)

The data are analyzed in three steps:

1. We compute a set of likelihood distribution functions $L(B_Z, N_{t\bar{t}})$ so each distribution corresponds to the given helicity structure of the FCNC decay (fraction of longitudinally polarized Z-bosons).

2. The likelihood distributions are turned into two-dimensional posterior probability density functions $P(Br(t \to Zc), N_{t\bar{t}}|observables)$. The posterior density functions are used to create "1σ" and "2σ" two-dimensional contours for each given structure of the FCNC coupling.

3. The the two-dimensional posterior distributions are integrated into one-dimensional posterior probability density functions $P(Br(t \to Zc)|observables)$. The functions $P(Br(t \to Zc)|observables)$ are used to calculate 95% C.L. upper limits on $Br(t \to Zc)$ so that we get a limit for each given fraction of longitudinally polarized Z's.

Each of the steps is presented below in more detail.

13.1 Numerical Computation of the Likelihood Distribution Function $L(B_Z, N_{t\bar{t}})$

We have discussed the construction of the likelihood function $L(B_Z, N_{t\bar{t}})$ earlier in the paper (See 2):

$$L(B_Z, N_{t\bar{t}}) = P(observables|B_Z, N_{t\bar{t}}). \tag{50}$$

The "observables" include the following numbers:

1. Number of observed events of $e + \not{E}_{\mathrm{T}} + 4jets$ where at least one jet is B-tagged
2. Number of observed events of $\mu + \not{E}_{\mathrm{T}} + 4jets$ where at least one jet is B-tagged
3. Number of observed events in the each bin of the M_{top} histogram of $e^+e^- + 4jets$ events where at least one jet is B-tagged
4. Number of observed events in the each bin of the M_{top} histogram of $\mu^+\mu^- + 4jets$ events where at least one jet is B-tagged

The ingredients for the expected numbers of events (which are used in the likelihood function) are presented in the following list:

1. Number of expected (non-$t\bar{t}$) events of $e + \not{E}_{\mathrm{T}} + 4jets$ where at least one jet is B-tagged
2. Number of expected (non-$t\bar{t}$) events of $\mu + \not{E}_{\mathrm{T}} + 4jets$ where at least one jet is B-tagged
3. Acceptance of the $t\bar{t}$ decaying to WbWb which decays to $e + \not{E}_{\mathrm{T}} + 4jets$ where at least one jet is B-tagged
4. Acceptance of the $t\bar{t}$ decaying to WbWb which decays to $\mu + \not{E}_{\mathrm{T}} + 4jets$ where at least one jet is B-tagged
5. Acceptance of the $t\bar{t}$ decaying to WbZc which decays to $e + \not{E}_{\mathrm{T}} + 4jets$ (the Z-boson is decaying into two jets) where at least one jet is B-tagged
6. Acceptance of the $t\bar{t}$ decaying to WbZc which decays to $\mu + \not{E}_{\mathrm{T}} + 4jets$ (the Z-boson is decaying into two jets) where at least one jet is B-tagged

7. Acceptance of the $t\bar{t}$ decaying to WbZc which decays to $e + \not{E}_{\rm T} + 4jets$ (the W-boson is decaying into two jets) where at least one jet is B-tagged

8. Acceptance of the $t\bar{t}$ decaying to WbZc which decays to $\mu + \not{E}_{\rm T} + 4jets$ (the W-boson is decaying into two jets) where at least one jet is B-tagged

9. Acceptance of the $t\bar{t}$ decaying to ZcZc which decays to $e + \not{E}_{\rm T} + 4jets$ where at least one jet is B-tagged

10. Acceptance of the $t\bar{t}$ decaying to ZcZc which decays to $\mu + \not{E}_{\rm T} + 4jets$ where at least one jet is B-tagged

11. Number of expected (SM background, non-$t\bar{t}$) events in the each bin of the M_{top} histogram of $Z^0 \rightarrow ee$ + four jets events where at least one jet is B-tagged

12. Number of observed (SM background, non-$t\bar{t}$) events in the each bin of the M_{top} histogram of "$Z^0 \rightarrow \mu\mu$ + four jets" events where at least one jet is B-tagged

13. Acceptance for each bin of the M_{top} histogram for the $t\bar{t} \rightarrow ZcWb \rightarrow e^+e^- + 4jets$ process. At least one jet is required to be B-tagged.

14. Acceptance for each bin of the M_{top} histogram for the $t\bar{t} \rightarrow ZcWb \rightarrow \mu^+\mu^- + 4jets$ process. At least one jet is required to be B-tagged.

15. Acceptance for each bin of the M_{top} histogram for the $t\bar{t} \rightarrow ZcZc \rightarrow e^+e^- + 4jets$ process (one Z is decaying leptonically and the other one is decaying hadronically). At least one jet is required to be B-tagged.

16. Acceptance for each bin of the M_{top} histogram for the $t\bar{t} \rightarrow ZcZc \rightarrow \mu^+\mu^- + 4jets$ process (one Z is decaying leptonically and the other one is decaying hadronically). At least one jet is required to be B-tagged.

The numbers are taken with the corresponding uncertainties and correlations. The numbers listed above are the acceptances: $A_{1,i}$, $A_{2,i}$, A_3, A_4, and A_5 (See Sec. 2) and backgrounds $Bgr(l\nu + 4jets)$ and $Bgr(l^+j^- + 4jets)$. All of these are taken for electrons and muons separately.

Numerical integration techniques allow us to incorporate all the correlations between the different acceptances and systematic uncertainties properly. We use the approach discussed and implemented in Ref. [13] to compute the values of the likelihood. The observed distribution of the likelihood (computed for 100% longitudinally polarized Z's) is presented in Figures 27 and 28.

A likelihood distribution is calculated for each given value of helicity of the $t \rightarrow Z^0c$ coupling since the acceptances A_i (i=1,..,5) vary for different structures of the FCNC coupling.

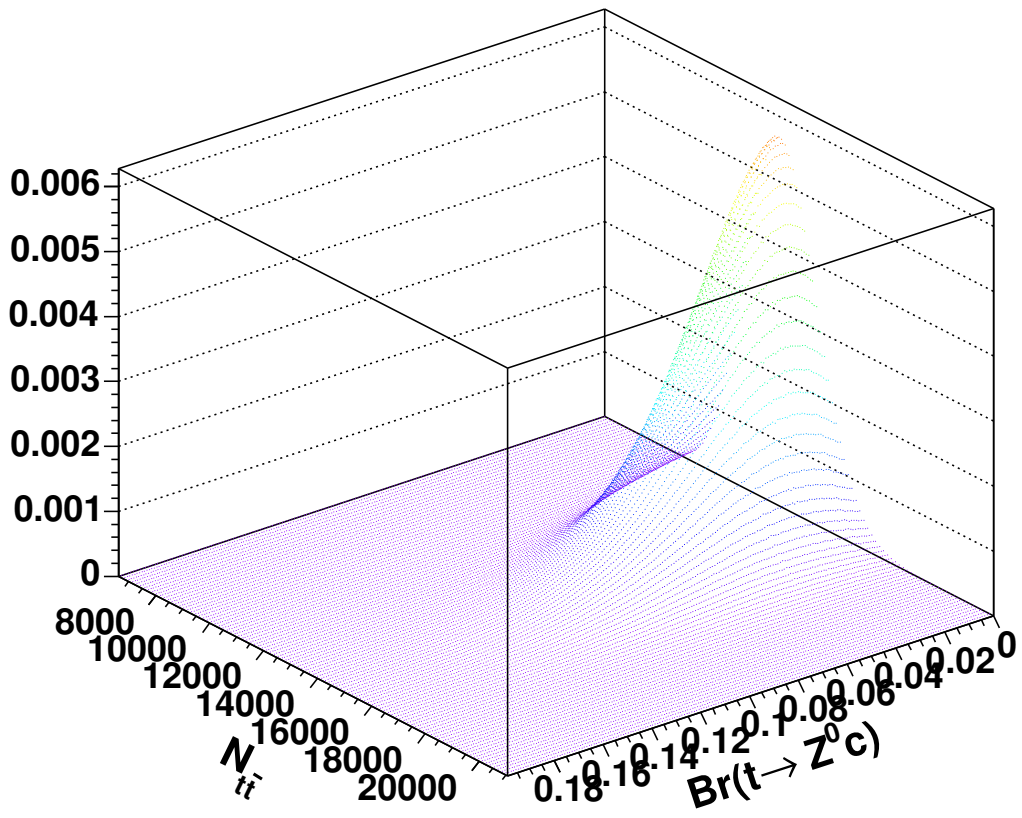

Figure 27: The 2D likelihood as a function of $N_{t\bar{t}}$ and $Br(t \to Z^0 c)$.

13.2 Computation of Posterior $P(Br(t \to Z^0 c)), N_{t\bar{t}}|observables)$ and "1σ" and "2σ" Contours

We obtain the posterior density functions $P(B_Z, N_{t\bar{t}}|observables)$ using the computed earlier distributions of $L(B_Z, N_{t\bar{t}})$. The calculation is performed for two distributions of $\pi_0(N_{t\bar{t}})$:

- Flat Prior and
- "Gaussian" prior.

The "Gaussian" prior is derived using the theoretical estimates of top pair production cross-section $\sigma(p\bar{p} \to t\bar{t})$ [14] as a function of top quark mass M_{top}, the measured M_{top} (with its uncertainties) and the uncertainty on the integrated luminosity. The measured top-quark mass is 170.9 $\pm$ 1.8 GeV [31]. The luminosity is 1.52 fb^{-1} with

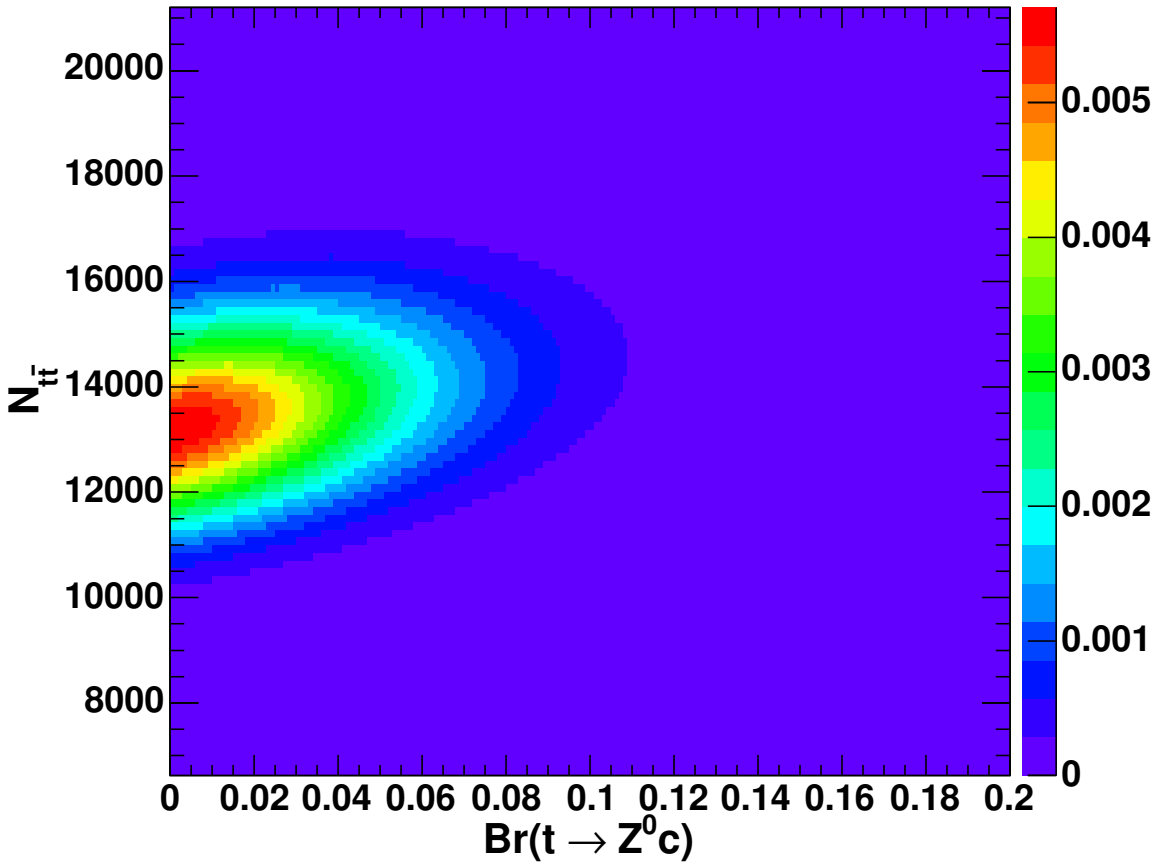

Figure 28: An alternative view of the 2D likelihood as a function of $N_{t\bar{t}}$ and $Br(t \to Z^0c)$.

an uncertainty of 6%. The "Gaussian" prior allows us to include the theoretical FCNC-independent knowledge of $\sigma(p\bar{p} \to t\bar{t})$.

A two-dimensional contour is a boundary of a set of points U with the following properties:

$$U \in \{(N_{t\bar{t}}, Br(t \to Z^0c))|N_{t\bar{t}} > 0 \; and \; 0 \leq Br(t \to Z^0c)) \leq 1\}, \tag{51}$$

$$\int\int_U dN_{t\bar{t}}dB_Z\{\; P(N_{t\bar{t}}, Br(t \to Z^0c)|observables)\} = \beta, \tag{52}$$

and

$$\forall \; x \in U \; and \; \forall \; y \in (\mathbb{R}^2 \backslash U) : \; P(x) > P(y). \tag{53}$$

The value of β is taken to be 0.95 to make a "2σ" contour and it is 0.68 for a "1σ" contour. The obtained contours are presented in Figures 29 and 43 for each fraction of longitudinally polarized Z-bosons in the FCNC decay.

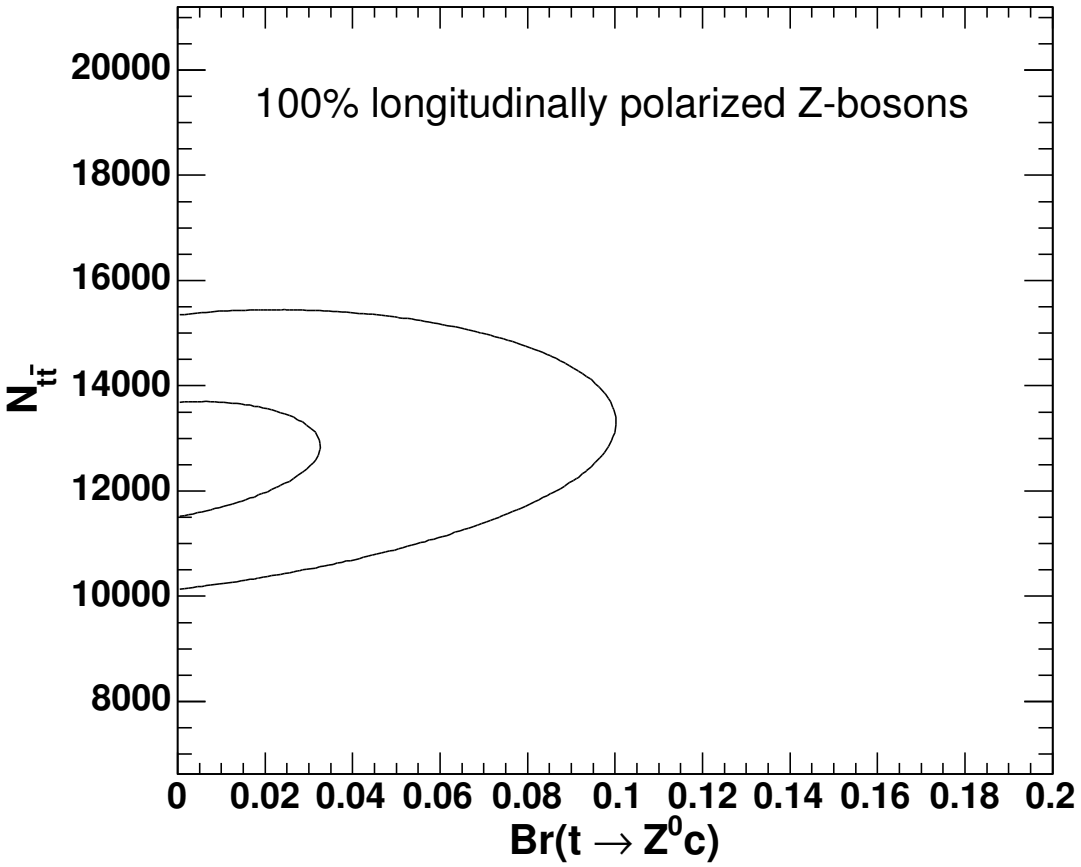

Figure 29: The "2σ"- and "1σ"- contours cover integrals of 0.95% ("2σ") and 0.68% ("1σ") of the posterior probability density function $P(N_{t\bar{t}}, Br(t \to Z^0c|observables)$ calculated using "Gaussian" prior. The points on the boundary of a given contour correspond to equal values of the posterior probability densities. In this figure we show contours for 100% longitudinally polarized Z-bosons.

13.3 Measurement of the Upper Limits on $Br(t \to Zc)$

We follow the procedure discussed in Section 2 to measure the upper limits B_Z^{lim} on $Br(t \to Zc)$ (i.e. B_Z):

$$P(observables|B_Z) = \int L(B_Z, N_{t\bar{t}}) \cdot \pi_0(N_{t\bar{t}}) dN_{t\bar{t}} \tag{54}$$

$$P(B_Z|observables) = \frac{P(observables|B_Z) \cdot \pi_1(B_Z)}{\int P(observables|B_Z) \cdot \pi_1(B_Z) dB_Z} \tag{55}$$

$$\beta = \int_0^{B_Z^{lim}} P(B_Z|observables)dB_Z, \tag{56}$$

where β is 0.95 (95% C.L). We calculate the limits for the two functions of $\pi_0(N_{t\bar{t}})$:

- Flat Prior and
- "Gaussian" prior.

The priors are described in more detail in the previous subsection.

The obtained upper limits for each given helicity and prior are summarized in Table 23. The distribution for $P(B_Z|observables)$ is shown in Figure 30. The distribution was calculated for 100% longitudinally polarized Z-bosons and "Gaussian" prior. The "Flat" prior does not include any expectation of $N_{t\bar{t}}$ so it is completely theory-independent.

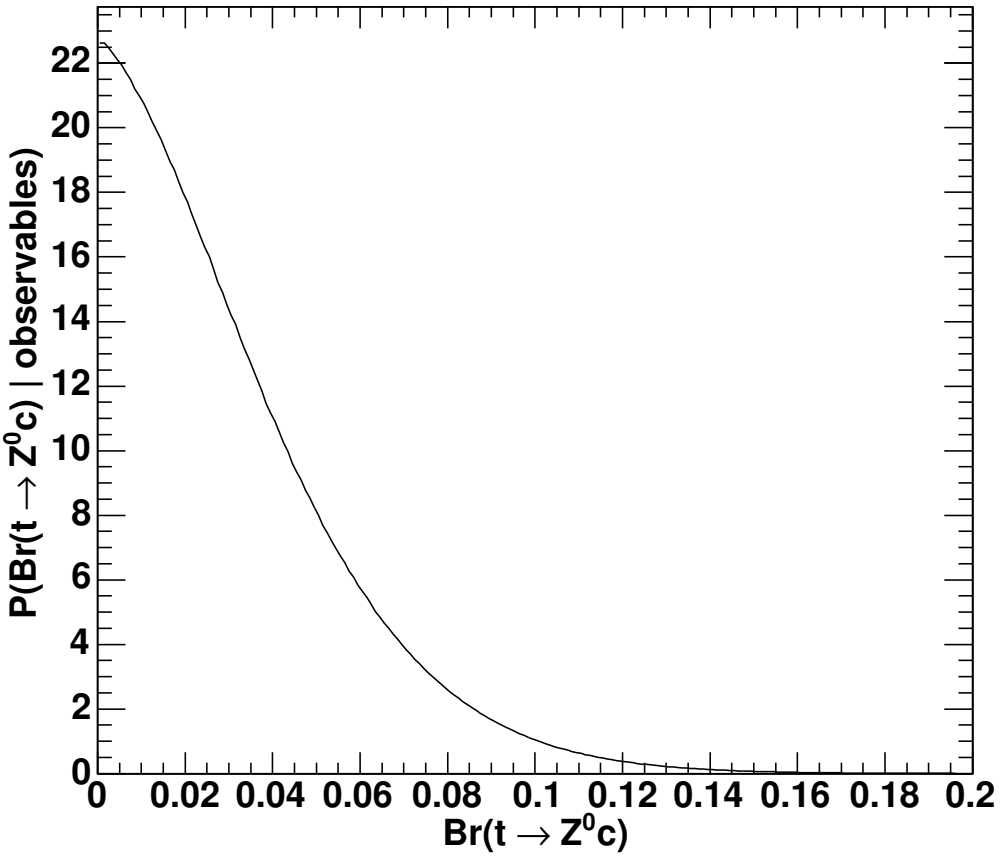

Figure 30: The distribution for $P(B_Z|observables)$. The distribution was calculated for 100% longitudinally polarized Z-bosons. The measured limit is 8.3% at 95% C.L.

We perform statistical cross-checks of the measured upper limits using pseudo-experiments. The pseudo-experiments are generated randomly assuming that the contribution from FCNC processes is not-existent (true $Br(t \to Z^0c)$ =0). The expected upper limit on $Br(t \to Z^0c)$ is 8.9 $\pm$ 2.8 % and it is consistent with the observed limit of 8.3%. The expected limit is obtained for 100% longitudinally polarized Z's and "Gaussian" prior. Also we calculate an expected limit for flat prior and 100% longitudinally polarized Z's and we obtain 9.9 $\pm$ 3.2 % (it agrees well with 9.2% observed).

14 Conclusions and Results

In the process of a signature-based search for new physics in events with high-Pt Z bosons, we came across what could be construed as a 'bump' at 175 GeV in the Z+jet mass distribution for events with a jet tagged by the 'Loose' SecVtx-tagger. However the significance of the feature depended on the shape and normalization of the SM backgrounds. We have now done a careful job on the SM backgrounds and added much more data (luminosity). The shape of the background is, unfortunately, consistent with the SM; what was left is to place a limit on the decay mode top goes to Z+charm. The analysis is performed in two stages, as described below.

In the first stage we validate reconstruction of inclusive W- and Z-bosons that play a crucial role in the the analysis. This checks lepton identification, geometric acceptances, and code for both data and Monte Carlo simulation datasets over the multi-year set of runs.

The second stage is the actual measurement of the upper limit on the branching ratio of the flavor-changing top quark decay $t \to Z^0c$. We assume and we know that this decay mode is small compared to the SM charged current decay of the top, $t \to W^+b$. We normalize to Z+2 jets, as the one-jet bin has matrix element contributions that differ from the those in the higher jet bins. We use a 2-dimensional likelihood $P(observables|N_{t\bar{t}}, Br(t \to Z^0c))$ to evaluate the posterior distribution $P(N_{t\bar{t}}, Br(t \to Z^0c)|observables)$ which is used to set limits on the FCNC branching ratio.

We then impose the prior knowledge of the top quark mass, 170.9 $\pm$ 1.8 GeV, to extract a 1-dimensional limit. Taking into account systematic uncertainties on Monte Modeling, B-tagging, mistag modeling, and lepton identification, etc., we find an upper limit at 95% C.L. on the branching ratio of $t \to Z^0c$ of 8.3% for FCNC decays where the Z-bosons are 100% longitudinally polarized. In addition to that we compute the same limits using flat prior for the distribution of $N_{t\bar{t}}$ so that it does not include any theoretical knowledge about the top-pair production cross-section.

To be assumption-independent we parametrize the limit on $Br(t \to Z^0c)$ as a function of the fraction of longitudinally polarized Z-bosons. The parametrization allows us to cover the full range of all possible helicity structures of the $t \to Z^0c$ vertex. The upper limits are calculated at 95% C.L. for five fractions of longitudinally polarized Z's using 1.52 fb^{-1} of data. The results are presented in Table 23.

Fraction of Longitudinal Z-bosons	0.00	0.25	0.50	0.75	1.0
Gaussian prior	9.0%	8.8%	8.6%	8.5%	8.3%
Flat prior	10.2%	10.0%	9.7%	9.5%	9.2%

Table 23: The upper limits on the Br($t \to Z^0c$) in % calculated for five helicity structures of the Z-bosons in the FCNC coupling ($t \to Z^0c$) at 95% CL. The limits with Gaussian prior include our knowledge about theoretical cross-section of $\sigma(p\bar{p} \to t\bar{t})$, and the ones with Flat prior are theory-independent.

15 Acknowledgments

We are grateful to Collin Wolfe, Carla Grosso-Pilcher, Fabio Maltoni, Johan Alwall, Michelangelo Mangano, and Charles Plager. Special thanks to Jahred Adelman for help modifying the top mass fitter for the FCNC case. We are in debt to Kevin Lannon, Jason Nielsen, and Beate Heinemann for their reviewing the paper. We thank Mary Heintz for her invaluable system support. We highly appreciate the help of Michele Papucci and Rikkert Fredrix in understanding the pitfalls of exotic FCNC models.

16 Possible Additions to the Analysis

There is a possibility of including an additional final state of $t\bar{t}$ decay which has two leptons, $\not\!\!E_{\mathrm{T}}$ and two jets. This will improve the analysis by putting an additional constraint on the $t\bar{t} \rightarrow WbWb \rightarrow l_1^+ l_2^- + bb + \not\!\!E_{\mathrm{T}}$ decay mode. Similarly, considering events with different number of B-tagged jets can play a valuable role in getting a better result. We do not use this two improvements due to low statistics of the observed events.

A Fractions of Backgrounds for Inclusive W- and Z-bosons

Process	0 Jets	1 Jet	2 Jets	3 Jets	4 Jets	≥5 Jets	All Jets
$W + jets$	649059.75±1384.83	114026.28±579.97	19360.37±238.96	2532.84±86.42	324.40±30.93	47.25±11.81	785350.89±1523.09
$W \to \tau\nu$	16256.40±115.44	3351.14±52.35	711.86±24.14	123.54±10.05	14.73±3.47	2.46±1.42	20460.14±129.48
$Z \to ee$	2948.51±16.18	1960.90±13.19	707.43±7.92	176.25±3.95	33.17±1.72	6.74±0.77	5833.00±22.76
dibosons	134.17±2.24	257.42±3.26	437.05±4.23	146.53±2.43	38.21±1.24	9.42±0.61	1022.80±6.43
$Z \to \tau\tau$	634.51±5.76	190.74±3.15	81.97±2.07	22.86±1.09	4.69±0.49	0.37±0.14	935.14±6.99
$t\bar{t}$	0.24±0.02	7.31±0.12	58.83±0.35	139.16±0.53	192.28±0.63	103.85±0.46	501.67±1.01
$Total$	669033.58±1389.74	119793.79±582.50	21357.51±240.35	3141.19±87.14	607.48±31.21	170.09±11.95	814103.64±1528.78
Observed	678362.00	108008.00	22332.00	4614.00	1081.00	331	814728

Table 24: Summary of observed events and backgrounds for production of $W \to e\nu$ + N jets. The uncertainties are due to statistics of the simulated processes.

Process	0 Jets	1 Jet	2 Jets	3 Jets	4 Jets	≥5 Jets	All Jets
$W + jets$	97.01±0.02	95.19±0.05	90.65±0.15	80.63±0.60	53.40±2.40	27.78±5.02	96.47±0.48
$W \to \tau\nu$	2.43±0.02	2.80±0.04	3.33±0.12	3.93±0.33	2.43±0.57	1.45±0.83	2.51±0.02
$Z \to ee$	0.44±0.00	1.64±0.01	3.31±0.05	5.61±0.20	5.46±0.39	3.96±0.52	0.72±0.00
dibosons	0.02±0.00	0.21±0.00	2.05±0.03	4.66±0.15	6.29±0.38	5.54±0.51	0.13±0.00
$Z \to \tau\tau$	0.09±0.00	0.16±0.00	0.38±0.01	0.73±0.04	0.77±0.09	0.22±0.08	0.11±0.00
$t\bar{t}$	0.00±0.00	0.01±0.00	0.28±0.00	4.43±0.12	31.65±1.63	61.06±4.29	0.06±0.00

Table 25: Summary of fractions of individual processes contributing to production of $W \to e\nu$ + N jets. The fractions are given in %.

Process	0 Jets	1 Jet	2 Jets	3 Jets	4 Jets	≥5 Jets	All Jets
$W + Jets$	509948.19±572.75	90896.29±241.82	15410.23±99.57	2231.47±37.93	299.43±13.87	48.78±5.61	618834.37±630.95
$W \to \tau\nu$	13047.02±99.97	2726.04±45.66	568.29±20.80	77.24±7.68	16.86±3.60	3.00±1.50	16438.43±112.19
$Z \to \mu\mu$	46322.91±67.19	9391.24±30.22	1842.96±13.38	295.48±5.37	47.94±2.15	5.38±0.72	57905.90±75.10
dibosons	95.40±1.80	184.76±2.66	312.15±3.45	105.43±1.99	27.70±1.02	6.63±0.50	732.07±5.24
$Z \to \tau\tau$	432.97±4.62	132.21±2.55	55.16±1.65	15.08±0.86	3.14±0.39	0.58±0.17	639.15±5.62
$t\bar{t}$	0.21±0.02	7.35±0.13	57.89±0.37	137.03±0.58	191.60±0.68	103.19±0.50	497.28±1.10
$Total$	569846.70±585.30	103337.90±247.97	18246.68±102.67	2861.73±39.14	586.66±14.55	167.54±5.90	695047.21±645.28
Observed	577785.00	93049.00	18917.00	3761.00	907.00	224	694643

Table 26: Summary of observed events and backgrounds for production of $W \to \mu\nu$ + N jets. The uncertainties are due to statistics of the simulated processes.

Process	0 Jets	1 Jet	2 Jets	3 Jets	4 Jets	≥5 Jets	All Jets
$W + Jets$	89.49±0.02	87.96±0.05	84.45±0.14	77.98±0.39	51.04±1.22	29.11±2.39	89.03±0.18
$W \to \tau\nu$	2.29±0.02	2.64±0.04	3.11±0.11	2.70±0.26	2.87±0.60	1.79±0.88	2.37±0.02
$Z \to \mu\mu$	8.13±0.01	9.09±0.03	10.10±0.09	10.33±0.22	8.17±0.39	3.21±0.43	8.33±0.01
dibosons	0.02±0.00	0.18±0.00	1.71±0.02	3.68±0.08	4.72±0.20	3.95±0.32	0.11±0.00
$Z \to \tau\tau$	0.08±0.00	0.13±0.00	0.30±0.01	0.53±0.03	0.53±0.07	0.35±0.10	0.09±0.00
$t\bar{t}$	0.00±0.00	0.01±0.00	0.32±0.00	4.79±0.07	32.66±0.81	61.59±2.16	0.07±0.00

Table 27: Summary of fractions of individual processes contributing to production of $W \to \mu\nu$ + N jets. The fractions are given in %.

Process	0 Jets	1 Jet	2 Jets	3 Jets	4 Jets	≥5 Jets	All Jets
Drell-Yan	66480.40±76.90	13267.55±34.31	2350.92±14.45	345.07±5.54	40.15±1.89	6.71±0.78	82490.80±85.64
ZZ	5.64±0.17	3.80±0.14	5.26±0.16	1.97±0.10	0.46±0.05	0.13±0.03	17.26±0.29
WZ	9.50±0.36	11.65±0.40	16.82±0.48	5.56±0.28	1.22±0.13	0.23±0.06	44.98±0.79
WW	20.93±0.98	5.05±0.48	1.36±0.25	0.13±0.08	0.05±0.05	0.00±0.00	27.52±1.12
$Z \to \tau\tau$	62.42±1.80	12.03±0.79	2.07±0.33	0.31±0.13	0.05±0.05	0.00±0.00	76.87±2.00
$t\bar{t}$	0.06±0.01	1.60±0.06	8.60±0.13	3.09±0.08	0.86±0.04	0.26±0.02	14.47±0.17
samesignee	47.90±18.23	20.74±9.21	4.71±4.06	5.97±2.71	-0.38±0.19	0.00±0.00	78.94±21.00
Total	66626.85±79.06	13322.42±35.54	2389.74±15.03	362.10±6.18	42.41±1.91	7.34±0.78	82750.85±88.21
Observed	68160.00	11834.00	2322.00	482.00	84.00	19	82901

Table 28: Summary of observed events and backgrounds for production of $Z^0 \to ee$ + N jets. The uncertainties are due to statistics of the simulated processes.

Process	0 Jets	1 Jet	2 Jets	3 Jets	4 Jets	≥5 Jets	All Jets
Drell-Yan	99.78±0.03	99.59±0.07	98.38±0.17	95.30±0.72	94.68±0.60	91.44±1.23	99.69±8.11
ZZ	0.01±0.00	0.03±0.00	0.22±0.01	0.54±0.03	1.08±0.12	1.79±0.39	0.02±0.00
WZ	0.01±0.00	0.09±0.00	0.70±0.02	1.53±0.08	2.87±0.32	3.19±0.82	0.05±0.00
WW	0.03±0.00	0.04±0.00	0.06±0.01	0.04±0.02	0.11±0.11	0.00±nan	0.03±0.00
$Z \to \tau\tau$	0.09±0.00	0.09±0.01	0.09±0.01	0.08±0.03	0.12±0.12	0.00±nan	0.09±0.00
$t\bar{t}$	0.00±0.00	0.01±0.00	0.36±0.01	0.85±0.03	2.04±0.13	3.58±0.49	0.02±0.00
samesignee	0.07±0.03	0.16±0.07	0.20±0.17	1.65±0.74	-0.89±-0.45	0.00±nan	0.10±0.03

Table 29: Summary of fractions of individual processes contributing to production of $Z^0 \to ee$ + N jets. The fractions are given in %.

Process	0 Jets	1 Jet	2 Jets	3 Jets	4 Jets	≥5 Jets	All Jets
Drell-Yan	42155.51±65.97	9038.71±30.51	1677.06±13.14	253.08±5.11	36.26±1.93	6.45±0.82	53167.06±74.07
WZ	6.62±0.30	8.40±0.34	11.84±0.40	3.92±0.23	1.26±0.13	0.19±0.05	32.23±0.67
ZZ	3.70±0.13	2.70±0.11	3.99±0.14	1.22±0.08	0.38±0.04	0.16±0.03	12.15±0.24
WW	21.16±0.99	5.10±0.49	1.38±0.25	0.13±0.08	0.05±0.05	0.00±0.00	27.83±1.13
$Z \to \tau\tau$	33.44±1.32	6.04±0.56	1.10±0.24	0.47±0.16	0.00±0.00	0.00±0.00	41.04±1.47
$t\bar{t}$	0.06±0.01	1.35±0.05	7.63±0.12	2.64±0.07	0.70±0.04	0.17±0.02	12.54±0.16
Total	42220.48±66.00	9062.30±30.52	1703.00±13.16	261.47±5.11	38.64±1.94	6.96±0.82	53292.85±74.10
Observed	43001.00	8285.00	1670.00	334.00	61.00	17	53368

Table 30: Summary of observed events and backgrounds for production of $Z^0 \to \mu\mu$ + N jets. The uncertainties are due to statistics of the simulated processes.

Process	0 Jets	1 Jet	2 Jets	3 Jets	4 Jets	≥5 Jets	All Jets
Drell-Yan	99.85±0.00	99.74±0.01	98.48±0.03	96.79±0.13	93.83±0.48	92.56±1.20	99.76±1.58
WZ	0.02±0.00	0.09±0.00	0.70±0.02	1.50±0.09	3.26±0.37	2.76±0.79	0.06±0.00
ZZ	0.01±0.00	0.03±0.00	0.23±0.01	0.47±0.03	0.98±0.12	2.29±0.47	0.02±0.00
WW	0.05±0.00	0.06±0.01	0.08±0.01	0.05±0.03	0.12±0.12	0.00±nan	0.05±0.00
$Z \to \tau\tau$	0.08±0.00	0.07±0.01	0.06±0.01	0.18±0.06	0.00±nan	0.00±nan	0.08±0.00
$t\bar{t}$	0.00±0.00	0.01±0.00	0.45±0.01	1.01±0.03	1.80±0.13	2.39±0.38	0.02±0.00

Table 31: Summary of fractions of individual processes contributing to production of $Z^0 \to \mu\mu$ + N jets. The fractions are given in %.

B Fractions of Backgrounds for W- and Z-bosons Produced with a B-tagged Jet.

Process	1 Jet	2 Jets	3 Jets	4 Jets	≥5 Jets	All Jets
$t\bar{t}$	4.06±0.10	45.13±0.34	113.12±0.53	167.11±0.65	90.38±0.48	419.81±1.03
$W + b\bar{b}$	246.32±1.26	216.87±1.02	77.58±0.44	21.81±0.19	5.94±0.08	568.52±1.70
$W + c\bar{c}$	105.63±0.92	106.33±0.78	43.86±0.36	13.50±0.16	4.14±0.08	273.46±1.27
$W + c$	424.74±3.49	161.74±1.38	41.34±0.50	8.78±0.15	1.99±0.06	638.60±3.79
mistags	715.83±6.26	365.69±4.99	131.59±3.50	38.76±1.98	15.06±1.43	1266.92±9.08
dibosons	7.67±0.52	26.83±0.95	11.71±0.64	4.03±0.37	0.95±0.17	51.19±1.32
$fakeW$	29.94±0.11	45.77±0.29	32.45±0.38	11.84±0.28	5.15±0.27	125.15±0.63
$Total$	1534.19±7.36	968.36±5.44	451.66±3.70	265.84±2.16	123.61±1.55	3343.66±10.22
Observed	1497.00	934.00	427.00	252.00	121	3231

Table 32: Summary of observed events and backgrounds for production of "$W \to e\nu$+ N jets" with at least one B-tagged jet. The uncertainties are due to statistics of the simulated processes.

Process	1 Jet	2 Jets	3 Jets	4 Jets	≥5 Jets	All Jets
$t\bar{t}$	0.26±0.01	4.66±0.04	25.05±0.22	62.86±0.50	73.12±0.88	12.56±0.05
$W + b\bar{b}$	16.06±0.10	22.40±0.15	17.18±0.16	8.20±0.09	4.80±0.09	17.00±0.08
$W + c\bar{c}$	6.88±0.06	10.98±0.09	9.71±0.11	5.08±0.07	3.35±0.07	8.18±0.05
$W + c$	27.68±0.20	16.70±0.15	9.15±0.12	3.30±0.06	1.61±0.05	19.10±0.13
mistags	46.66±0.25	37.76±0.33	29.13±0.55	14.58±0.64	12.18±1.02	37.89±0.28
dibosons	0.50±0.03	2.77±0.10	2.59±0.14	1.52±0.14	0.77±0.14	1.53±0.04
$fakeW$	1.95±0.01	4.73±0.04	7.19±0.10	4.46±0.11	4.17±0.22	3.74±0.02

Table 33: Summary of fractions of individual processes contributing to production of "$W \to e\nu$+ N jets" with at least one B-tagged jet. The fractions are given in %.

Process	1 Jet	2 Jets	3 Jets	4 Jets	≥5 Jets	All Jets
$t\bar{t}$	3.14±0.08	34.78±0.28	87.24±0.45	129.91±0.55	70.70±0.41	325.76±0.87
$W + b\bar{b}$	192.20±1.07	170.32±0.87	60.09±0.37	16.79±0.15	4.77±0.07	444.18±1.44
$W + c\bar{c}$	81.82±0.77	83.04±0.66	34.58±0.31	10.87±0.14	3.30±0.07	213.60±1.07
$W + c$	335.37±2.96	122.28±1.13	31.97±0.42	6.79±0.15	1.47±0.06	497.89±3.20
$mistags$	621.81±5.57	302.63±4.44	105.73±3.01	32.32±1.81	10.48±1.27	1072.98±8.04
dibosons	5.64±0.43	19.50±0.78	7.77±0.49	2.79±0.31	0.80±0.16	36.50±1.08
$fakeW$	4.29±0.02	6.80±0.04	4.04±0.05	5.69±0.14	2.16±0.13	22.99±0.20
$Total$	1244.27±6.46	739.37±4.78	331.43±3.15	205.16±1.94	93.68±1.35	2613.90±8.95
Observed	1430.00	756.00	311.00	219.00	83	2799

Table 34: Summary of observed events and backgrounds for production of "$W \to \mu\nu$ + N jets" with at least one B-tagged jet. The uncertainties are due to statistics of the simulated processes.

Process	1 Jet	2 Jets	3 Jets	4 Jets	≥5 Jets	All Jets
$t\bar{t}$	0.25±0.01	4.70±0.05	26.32±0.27	63.32±0.58	75.47±1.04	12.46±0.06
$W + b\bar{b}$	15.45±0.11	23.04±0.17	18.13±0.19	8.18±0.10	5.09±0.10	16.99±0.09
$W + c\bar{c}$	6.58±0.07	11.23±0.11	10.43±0.13	5.30±0.08	3.52±0.08	8.17±0.05
$W + c$	26.95±0.21	16.54±0.16	9.65±0.15	3.31±0.08	1.57±0.06	19.05±0.14
mistags	49.97±0.26	40.93±0.37	31.90±0.63	15.75±0.75	11.19±1.20	41.05±0.32
dibosons	0.45±0.03	2.64±0.10	2.34±0.15	1.36±0.15	0.86±0.17	1.40±0.04
fake W	0.34±0.00	0.92±0.01	1.22±0.02	2.78±0.07	2.30±0.14	0.88±0.01

Table 35: Summary of fractions of individual processes contributing to production of "$W \to \mu\nu$ + N jets" with at least one B-tagged jet. The fractions are given in %.

Process	1 Jet	2 Jets	3 Jets	4 Jets	≥5 Jets	All Jets
$Z + b\bar{b}, Alpgen$	35.05±0.32	28.49±0.25	10.00±0.11	2.62±0.04	0.72±0.02	76.88±0.42
$Z + c\bar{c}, Alpgen$	14.94±0.26	13.65±0.21	5.36±0.10	1.53±0.04	0.42±0.02	35.90±0.35
$mistags$	73.50±1.87	32.34±1.39	12.17±1.02	2.96±0.50	1.41±0.56	122.38±2.65
ZZ	0.20±0.03	0.75±0.06	0.33±0.04	0.05±0.02	0.04±0.01	1.39±0.08
WZ	0.22±0.05	0.66±0.09	0.31±0.06	0.09±0.03	0.01±0.01	1.30±0.13
$t\bar{t}$	0.67±0.04	5.24±0.10	1.87±0.06	0.52±0.03	0.15±0.02	8.45±0.13
$Total$	124.58±1.91	81.15±1.43	30.04±1.04	7.77±0.51	2.75±0.56	246.29±2.71
Observed	150.00	76.00	35.00	6.00	3	270

Table 36: Summary of observed events and backgrounds for production of "$Z^0 \to ee$ + N jets" with at least one B-tag. The uncertainties are due to statistics of the simulated processes.

Process	1 Jet	2 Jets	3 Jets	4 Jets	≥5 Jets	All Jets
$Z + b\bar{b}, Alpgen$	28.13±0.46	35.12±0.64	33.28±1.17	33.68±2.22	26.23±5.34	31.21±0.52
$Z + c\bar{c}, Alpgen$	11.99±0.26	16.83±0.36	17.85±0.67	19.70±1.34	15.08±3.10	14.58±0.23
mistags	59.00±0.65	39.85±1.04	40.53±2.04	38.08±4.02	51.26±9.90	49.69±1.10
ZZ	0.16±0.02	0.93±0.07	1.11±0.14	0.70±0.21	1.36±0.55	0.56±0.03
WZ	0.18±0.04	0.82±0.11	1.02±0.21	1.15±0.44	0.50±0.51	0.53±0.05
$t\bar{t}$	0.54±0.03	6.46±0.16	6.21±0.29	6.68±0.58	5.56±1.28	3.43±0.07

Table 37: Summary of fractions of individual processes contributing to production of "$Z^0 \to ee$+ N jets" with at least one B-tag. The fractions are given in %.

Process	1 Jet	2 Jets	3 Jets	4 Jets	≥5 Jets	All Jets
$Z + b\bar{b}, Alpgen$	29.90±0.29	25.18±0.23	8.90±0.10	2.40±0.04	0.67±0.02	67.04±0.38
$Z + c\bar{c}, Alpgen$	12.89±0.24	11.87±0.19	4.69±0.09	1.41±0.04	0.45±0.02	31.31±0.32
$mistags$	60.80±1.63	26.71±1.25	8.67±0.79	2.20±0.47	1.25±0.37	99.64±2.29
ZZ	0.17±0.03	0.55±0.05	0.19±0.03	0.05±0.01	0.03±0.01	1.00±0.07
WZ	0.16±0.05	0.67±0.09	0.26±0.06	0.08±0.03	0.06±0.03	1.22±0.13
$t\bar{t}$	0.58±0.03	4.90±0.10	1.64±0.06	0.46±0.03	0.11±0.01	7.68±0.12
$Total$	104.50±1.68	69.88±1.30	24.35±0.81	6.59±0.47	2.56±0.37	207.88±2.35
Observed	134.00	75.00	32.00	8.00	3	252

Table 38: Summary of observed events and backgrounds for production of "$Z^0 \to \mu\mu$ + N jets" with at least one B-tag. The uncertainties are due to statistics of the simulated processes.

Process	1 Jet	2 Jets	3 Jets	4 Jets	≥5 Jets	All Jets
$Z + bb, Alpgen$	28.61±0.49	36.03±0.69	36.53±1.23	36.38±2.62	26.04±3.82	32.25±0.56
$Z + c\bar{c}, Alpgen$	12.33±0.28	16.99±0.39	19.28±0.70	21.37±1.59	17.46±2.61	15.06±0.25
mistags	58.18±0.69	38.23±1.12	35.60±2.11	33.37±4.72	48.85±7.45	47.93±1.12
ZZ	0.17±0.03	0.79±0.07	0.79±0.12	0.75±0.23	1.08±0.46	0.48±0.03
WZ	0.16±0.04	0.95±0.13	1.05±0.24	1.15±0.47	2.45±1.13	0.59±0.06
$t\bar{t}$	0.55±0.03	7.01±0.18	6.75±0.31	6.97±0.65	4.12±0.80	3.70±0.07

Table 39: Summary of fractions of individual processes contributing to production of "$Z^0 \to \mu\mu$ + N jets" with at leas one B-tag. The fractions are given in %.

C Jet Multiplicity Modeling in Alpgen.

Process	0 Jets	1 Jet	2 Jets	3 Jets	4 Jets	$\geq$5 Jets	All Jets
$Drell-Yan$	42792.14±77.26	7654.95±20.00	1377.66±5.67	244.66±1.73	43.38±0.58	8.25±0.11	52121.04±80.03
$Z+c, Alpgen$	349.59±1.29	255.04±0.96	121.14±0.55	35.16±0.23	8.45±0.09	2.15±0.04	771.54±1.72
$Z+b, Alpgen$	150.99±0.66	130.31±0.56	65.76±0.34	20.11±0.14	5.05±0.05	1.29±0.02	373.50±0.94
WZ	6.07±0.28	7.71±0.31	10.87±0.37	3.60±0.21	1.16±0.12	0.18±0.05	29.59±0.61
ZZ	3.40±0.12	2.48±0.10	3.67±0.13	1.12±0.07	0.35±0.04	0.15±0.03	11.16±0.22
WW	19.43±0.91	4.69±0.45	1.26±0.23	0.12±0.07	0.04±0.04	0.00±0.00	25.55±1.04
$Z \to \tau\tau$	30.70±1.22	5.55±0.52	1.01±0.22	0.43±0.14	0.00±0.00	0.00±0.00	37.68±1.35
$t\bar{t}$	0.06±0.01	1.40±0.05	7.94±0.13	2.75±0.08	0.73±0.04	0.17±0.02	13.06±0.17
$Total$	43352.38±77.29	8062.13±20.05	1589.32±5.74	307.96±1.78	59.15±0.60	12.18±0.13	53383.12±80.07
Observed	43001.00	8285.00	1670.00	334.00	61.00	17	53368

Table 40: Summary of observed events and backgrounds for production of $Z^0 \to \mu\mu$ + N jets. The uncertainties are due to statistics of the simulated processes. The simulated "Z+Jets" (Drell-Yan, Z+c, and Z+b) processes are produced with Alpgen.

Process	0 Jets	1 Jet	2 Jets	3 Jets	4 Jets	≥5 Jets	All Jets
$Drell-Yan$	98.71±0.01	94.95±0.02	86.68±0.07	79.45±0.15	73.34±0.34	67.73±0.49	97.64±0.26
$Z+c, Alpgen$	0.81±0.00	3.16±0.01	7.62±0.04	11.42±0.09	14.29±0.20	17.63±0.32	1.45±0.00
$Z+b, Alpgen$	0.35±0.00	1.62±0.01	4.14±0.03	6.53±0.06	8.53±0.12	10.57±0.19	0.70±0.00
WZ	0.01±0.00	0.10±0.00	0.68±0.02	1.17±0.07	1.95±0.20	1.45±0.38	0.06±0.00
ZZ	0.01±0.00	0.03±0.00	0.23±0.01	0.36±0.02	0.59±0.07	1.20±0.21	0.02±0.00
WW	0.04±0.00	0.06±0.01	0.08±0.01	0.04±0.02	0.07±0.07	0.00±nan	0.05±0.00
$Z \to \tau\tau$	0.07±0.00	0.07±0.01	0.06±0.01	0.14±0.05	0.00±nan	0.00±nan	0.07±0.00
$t\bar{t}$	0.00±0.00	0.02±0.00	0.50±0.01	0.89±0.02	1.23±0.07	1.42±0.15	0.02±0.00

Table 41: Summary of fractions of individual processes contributing to production of $Z^0 \to \mu\mu$ + N jets. The fractions are given in %. The uncertainties are due to statistics of data and simulations. The simulated "Z+Jets" (Drell-Yan, Z+c, and Z+b) processes are produced with Alpgen.

D Plots for Inclusive W- and Z-bosons on a Linear Scale

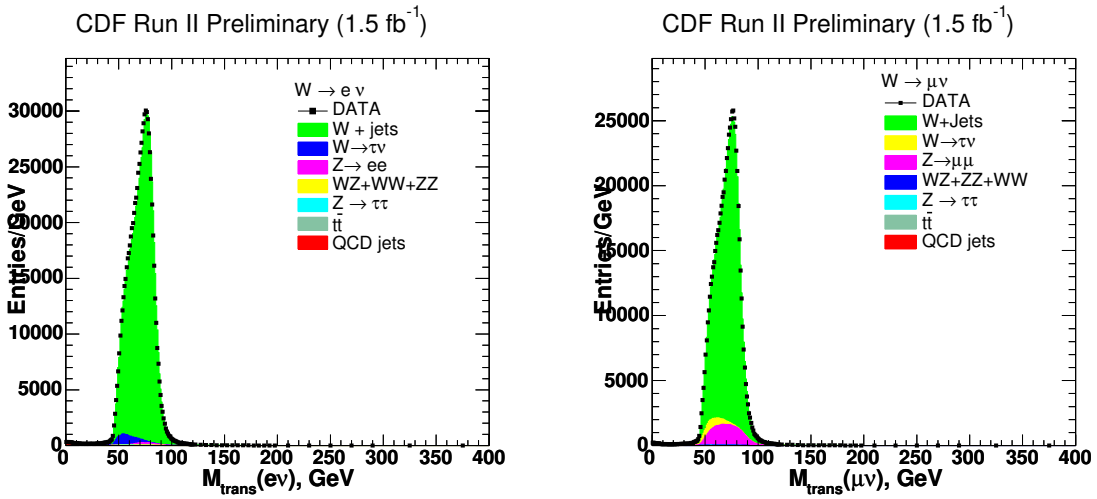

Figure 31: The observed (points) and expected ("stacked" histogram) distributions in transverse mass for $W \to e\nu$ (left) and $W \to \mu\nu$ (right).

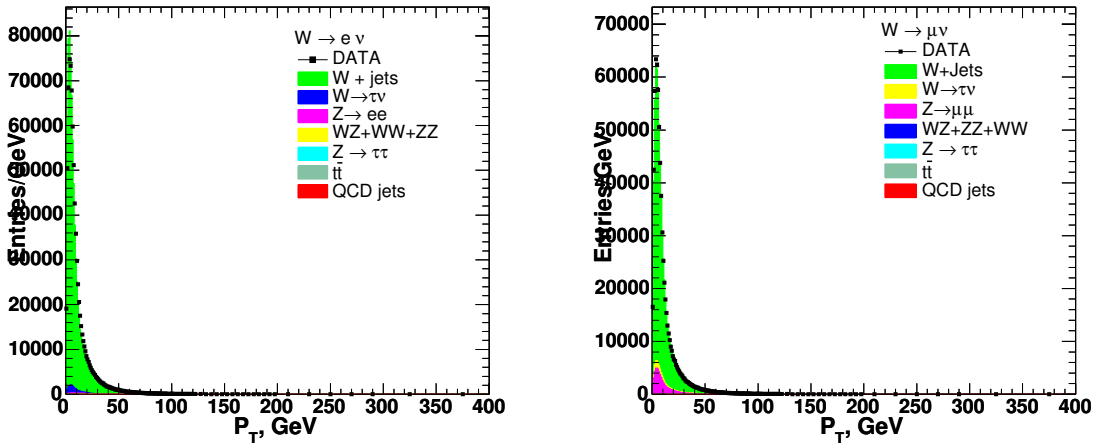

Figure 32: The observed (points) and expected (stacked histogram) distributions in the transverse momentum of the W boson for $W \to e\nu$ (left) and $W \to \mu\nu$ (right) with $M_T > 20$ GeV. (The discrepancy at large p_T in the electron sample seems to be a feature of the wtopli sample, but has negligible effect on this analysis.)

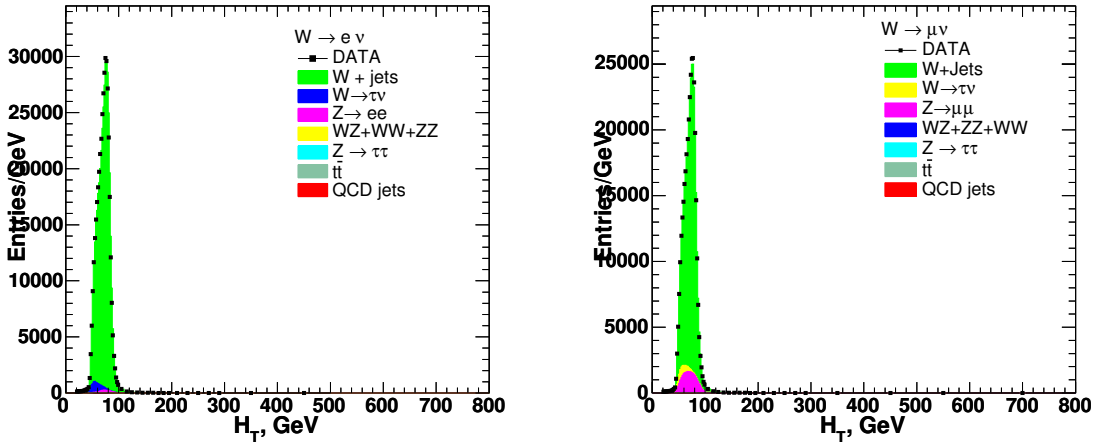

Figure 33: The observed (points) and expected (stacked histogram) distributions in H_T for $W \to e\nu$ (left) and $W \to \mu\nu$ (right) with $M_T > 20$ GeV. The discrepancy at large H_T in the wewk8m muon sample does not appear in the analogous plot for $Z^0 \to \mu\mu$, and so has no effect on this analysis (we show it for others to beware of).

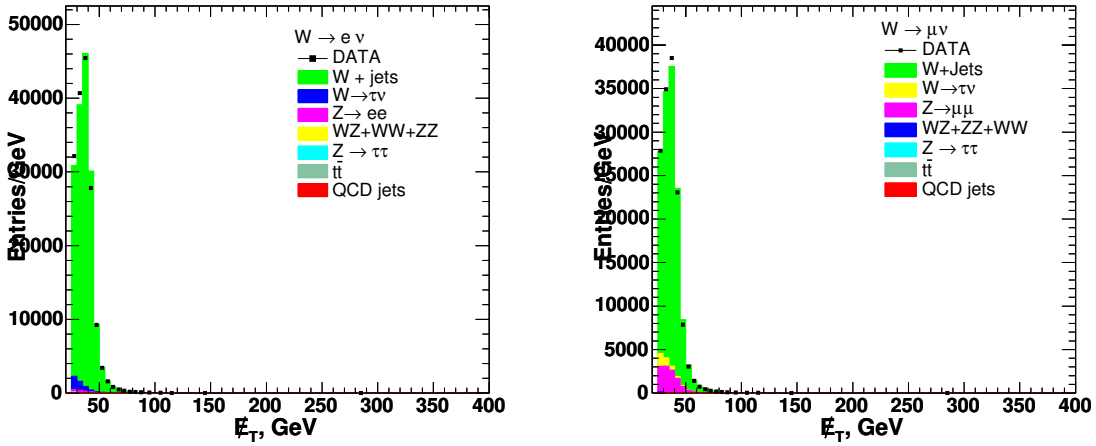

Figure 34: The observed (points) and expected (stacked histogram) distributions in $\not\!\!E_{\rm T}$ for $W \to e\nu$ (left) and $W \to \mu\nu$ (right). We select only events with $M_T > 20$ GeV to make the distribution.

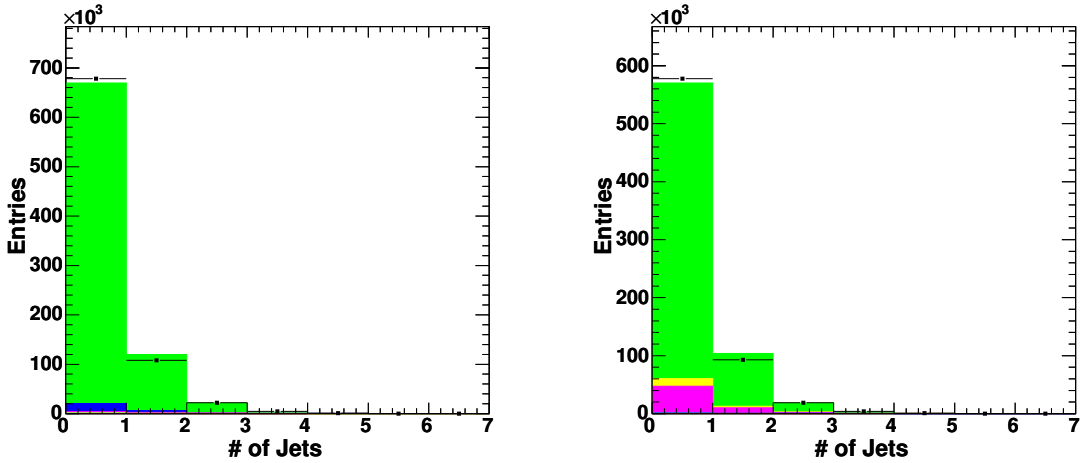

Figure 35: The observed (points) and expected (stacked histogram) distributions in the number of jets, N_{jets}, for $W \to e\nu$ (left) and $W \to \mu\nu$ (right) with $M_T > 20$ GeV.

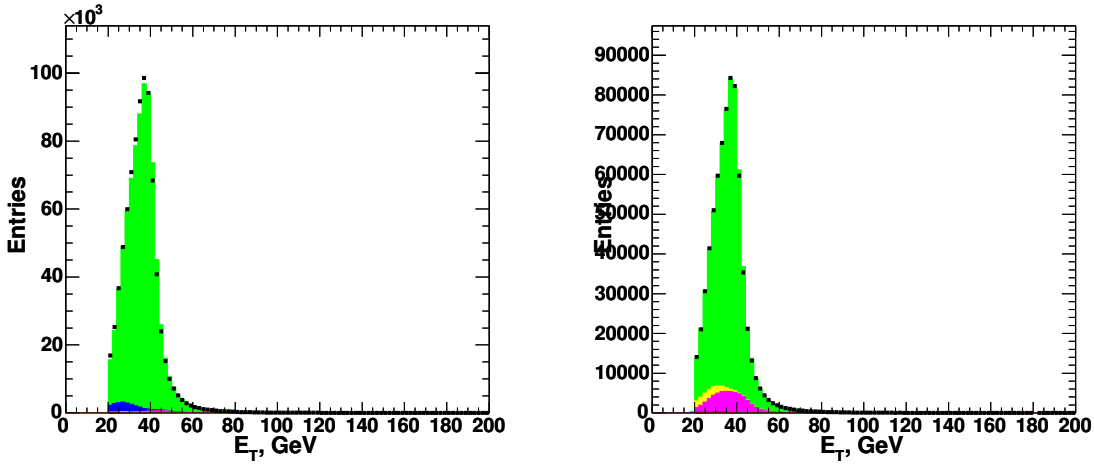

Figure 36: The observed (points) and expected (stacked histogram) distributions in the P_T of the lepton for $W \to e\nu$ (left) and $W \to \mu\nu$ (right) with $M_T > 20$ GeV.

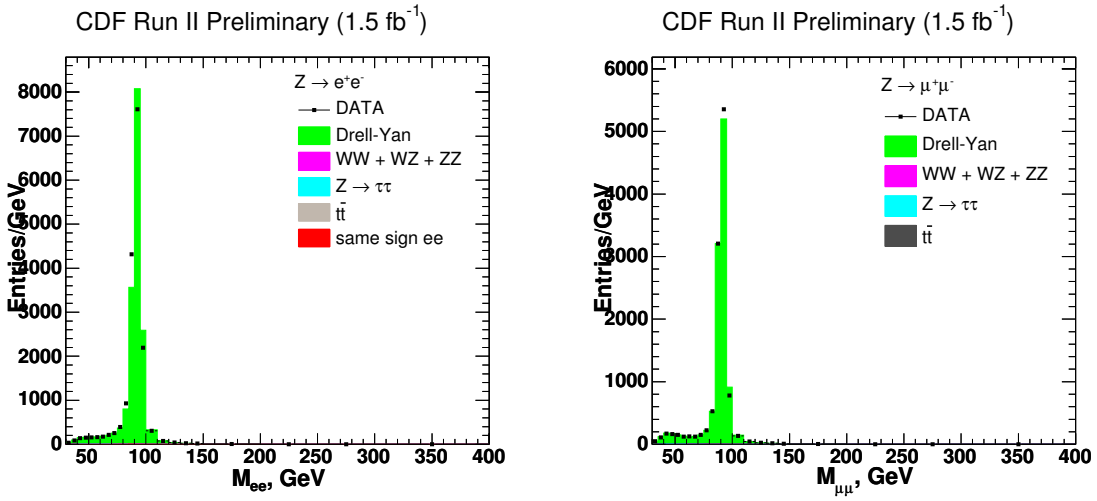

Figure 37: The observed (points) and expected (stacked histogram) distributions in the invariant mass for $Z^0 \to ee$ (left) and $Z^0 \to \mu\mu$ (right).

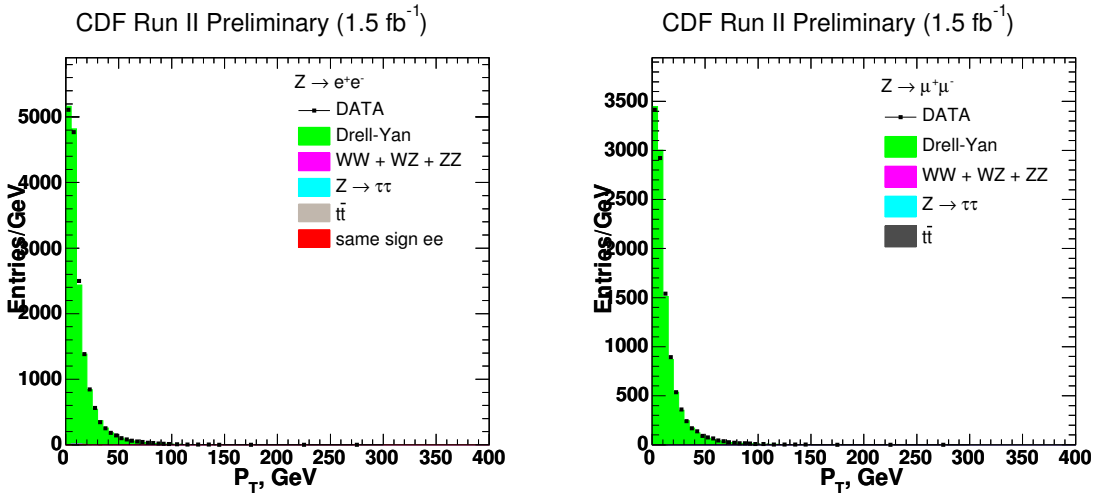

Figure 38: The observed (points) and expected (stacked histogram) distributions in transverse mass for $Z^0 \to ee$ (left) and $Z^0 \to \mu\mu$ (right). We select events with $66 < M(l^+l^-) < 116$ GeV for the histograms.

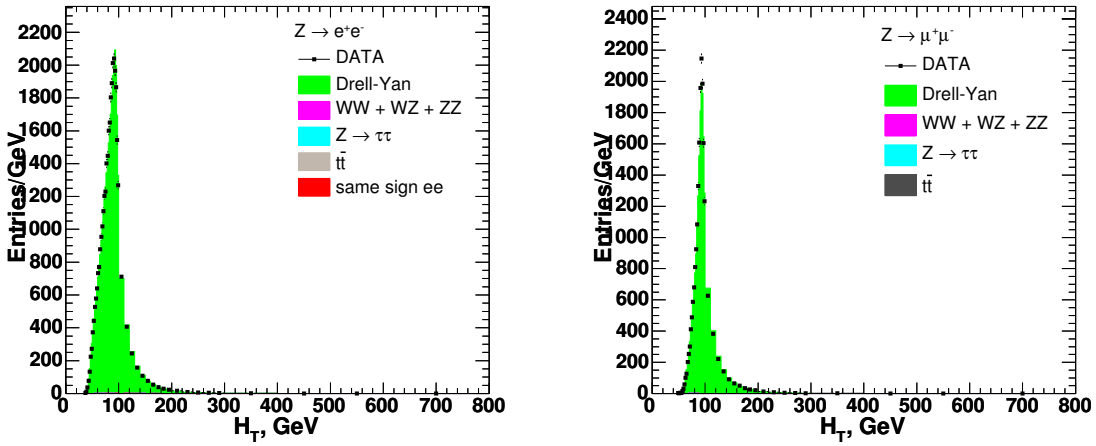

Figure 39: The observed (points) and expected (stacked histogram) distributions in H_T for $Z^0 \to ee$ (left) and $Z^0 \to \mu\mu$ (right). We select events with $66 < M(l^+l^-) < 116$ GeV for the histograms.

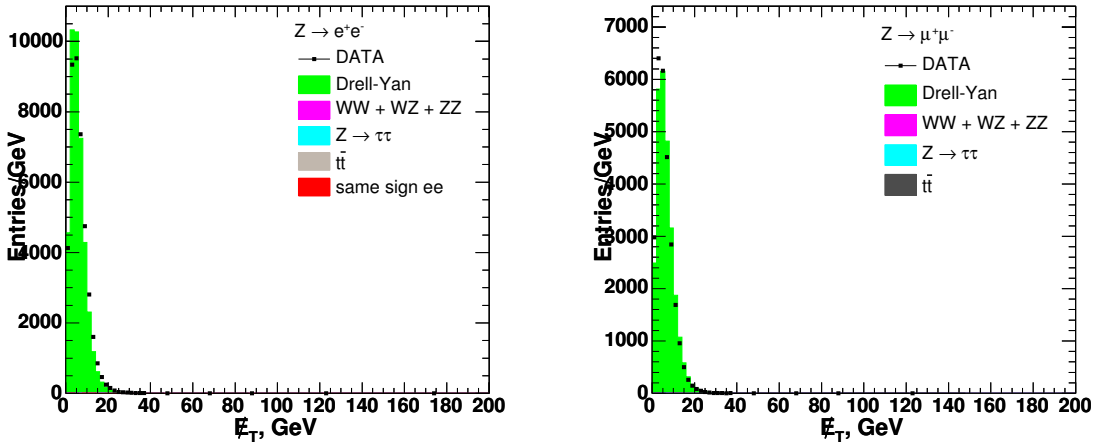

Figure 40: The observed (points) and expected (stacked histogram) distributions in $\not\!\!E_{\rm T}$ for $Z^0 \to ee$ (left) and $Z^0 \to \mu\mu$ (right). We select events with $66 < M(l^+l^-) < 116$ GeV for the histograms.

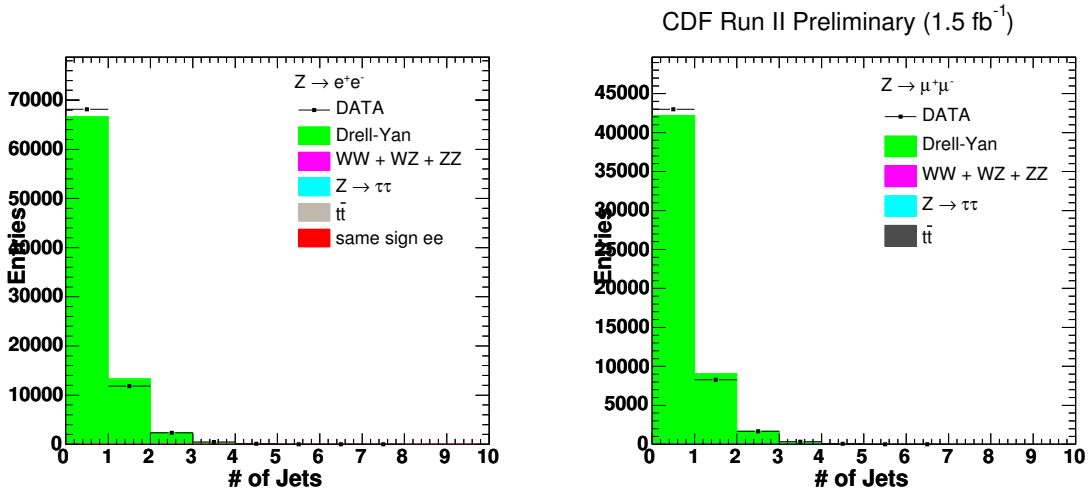

Figure 41: The observed (points) and expected (stacked histogram) distributions in the number of jets, N_{jets}, for $Z^0 \to ee$ (left) and $Z^0 \to \mu\mu$ (right). We select events with $66 < M(l^+l^-) < 116$ GeV for the histograms.

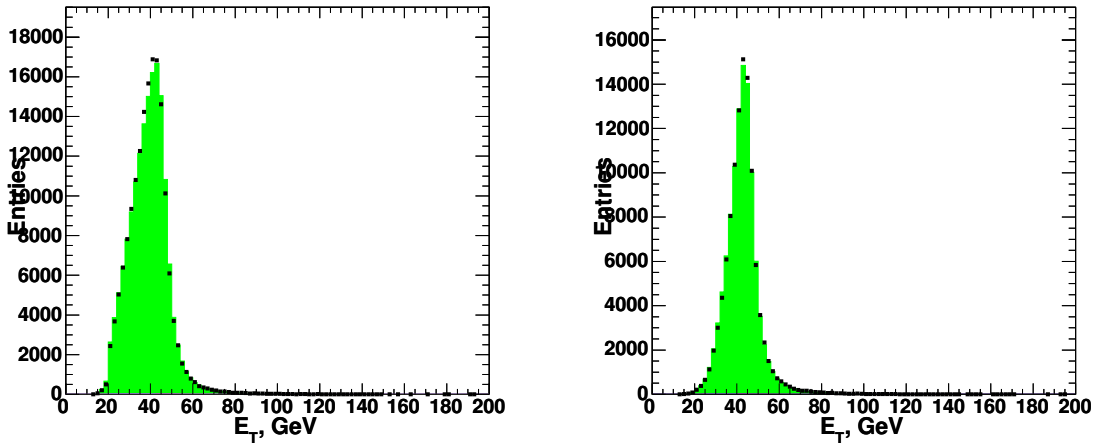

Figure 42: The observed (points) and expected (stacked histogram) distributions in the P_T of the lepton for $Z^0 \to ee$ (left) and $Z^0 \to \mu\mu$ (right).

E Additional "1σ"- and "2σ"- Contours

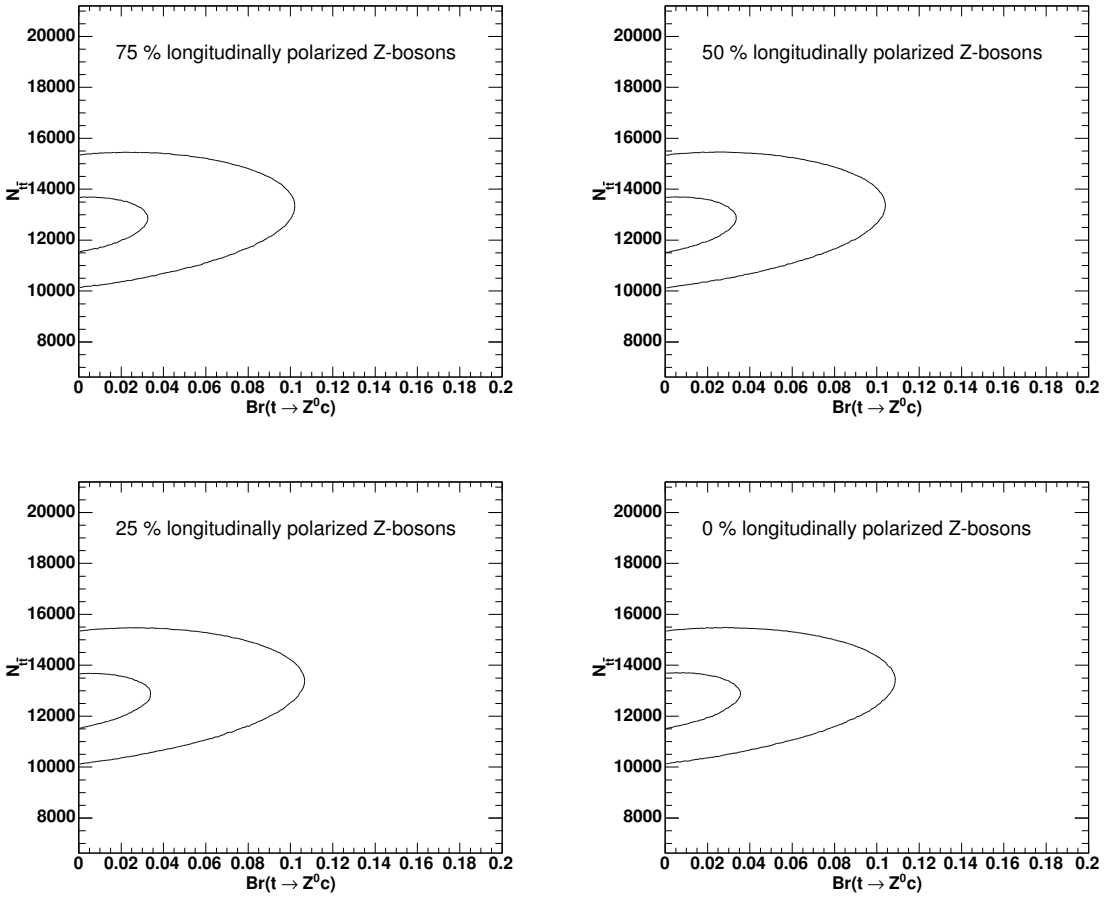

Figure 43: The "1σ"- and "2σ"- contours cover integrals of 0.95% ("2σ") and 0.68% ("1σ") of the posterior probability density function $P(N_{t\bar{t}}, Br(t \to Z^0c|observables)$. Boundary points of a given contour correspond to equal values of the posteriory probability densities. In this figure we show contours for FCNC decays with 0.75, 0.50, 0.25, and 0.0 fractions of longitudinally polarized Z-bosons.

References

[1] H.Fritzsch. t-quarks may decay into z-bosons and charm. *Phys. Lett.*, B224:423, 1989.

[2] J.A. Aguilar-Saavedra. Top flavour-changing neutral interactions: Theoretical expectations and experimental detection. *Acta Phys. Polon.*, B35:2695–2710, 2004, hep-ex/0409342.

[3] F. Larios, R. Martinez, and M. A. Perez. Constraints on top-quark FCNC from electroweak precision measurements. *Phys. Rev.*, D72:057504, 2005, hep-ph/0412222.

[4] Z. Ligeti, M. Papucci, G. Perez, M. D. Schwartz P.J. Fox. Deciphering top flavor violation at the lhc with b factories. page 2, 2007, arXiv:0704.1482 [hep-ph]. http://arxiv.org/abs/0704.1482.

[5] N. Cabbibo, II Topical Conference on Proton-Antiproton Collider PHysics, Rome, Jan. 1982; F. Halzen and M. Marsula, Phys. Rev. Lett. 51, 857 (1983); K. Hikasa, Phys. Rev. D29, 1939 (1984); N.G. Deshpande et al, Phys. Rev. Lett. 54, 1757 (1985); A.D. Martin, R.G. Roberts, and W. J. Stirling, Phys. Lett. 189B, 220 (1987): E.L. Berger, F. Halzen, C.S. Kim, and S. Willenbrock, Phys. Rev. D40, 83 (1989).

[6] Michelangelo L. Mangano, Mauro Moretti, Fulvio Piccinini, Roberto Pittau, and Antonio D. Polosa. Alpgen, a generator for hard multiparton processes in hadronic collisions. *JHEP*, 07:001, 2003, hep-ph/0206293.

[7] Michelangelo L. Mangano, Mauro Moretti, Fulvio Piccinini, and Michele Treccani. Matching matrix elements and shower evolution for top-quark production in hadronic collisions. *JHEP*, 01:013, 2007, hep-ph/0611129.

[8] Torbjorn Sjostrand, Leif Lonnblad, and Stephen Mrenna. Pythia 6.2: Physics and manual. 2001, hep-ph/0108264.

[9] W. M. Yao et al. Review of particle physics. *J. Phys.*, G33:1–1232, 2006.

[10] Thomas J. LeCompte, Robert M. Roser, and Robin L. Coxe. Common Limit Calculations on Top FCNC Decays. CDF Note 3813, Aug. 7, 1996.

[11] LEP Electroweak Working Group (EWWG), http://lepewwg.web.cern.ch/LEPEWWG/.

[12] C. Plager, D. Saltzberg, M. Sutherland, M. Franklin, I. Zaw, J. Gimmell, U. Husemann, and P. Tipton. Search for the Flavor Changing Neutral Current Decay t→Zc in $p\bar{p}$ Collisions at $\sqrt{S}$=1.96 TeV. CDF Note 8888, Jul. 13, 2007.

[13] Joel Heinrich. Bayesian limit software: multi-channel with correlated backgrounds and efficiencies. CDF Note 7587, University of Pennsylvania, 2005.

[14] Matteo Cacciari, Stefano Frixione, Giovanni Ridolfi, Michelangelo L. Mangano, and Paolo Nason. The $t\bar{t}$ cross-section at 1.8 and 1.96 tev: a study of the systematics due to parton densities and scale dependence. *Journal of High Energy Physics*, 2004(04):068–068, 2004. http://stacks.iop.org/1126-6708/2004/i=04/a=068.

[15] F. A. Berends, W. T. Giele, H. Kuijf, R. Kleiss, and W. James Stirling. Multi - jet production in w, z events at p anti-p colliders. *Phys. Lett.*, B224:237, 1989.

[16] Larry Nodulman. Curvature Corrections for 5.3.1 and 6.1.1. CDF Note 6971, Fermilab, 2005.

[17] U. Grundler, L. Lovas, and A. Taffard. High-Pt muons recommended cuts and efficiencies for Winter 2007. CDF Note 8618, University of Illinois - Urbana-Champaign and Comenius University, Nov. 29, 2006.

[18] Mircea Coca and Eva Halkiadakis. Central Electron Identification Efficiencies for the 200 pb^{-1} Run 2 Dataset. CDF Note 6580, University of Rochester, Jan. 6, 2004.

[19] Sam Harper and Greg Veramendi. Very High-Pt Electron Identification. CDF Note 7527, Fermilab, 2005.

[20] Mircea Coca and Eva Halkiadakis. Plug Electron Baseline Cuts Defined in Summer 2003 and Cut Efficiencies. CDF Note 6580, for the ETF group, Feb. 16, 2004.

[21] D. Hare, E. Halkiadakis, and T. Spreitzer. Electron ID Efficiencies and Scale Factors for Winter 2007 Analyses. CDF Note 8614, Rutgers University and University of Toronto, Dec. 7, 2006.

[22] Bo-Young Han and Veronique Boisvert. Trigger Efficiencies for the High E_T Central Electrins in the Gen6 data. CDF Note 8629, University of Rochester, 2006.

[23] We use the jetCorr08 corrections: see http://www-cdf.fnal.gov/internal/physics/top/jets/how-to-apply.html.

[24] See: Baseline Analysis Cuts for High Pt Photons V2.3, http://www-cdf.fnal.gov/internal/physics/photon/docs/cuts.html.

[25] See http://www-cdf.fnal.gov/internal/people/links/SarahBudd/mistag3.html.

[26] S.Grinstein and D.Sherman. SecVtx Scale Factors and Mistag Matrices for the 2007 Summer Conferences. CDF Note 8910, 2007.

[27] Johan Alwall et al. MadGraph/MadEvent v4: The New Web Generation. *JHEP*, 09:028, 2007, arXiv:0706.2334 [hep-ph].

[28] Patrick J. Fox, Zoltan Ligeti, Michele Papucci, Gilad Perez, and Matthew D. Schwartz. Deciphering top flavor violation at the lhc with b factories. 2007, arXiv:0704.1482 [hep-ph].

[29] Ben Cooper and Andrea Messina. Estimation of the Background to $W \to e\nu + n$ Jet Events. CDF Note 7760, University College London, UK; INFN, Rome, Italy, Aug. 4, 2005.

[30] Heather K Gerberich, Ashutosh V. Kotwal and Chris Hays. Cosmic Ray Tagging using COT Hit Timing. CDF Note 6089, 2002.

[31] A Combination of CDF and D0 results on the mass of the top quark. 2007, hep-ex/0703034. http://xxx.lanl.gov/abs/hep-ex/0703034.

[32] J.-F. Arguin. Measurement of the Top Quark Mass with In Situ Jet Energy Scale Calibration at CDF-II. CDF Note 7968, 2005.

[33] Franklin, Grinstein, Guimaraes da Costa, and Sherman. Measurement of the Top Pair Cross Section in Lepton+Jets in 1.12/fb. CDF Note 8767, Harvard, CDF Collaboration, April 26, 2007.

[34] S. Grinstein and D. Sherman. SecVtx Scale Factors and Mistag Matrices for the 2007 Summer Conferences. CDF Note 8910, Harvard, CDF Collaboration, 2007.

[35] Sebastian Grinstein, Jao Guimaraes da Costa, and Daniel Sherman. SecVtx Mistag Asymmetry for Winter 2007. CDF Note 8626, CDF Collaboration, Jan. 4, 2007.

[36] Sarah Budd, Thomas Junk, Tony Liss, and Christopher Neu. Tight, Loose, and Ultratight Secvtx Tag Rate Matrix with $1.2/fb^{-1}$. CDF Note 8519, University of Illinois, Urbana-Champaign and University of Pennsylvania, Dec. 12, 2006.